universität wien

DISSERTATION

Titel der Dissertation

„Insights into telomere protection by the Ku heterodimer“

Verfasserin

Soňa Valuchová

angestrebter akademischer Grad

Doctor of Philosophy (PhD)

Wien, 12. September 2014

Studienkennzahl lt. Studienblatt:	A 094 490
Dissertationsgebiet lt. Studienblatt:	Molekulare Biologie
Betreut von:	Dr. Karel Riha

Ever tried. Ever failed. No matter.
Try again. Fail again. Fail better.
Samuel Beckett

Dedicated to Eduard Valuch - education is a privilege.

Abstract

The Ku heterodimer is an essential protein in human cells for its role in telomere protection. It is also a key factor in DNA double strand break repair via non-homologous end joining (NHEJ). Telomere protection and maintenance as well as NHEJ are important for genome integrity and deficiencies in these processes were associated with human diseases. The function of Ku at telomeres is puzzling as it is unclear how Ku protects telomeres without mediating NHEJ and telomere fusions.

In many eukaryotes, Ku is required for protection of telomeres from resection by nucleases, recombination and fusion. It was proposed that Ku protects chromosome ends by directly binding to DNA. To investigate the Ku-DNA interaction, I designed and *in vitro* reconstituted human and *Arabidopsis thaliana* Ku complexes carrying mutations in conserved residues located on the DNA-protein interaction surface. I analyzed DNA binding capability of the mutant complexes by a set of biochemical assays and identified mutations that altered DNA binding. To study the significance of Ku-DNA binding for telomere biology I set up functional complementation of human cells and *A. thaliana* with selected mutated complexes.

Data obtained from complemented *A. thaliana ku* mutants suggest that direct DNA interaction might be required for telomere function. I further propose that Ku-DNA binding activity is in the context of telomeric chromatin modified by telomere binding proteins (TBPs). However, the plant TBPs have not yet been identified, likely due to genetic redundancy in higher plants. To find plant TBPs, I surveyed the genome of the unicellular green algae *Chlamydomonas reinhardtii* and biochemically characterized one putative TBP. Further analysis of this gene might help to shed light on TBPs in the plant lineage.

Zusammenfassung

Im Menschen spielt der Ku Heterodimer eine essenzielle Rolle indem er das Ende der Telomere beschützt. Er ist auch einer der Schlüsselfaktoren im DNA Doppelstrangbruch Reparaturmechanismus “Non-Homologous end joining” (NHEJ). Der Schutz der Telomere, deren Instandhaltung und auch NHEJ sind wichtig für die Genomintegrität eines Organismus, und Fehler in diesen Prozessen sind mit Krankheiten im menschlichen Organismus asoziiert. Die Funktion von Ku an den Telomeren ist erstaunlich, da nicht klar ist wie Ku das Telomer beschützen kann, ohne NHEJ zu aktivieren, was zu Telomerfusionen führen würde.

In vielen Eukaryoten wird Ku benötigt um das Telomerende vor nukeolytischer Resektion, Rekombination und Fusion zu beschützen. Es wurde vorgeschlagen, dass Ku das Telomereende beschützt, indem es direkt an die DNA bindet. Um diese direkte DNA-Protein Interaktion zu testen, entwarf ich in vitro rekonstituierte humane und *Arabidopsis thaliana* Ku Komplexe mit Mutationen in konservierten DNA Resten die sich an der DNA-Protein Interaktionsoberfläche befinden. Ich analysierte die DNA Bindekapazität dieser mutanten Komplexe mit Hilfe biochemischer Verfahren und identifizierte Mutationen die die DNA Bindefähigkeit veränderten. Um die Signifikanz der Ku-DNA Bindung für Telomerbiologie zu evaluieren, testete ich funkionelle Komplementationen von humanen Zellen und *A. thaliana* mit ausgesuchten, mutierten Komplexen.

Die Daten, die ich von den komplementierten *A. thaliana* Mutanten erhielt, deuten darauf hin, dass eine direkte Interaktion von Ku mit DNA für dessen Telomerfunktion notwendig ist. Weiters, schlage ich vor, dass die Ku-DNA Bindungsaktivitiät, im Hinblick auf telomerisches Chromatin, durch Telomerbindeproteine (TBPs) modifiziert wird. Allerdings sind die TBPs in Pflanzen noch nicht identifiziert worden, wahrscheinlich auf Grund von genetischer Redundanz in höheren Pflanzen. Um diese TBPs zu bestimmen, untersuchte ich das Genom der einzelligen Grünalge *Chlamydomonas reinhardtii* und charakterisierte auf biochemische Weise eine putatives TBP. Eine weitere Analyse dieses Gens könnte helfen, die TBPs in der Pflanzenlinie zu identifizieren.

Table of Contents

1 Introduction

1.1 Telomeres

1.1.1 History, definition, evolution and importance

Stability and integrity of genetic information is essential for reproduction and function of organisms. Telomeres represent one of the key elements necessary for maintaining genome stability. In 1930s Hermann Muller and Barbara McClintock independently concluded that natural chromosome ends differ from chromosome breaks. Muller worked with fruit flies *Drosophila melanogaster*, where he induced chromosome breaks using X-ray. He was unable to isolate chromosomal terminal deletions. He predicted protective function of terminal regions and called them telomeres (from Greek: *telos* = ends, *meros* = part) (E. H. Blackburn 2001; Boukamp and Mirancea 2007; Chan and Blackburn 2004). In the same time period McClintock came to conclusion that telomeres protect chromosomes from end-to-end fusions and their negative consequences. This conclusion was stimulated by her studies of plants *Zea mais*. She noticed that natural chromosome ends are not a substrate for chromosome rearrangements, as it was the case for DNA double strand breaks (DSBs). She could not observe a fusion of chromosome fragment with an intact chromosome. The discovery of DNA structure and replication forewent the detailed characterization of telomeres (E. H. Blackburn 2001; G. L. Blackburn and Mun 2004; E. H. Blackburn 2005; E. H. Blackburn et al. 2006; Boukamp and Mirancea 2007; Chan and Blackburn 2004).

The linear genome configuration likely represents an evolutionary advantage. It is ubiquitous in nuclei of eukaryotes and can be also found in some eukaryotic organelles, bacteria and viruses. The benefits of linearity of nuclear genomes in eukaryotes are seen in enabling of sexual reproduction and recombination (Fulcher et al. 2014). However, natural DNA end of linear genome also present major challenges to cellular metabolism. DNA replication is semiconservative and dis-continual. Standard DNA polymerases synthetize DNA in the 5’ -> 3’ direction and require RNA primer for initiation. After the last RNA primer removal on the lagging strand an unfilled gap arises and forms a 3’ overhang. The problem of the loss of genetic information in every replication cycle was named the end replication problem (Olovnikov 1973).

Furthermore, natural DNA ends formally resemble DSB. During the evolution organisms adopted several strategies how to provide solutions to the chromosome end replication problem and DNA double strand break repair (DSBR) regulation (E. H. Blackburn 2001; de Lange 2004; Fulcher et al. 2014; Nelson and Shippen 2012; Olovnikov 1971; Watson 1972).

Telomeres shorten progressively due to the end replication problem. Emergence of short telomeres eventually leads to cell growth arrest also known as replicative senescence. Activation of specialized programs such as cellular senescence or apoptosis protects the integrity of genome and limits cellular proliferation. In absence of cell cycle arrest, short and deprotected telomeres become substrate for DNA repair and chromosome fusions cause genomic instability that was observed to drive carcinogenesis. Telomeres are therefore important for prevention of malignancies (O'Sullivan and Karlseder 2010; Zhou and Elledge 2000).

On the other hand, short telomeres cause problems in proliferating tissues. Stem and immune cell deficit might develop with progressive telomere shortening and is associated with aging process. Nowadays, several human telomere syndromes have been identified that are caused by impaired telomere maintenance. Patients that harbor short telomeres suffer from a spectrum of symptoms such as idiopathic pulmonary fibrosis, familial liver cirrhosis, aplastic anemia in adulthood, sporadic acute myelogenous leukemia, dyskeratosis congenita characterized by the “diagnostic triad” of oral leukoplakia, skin hyperpigmentation, and nail dystrophy and in severe cases Hoyeraal-Hreidersson, Coats Plus, and Revesz syndrome. Because these symptoms often overlap, it has been proposed that they represent a single disease entity with multiple genetic mechanisms. (Aubert 2014; Holohan et al. 2014; Horn et al. 2013; O'Sullivan and Karlseder 2010; Zhou and Elledge 2000). Studying the structure, protection and maintenance mechanisms of telomeres is therefore medically relevant.

1.2 Structure of telomeres

1.2.1 DNA sequence and structure

In eukaryotic organisms the most distal part of chromosomes consists of tandem repeats. Majority of studied protista, fungi, plants and mammals harbor short repeat

units that are usually rich on guanine, with the general structure of $T_xA_yG_z$ and are added by an enzyme telomerase. Some exceptions include *D. melanogaster* or plants from the genus *Allium* that contain a complex tandem repeats maintained via transposition or recombination (Fulcher et al. 2014).

The telomeric DNA is mostly double-stranded, however the G-rich strand forms on the 3' end of a chromosome a single stranded overhang (G-overhang). The exception is *Caenorhabditis elegans* that forms also single-stranded overhangs of the complementary C-rich strand (C-strand) (Raices et al. 2008). The G-overhang is formed naturally during the DNA replication after the removal of the RNA primer from the last Okazaki fragment. However, the length of observed G-overhang and its presence on majority of telomeres suggests that highly regulated post-replicative 5' -> 3' exonucleolytic degradation of C-strand also contributes to G-overhang formation. The G-overhang is evolutionary conserved feature of telomeres what demonstrates its functional importance and involvement in telomere protection (Fulcher et al. 2014; Louis 2002; O'Sullivan and Karlseder 2010; Verdun and Karlseder 2007). Interesting property of G-overhang is a capability to form G-quadruplex (G4) structures. Groups of guanine nucleotides separated by short sequences are able to bind one another and form stable secondary structures *in vitro* (Figure 1). Recently G4 have been identified *in vivo*, but their function in telomere protection requires further research (Burge et al. 2006; Tarsounas and Tijsterman 2013). G-overhangs further mediate the formation of higher organized structure called t-loop (Griffith et al. 1999). The single-stranded DNA invades the proximal double-strand of telomeric DNA. G-overhang hybridizes with C-strand and displaces G-strand into a displacement loop (D-loop, Figure 1). The size of the t-loop may vary. It is believed that t-loop physically protects the chromosome end from being recognized as DSB (de Lange 2005). Although, plants form G-overhangs and are capable of forming t-loops, some angiosperm plants seem to lack long G-overhangs on 50% of telomeres. Surprisingly, subset of these telomeres is blunt-ended and has been confirmed in *Arabidopsis thaliana*, *Silene latifolia* and *Zea mais* and suggests a G-overhang independent form of telomere protection (Cesare et al. 2003; Kazda et al. 2012; Riha et al. 2000).

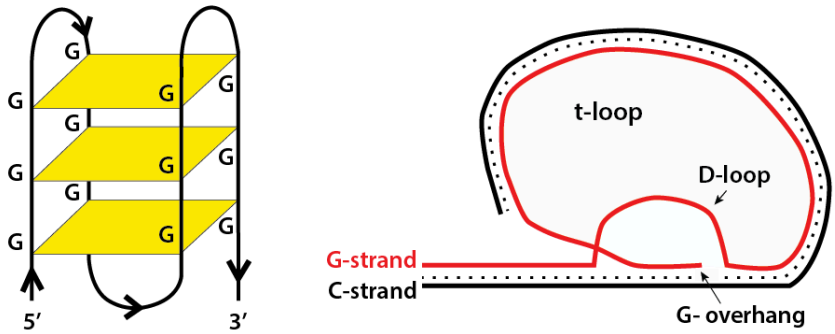

Figure 1: Telomeric DNA structures
Telomere DNA can form higher structures such as G-quadruplexes (G4) where groups of guanine nucleotides separated by short sequences are able to bond one another. The example of parallel topology of G4 is shown (left). T-loops can form when G-overhang invades proximal double-stranded region forming a D-loop (right).

1.2.2 Telomere synthesis

After the discovery of the first telomeric repeats in *Tetrahymena thermophilla* (E. H. Blackburn and Gall 1978) unusual characteristics of telomeres have been observed. Linear plasmids in *Saccharomyces cerevisiae* containing telomeres of *T. thermophilla* started to accumulate telomeric sequence of the budding yeast. Also *de novo* synthesis of telomeres and telomere length heterogeneity in *T. thermophilla* has been observed and suggested a new mechanism for DNA synthesis (E. H. Blackburn et al. 2006). In 1985 was for the first time described a biochemical activity of telomere specific terminal transferase, called telomerase. The enzyme added telomeric repeats to the ends of chromosomes (Greider and Blackburn 1985, 1987).

Telomerase is a ribonucleoprotein complex with a reverse transcriptase activity. Catalytic core is composed of RNA subunit (TR, TER or TERC in mammals and *Tlc1* in budding yeast) forming a template for telomere repeats and protein subunit TERT (telomerase reverse transcriptase) with the enzymatic activity. Additional protein components have been shown to contribute to activity of telomerase. Est1 and Est3 in *S. cerevisiae* are essential for telomere elongation *in vivo* (Osterhage and Friedman 2009). In human cells an accessory protein dyskerin (DKC1) binds RNA and stabilizes TR and forms with TERT an active telomerase. Further, TCAB1 (telomerase Cajal body protein 1) associates with DKC1 and is important for telomere maintenance. Telomerase is modified to active conformation by ATPases pontin and reptin. In different organisms, different accessory proteins associate with telomerase (Cohen et

al. 2007; Collins 2006; O'Sullivan and Karlseder 2010; Riha et al. 2006; Venteicher et al. 2008; Venteicher et al. 2009; Venteicher and Artandi 2009).

To synthetize telomeric repeats, RNA subunit of telomerase associates with the last nucleotides of G-overhang. TERT catalyzes the synthesis of telomere DNA by extending the G-overhang and then telomerase translocates allowing the synthesis of following repeats (Figure 2). This process is tightly regulated (O'Sullivan and Karlseder 2010). To complete the process of telomere elongation, the complementary C-strand is synthesized by fill in synthesis (Chen and Lingner 2013).

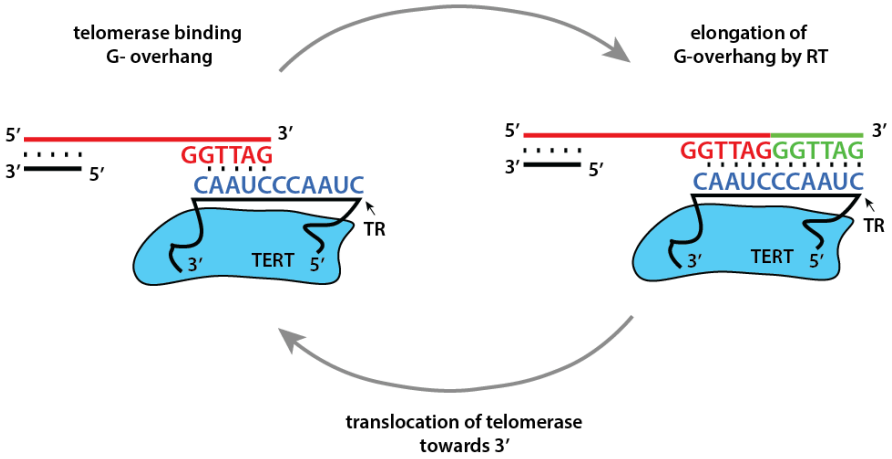

Figure 2: Telomere elongation by telomerase
Telomerase associates with the terminal nucleotides of G-overhand and elongation occurs via reverse transcription (RT) catalyzed by TERT and TR serves as a template. After synthesis, telomerase can translocate towards the 3' end and continue elongation.

1.2.3 Telomere end structure and processing

The end replication problem leads to the loss of DNA on lagging strand during DNA replication when the last RNA primer is removed. Telomerase counteracts the loss of genetic information by elongation of the 3' G-overhang and allows for additional Okazaki fragment synthesis. However, during DNA replication blunt ends arise on telomeres synthesized via leading strand mechanism (Figure 3).

G-overhang is required for priming the telomerase and maintaining telomere length. It is further involved in telomere protection as a substrate for secondary structure formation and binding of telomere proteins (Baumann and Cech 2001; Griffith et al. 1999; Horvath et al. 1998; Lingner and Cech 1996). The importance of 3' overhangs indicates that cells harbor a resection mechanism that turns blunt ends formed by

leading strand synthesis into G-overhangs (Lingner et al. 1995). It appears that the resection is influenced by multiple nucleases and telomere chromatin. The MRX (Mre11-Rad50-Xrs2) complex in budding yeast and the MRN (Mre11-Rad50-Nbs1) in human cells have been shown to be important for G-overang formation (Chai et al. 2006; Larrivee et al. 2004). Further, Sae2 (orthologue of CtIP in human), Exol, Sgs1, Dna2 and Apollo (Balestrini et al. 2013; Bonetti et al. 2009; Kazda et al. 2012; P. Wu et al. 2010) might have overlapping functions at DNA ends. The end resection is limited in angiosperm plants resulting into blunt-ended telomeres on a portion of chromosome ends (Kazda et al. 2012).

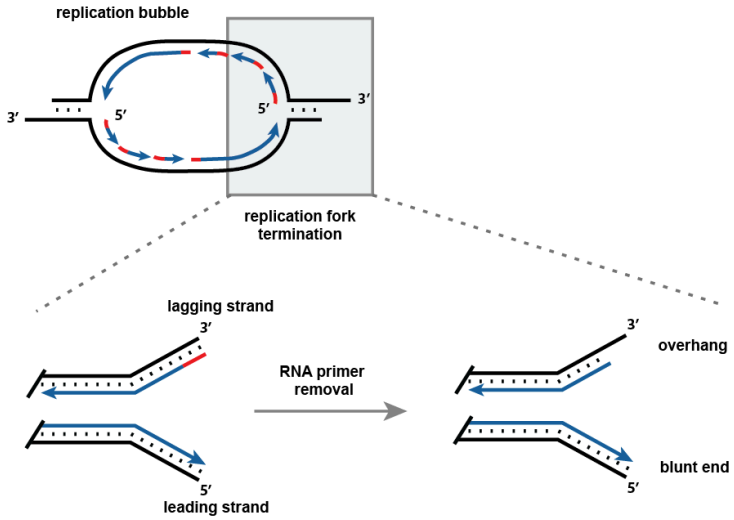

Figure 3: Semiconservative DNA replication
DNA is synthetized in 5' -> 3' direction. In replication fork, leading strand progresses continuously while lagging strand consists of Okazaki fragments. When the terminal RNA primer is removed from lagging strand, 3' single stranded overhang cannot be filled in.

1.3 Telomeric proteins

1.3.1 Telomere-binding proteins

Telomeric DNA interacts with many proteins that regulate its length, function, or help mediate formation of higher organized structures. Four mechanisms of telomere association have been described. First, a Myb-like domain (SANT/Myb) ensures binding of proteins to double-stranded DNA. Sequence specific binding is achieved due to presence of a conserved telobox motif (Konig et al. 1996; Peska et al. 2011). Telobox was used to search for telomere proteins in yeast, animals and plants. Mammalian TRF1 and TRF2 (telomeric repeat-binding factor 1, 2) harbor C' terminal single Myb-like

domain and form dimers to bind telomeres. Rap1 with two Myb-like subdomains from *S. cerevisiae* can bind as a monomer (Court et al. 2005; Konig et al. 1996; Palm and de Lange 2008; Peska et al. 2011; Wahlin and Cohn 2000). Second, sequence specific binding of single-stranded overhangs occurs via OB-fold (oligonucleotide-oligosaccharide-binding). It can be found in budding yeast Cdc13, *Oxytricha nova* TEBPα/β, mammalian Pot1 (protection of telomeres 1) (Horvath et al. 1998; Lei et al. 2004; Mitton-Fry and Wuttke 2002). Third, sequence unspecific binding of DNA through DNA-binding channel was observed in Ku heterodimer of budding yeast (Lopez et al. 2011). Last, proteins associate with telomeres via protein-protein interactions. Examples of such proteins are Sir3 and Sir4 associating with Rap1 in budding yeast or TIN2 associating with TRF1 and TRF2 in mammals (Cockell et al. 1995; Ye et al. 2004).

Protection of telomeres and formation of t-loop is facilitated in mammals by protein complex Shelterin. Shelterin consists from six proteins: TRF1, TRF2, POT1, TIN2, TPP1 and RAP1 (Figure 4). Removal of TRF1 and TRF2 cause removal of Shelterin and reveal it's role in telomere protection DNA damage signaling via ATM (ataxia telangiectasia mutated) and ATR (ataxia telangiectasia and Rad3 related), classical and alternative non-homologous end joining (C-NHEJ, alt-NHEJ), homologous recombination, and resection (Sfeir and de Lange 2012). TRF2 plays major role in suppressing C-NHEJ (Bae and Baumann 2007; Ribes-Zamora et al. 2013). POT1 binds single stranded G-overhang and protects from DNA response at telomeres (L. Wu et al. 2006).

Telomere integrity in budding yeast relies on CST complex Cdc13, Stn1 and Ten1 (Figure 4). CST is essential for telomere maintenance and protection of telomeres from nucleolytic degradation and DNA damage checkpoint activation (Chen and Lingner 2013; Fulcher et al. 2014).

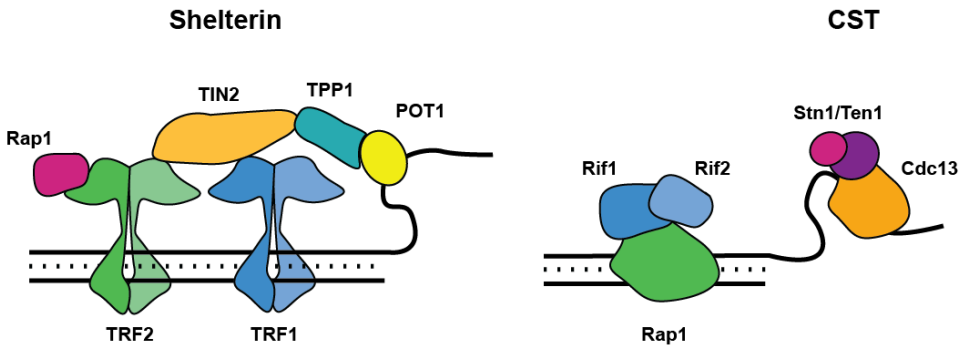

Figure 4: Shelterin and CST complex
Mammalian telomere protection is carried out by protein complex Shelterin (TRF1, 2, Rap1, TIN2, TPP and POT1) anchored by Myb-like domains of TRF proteins to double-stranded telomeres. In *S. cerevisiae* Rap1/Rif1/Rif2 is anchored via two Myb-like domains of Rap1 and CST complex (Cdc13/Stn1/Ten1) is bound to G-overhang via OB fold of Cdc13.

Plant telomeres are not very well studied. The telomere length vary from 0,5 kb in *Chlorella vulgaris* to 150 kb in *Nicotiana tabacum*. The most studied are telomeres in *A. thaliana* with telomere repeat unit TTTAGGG (different from mammalian TTAGGG). T-loops have been observed in *Pisum sativum*. Due to gene duplication the Shelterin subunits have not yet been identified. In *A. thaliana* telomere binding proteins (TBPs) has undergone major gene duplication. Two major groups of TBPs have been identified: TRF-like (TRFL) and SMH-like (single myb histone). TRFL harbor C' terminal Myb-like domain and one subfamily contains central ubiquitin-like region and 40 amino acid extension domain that has been shown to be essential for binding telomere sequence *in vitro*. SMH-like family contains N' terminal Myb-like domain and one member TRB1 has been shown to localize to telomeres *in vivo* (Cesare et al. 2003; Karamysheva et al. 2004; Schrumpfova et al. 2014; Zellinger and Riha 2007).

Chlamydomonas reinhardtii telomeres consist of TTTTAGGG repeats. Telomeric DNA is relatively guanine-poor (37,5 % GC) and contrasts with the high GC content of the genomic DNA (64 % GC). The TTTTAGGG sequence forms G-quadruplexes with lower stability and cannot fully complement telomeric function in *S. cerevisiae*. However, it is able to serve as a substrate for endogenous telomerase. Telomeric DNA cloned from *C. reinhardtii* was approximately 300 bp. Nevertheless, the real telomere length is likely longer because nucleases were used during the cloning process (Fulneckova et al. 2012; Petracek et al. 1990). Only one telomere-associated protein has been

investigated in *C. reinhardtii*: G-strand binding protein GBP with 34kDa contains RNA binding motifs (Hails et al. 1995; Petracek et al. 1990; Petracek and Berman 1992).

1.3.2 DNA repair proteins on telomeres

DNA double-strand breaks (DSBs) are considered to be the most deleterious form of DNA damage. A single unrepaired DSB results in cellular death (Bennett et al. 1993; Symington and Gautier 2011). Broken DNA ends are recognized predominantly by two kinases of the PIKK family: ATM and ATR. ATM is preferentially activated by blunt-ended DNA having none or short overhangs. ATR recognizes longer stretches of single stranded DNA (Shiotani and Zou 2009). Homologous recombination (HR) or non-homologous end joining (NHEJ) pathway are responsible for DNA repair. The canonical C-NHEJ depends on Ku and XRCC4/LigIV, while alternative alt-NHEJ requires PARP1, Mre11 and CtIP and involves resection (Betermier et al. 2014).

Recognition of the chromosome ends by the DNA repair machinery can lead to cell cycle arrest, chromosome end-to-end fusions or cell death (Longhese 2008; O'Sullivan and Karlseder 2010). However, DNA repair proteins such as ATM, ATR, Mre11 or Ku are present at telomeres and are important for their maintenance as well as protection. Furthermore, temporary recognition of telomeres by the DNA repair machinery during S-phase seems to be required for replication and folding of functional telomeres (Longhese 2008; Riha et al. 2006; Verdun and Karlseder 2007). Nevertheless, most of the time a full DNA damage response is repressed at the chromosome termini (Denchi, 2009). DNA repair proteins thus play a seemingly contradictory role in telomere biology. One of the most interesting proteins involved in both DNA repair and telomere biology is Ku heterodimer. Ku protects both DSBs and telomeres from excessive nucleolytic processing (Kazda et al. 2012; Liang and Jasin 1996; Lopez et al. 2011). However, C-NHEJ is repressed at functional telomeres (Smogorzewska et al. 2002). The exact mechanism of DNA protection and inhibition of DNA repair on telomeres by Ku is yet to be determined.

1.4 Ku heterodimer

1.4.1 History and structure

The Ku protein complex was discovered as autoantigen in serum of patients with autoimmune diseases of connective tissues. Ku was identified as acidic nuclear protein and was named after first two letters of the name of Japanese patient whose serum served as a prototype (Mimori et al. 1981). The association of Ku with autoimmune diseases is most likely not connected to its biochemical functions. The protein is present in high abundance (0,5 x 10^6 molecules per cell) and it has higher probability to become an autoantigen then less abundant proteins (Tuteja et al. 1994).

Ku is highly conserved complex that can be found in eukaryotic organisms, but homologues were found also in some bacteria (Doherty et al. 2001) and bacteriophage Mu (d'Adda di Fagagna et al. 2003). In eukaryotes Ku consists from two polypeptides of approximate weight 70 and 80 kDa with size-derived names Ku70 and Ku80 respectively. Ku80 in mammals is according to some sources also known as Ku86. Both names probably origin from under- and overestimation of the actual size in human cells 82,713 kDa. Ku83 would represent more accurate name (Mimori et al. 1990).

The crystal structure of human Ku bound to DNA revealed its ring-like shape (Walker et al. 2001). Both subunits form stable quasi-symmetrical dimer with expansive base and narrow bridge creating a channel. Although Ku70 and Ku80 evolved from a single ancestor, divergence within dimer interface precludes formation of homodimers. Structurally, both subunits share three-domain topology: (i) N-terminal α/β domain (Ku70 34-250 aa, Ku80 6-238 aa), (ii) central β-barrel, (iii) C-terminal helical arm (Figure 5). Majority of the central region (core) adopts β-barrel conformation and with the narrow bridge it is responsible for DNA binding (d'Adda di Fagagna et al. 2003; Grundy et al. 2014; Walker et al. 2001). The core is shared among Ku proteins from different species (Grundy et al. 2014). N' terminal α/β domain in eukaryotes contains Von Willebrand factor type A (vWA)-like domain that often mediates protein-protein interactions. C-terminal region harbors nuclear localization signal in both subunits. Further, additional DNA interacting SAP domain is present on Ku70 and C-terminal domain (CTD) on Ku80 was deleted from for crystallography. In vertebrates, Ku forms a

DNA dependent protein kinase (DNA-PK) with the catalytic subunit DNA-PKcs. The interaction region is localized on C-terminus of Ku80 (Figure 5) (Grundy et al. 2014).

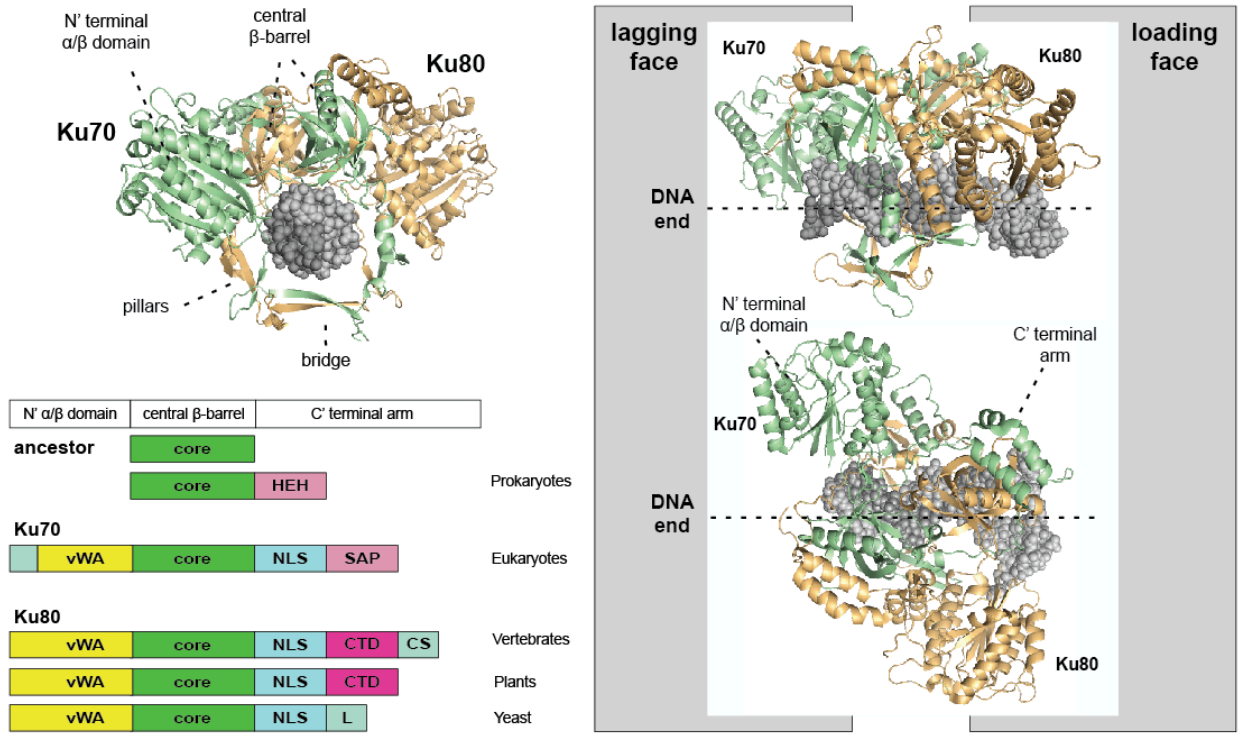

Figure 5: Structure and domains of Ku

Crystal structure of human Ku heterodimer encircles DNA in ring-like manner. The frontal view (left top) illustrates bridge and pillars forming DNA channel with wide base of the protein. Loading of the complex through N-terminus of Ku80 (loading face) is illustrated with the side and top view (right top and bottom). Structural images were generated using Pymol. In addition to the core domain of Ku, several domains were adopted in different organisms (left bottom): HEH = helix-extension-helix, vWA = Von Willebrand factor type A-like domain, NLS = nuclear localization sequence, SAP = common to SAF-A/B, Acinus PIAS proteins, CTD = C-terminal domain, CS = DNA-PKcs binding region, L = leucine rich helix (modified according to (Grundy et al. 2014)).

Ku binds DNA through its channel in a nut-and-bolt manner in preferred orientation. N-terminus of Ku80 subunit loads onto DNA (loading face) and N-terminus of Ku70 is proximal to the DNA end (lagging face). Internal surface of DNA channel has positive electrostatic charge localized on the base (opposite the bridge). Although no obstruction was detected on either end, many residues lie within the exclusion volume. Therefore, helical path of DNA through Ku channel was suggested (Walker et al. 2001; Yoo et al. 1999). Partial asymmetry of the complex, where α/β domain of Ku70 is closer to the DNA, might be responsible for directional loading and impose an energetic barrier

to inward movement of Ku. This is the rate-limiting step in binding to internal sequences (de Vries et al. 1989). Ku does not bind to circular dsDNA. The highest affinity was observed for free dsDNA ends, however linear DNA, as well as RNA binding was observed. Blunt ends, single strand overhangs as well as hairpins can be bound with different affinities. Binding is not sequence specific, does not require ATP and appears to be non-cooperative. Ku is also able to translocate inward (slide) along the DNA (Arosio et al. 2002; Arosio et al. 2004; Blier et al. 1993; Falzon et al. 1993; Fisher and Zakian 2005; Ma and Lieber 2001; Mimori and Hardin 1986; Pfingsten et al. 2012). Sequence non-specific binding can be explained by interaction of Ku protein with DNA backbone rather than individual bases. The interaction is electrostatic and involves several lysine residues from both subunits and leads to conformational changes in Ku (Arosio et al. 2004; Lehman et al. 2008; Walker et al. 2001). Interestingly, Ku can also bind to nucleosomal DNA by peeling away a short stretch of DNA from histone octamer (Roberts and Ramsden 2007).

Due to the high affinity to DNA ends, Ku has a general conserved role in protecting DNA from excessive nucleolytic degradation across species (d'Adda di Fagagna et al. 2003; Shee et al. 2013). DNA interaction and protein-protein interaction domains of Ku are important for several cellular mechanisms. The best studied is its function in DNA DSB repair via C-NHEJ. It also contributes to the immune system gene variability by V(D)J recombination (variable, diversity and joining) and class-switch recombination. Surprisingly, Ku also plays an important role in telomere biology in many organisms. It can also be found in cytoplasm, where it is able to inhibit apoptosis by restricting the entry of BAX protein to mitochondria (Downs and Jackson 2004).

1.4.2 Main component of C-NHEJ

Eukaryotic cells use two main pathways to repair DSBs: homologous recombination (HR) and non-homologous end joining (NHEJ). While HR is mainly used by lower eukaryotes, NHEJ was described to be the main repair mechanism in multicellular as well as some unicellular organisms such as *C. reinhardtii* (Debuchy et al. 1989; Mahaney et al. 2009).

Analysis of hamster cell lines sensitive to X-rays uncovered the connection of Ku and DSB repair in NHEJ (Rathmell and Chu 1994). Ku binds DSBs and protects them from excessive nuclease degradation (Boulton and Jackson 1996; Feldmann et al. 2000; Liang and Jasin 1996). It helps to bridge DNA ends to facilitate the ligation and recruits other proteins involved in this pathway to recognize and repair the damaged site. Ku acts at the first step of NHEJ pathway where it recognizes a DBS and binds to it. After DNA binding it must translocate inwards to free DNA end for further processing (Kysela et al. 2003). In vertebrates it forms with the catalytical subunit of proteinkinase (DNA-PKcs) an active DNA dependent protein kinase (DNA-PK). DNA-PK holds DNA ends in close proximity in synaptic complex. In case that the DNA ends are modified due to the initial damage, they become enzymatically processed to ensure ligation by complex of DNA ligase IV with XRCC4 (Downs and Jackson 2004; Mahaney et al. 2009). There is evidence that Ku itself might bridge DNA via Ku70 interaction surfaces (Ribes-Zamora et al. 2013). After DNA ligation, Ku becomes trapped on DNA and could interfere with DNA replication or transcription. Ku80 subunit is therefore polyubiquitinated and degraded (Grundy et al. 2014).

The main phenotypical manifestation of Ku mutations is increased sensitivity to agents promoting formation of DSBs (Rathmell and Chu 1994). Surprising results were obtained from mutations of yeast homologues, where *S. cerevisiae* mutants in genes YKU70 and YKU80 did not show DSB sensitivity. Decrease in survival was observed in YKU mutants only when the HR pathway was inactivated simultaneously. The explanation of this phenomenon comes from the preference to repair DSB via HR in budding yeast. When HR is inactive, NHEJ forms a backup mechanism to ensure DSB repair (Siede et al. 1996). Similarly, it is possible to increase the HR rate in organisms preferring NHEJ as the main repair mechanism by Ku inactivation. This can be used in gene targeting (Fox et al. 2009).

Two NHEJ pathways have been described: the classical or canonical (C-NHEJ or D-NHEJ as DNA-PK dependent) and alternative or backup (alt-NHEJ or B-NHEJ) pathway (Mladenov and Iliakis 2011). Ku initiates and is required for C-NHEJ and suppresses alt-NHEJ at DSBs and telomeres (Bombarde et al., 2010; Fattah et al., 2010; Sfeir and de Lange, 2012; Wang et al., 2006).

1.4.3 Telomere functions of Ku

In all studied eukaryotes, the Ku contributes to telomere length homeostasis and chromosome end protection. In *S. cerevisiae, S. pombe* and trypanosomes, telomere length declines due to Ku deficiency (Fisher and Zakian 2005; Riha et al. 2006). In *S. cerevisiae* Ku binds directly RNA subunit of telomerase in mutually exclusive manner with DNA. Nuclear accumulation of the RNA subunit and recruitment to DNA end via Ku was proposed to be the mechanism of positive telomere length regulation (Pfingsten et al. 2012). By contrast, Ku acts as negative regulator of telomerase in *A. thaliana*. *Ku* mutants exhibit telomerase-dependent telomere lengthening. In the absence of Ku, the amount of G-overhangs increases. G-overhangs present a substrate for telomerase and thus limiting the formation of G-overhangs could be the underlying mechanism of Ku regulation of the telomere length (Kazda et al. 2012; Riha et al. 2002). Data from mouse and human cells are less clear and both telomere shortening and elongation has been observed. Different levels of telomerase expression could contribute to this heterogeneity. In absence of telomerase, Ku deficient *A. thaliana* also exhibit telomere shortening (Riha et al. 2006).

Interestingly, Ku is an essential protein in human cells due to its function at telomeres and not in DNA repair. Ku deficiency causes massive telomere loss via t-circle excision presumably due to homologous recombination (Wang et al. 2009). Excision of t-circles was also observed in *A. thaliana ku* mutants (Zellinger et al. 2007). Suppression of recombination and alt-NHEJ (Bombarde et al. 2010) on telomeres is analogous to the function of Ku on DSBs as Ku has been previously implicated in regulation of DSB repair pathway choice in plants and human (F. Fattah et al. 2010; Qi et al. 2013).

Ku further regulates length of the G-overhang: deficiency results in G-overhang extension in plants and yeast. Reduction of Ku86 leads also to extension of G-overhang in human cells (Fisher and Zakian 2005; Myung et al. 2004; Riha et al. 2006). Interestingly, EXO1 nuclease was implicated in G-overhang elongation (Kazda et al. 2012; Maringele and Lydall 2002).

Surprisingly, Ku protects telomeres in a similar fashion as DSBs: via suppression of extensive nucleolytic degradation and recombination. However, it fails to initiate

NHEJ on intact telomeres. The mechanism that prevents initiation of Ku-dependent DNA repair selectively on telomeres is not well understood. There is evidence, that telomere binding proteins are involved in this process. Deficiency of TRF2 in mammals, Taz1 in *S. pombe* or Rap1 in *S. cerevisiae* lead to Ku-dependent chromosome end-to-end fusions (Riha et al. 2006). In *S. cerevisiae* has been proposed a “two face” model of Ku function on telomeres. A conserved α-helix on N-terminal α/β domain of Ku70 is important for NHEJ, while orthologous helix on Ku80 is responsible for telomere silencing. The α-helix in human Ku70 is responsible for formation of heterotetrameres with another Ku complex and it is also involved in TRF2 interaction. It has been proposed, that limiting heteroteramerization by TRF2 interaction on telomeres helps preventing NHEJ and therefore chromosome end-to-end fusions (Ribes-Zamora et al. 2007; Ribes-Zamora et al. 2013).

Furthermore, data from *S. cerevisiae* show that Ku must bind directly to telomeric DNA in order to ensure telomere protection (Lopez et al. 2011). Interestingly, sliding of Ku is important for successful NHEJ (Kysela et al. 2003) and mutant Ku complexes with enhanced sliding failed to protect telomeres from nucleolytic degradation (Balestrini et al. 2013). This suggests, that sliding restriction might play a role in the inhibition of NHEJ on telomeres. In angiosperm plants Ku contributes to integrity of blunt-ended telomeres by protecting them from nucleolytic resection (Kazda et al. 2012). Based on this data we propose a model where NHEJ is inhibited on telomeres due to limited sliding (Figure 6). In angiosperm plants, formation of blunt ended telomeres might be therefore a result of extremely limited sliding. Ku could load onto newly replicated DNA ends that are blunt thanks to leading strand replication and physically protect DNA end from exonucleolytic processing. In organisms lacking blunt-ended telomeres, the sliding might be partially permitted, however the rate of resection might be regulated by the sliding ability. Presence of telomere binding proteins could restrict sliding of Ku and therefore end-to-end fusions.

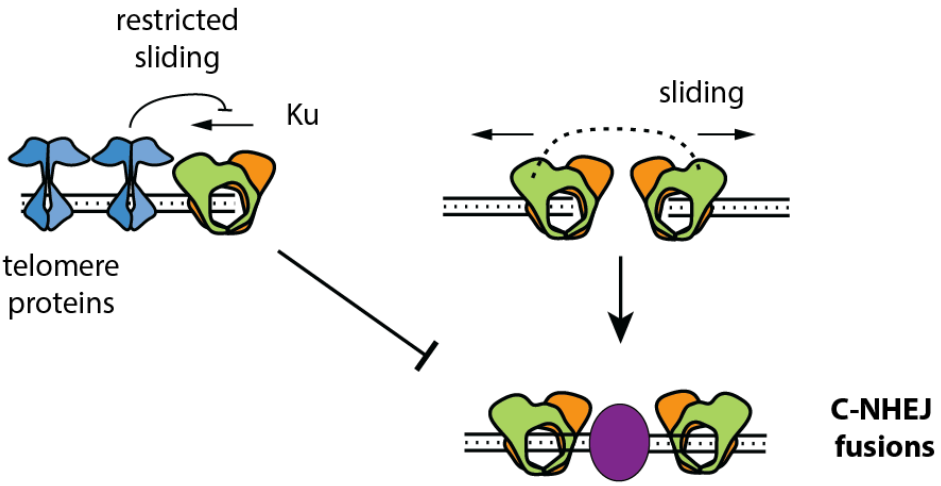

Figure 6: Suggested model of NHEJ regulation by Ku on telomeres
Ku has high affinity to dsDNA ends. Restricted sliding by telomere binding proteins might prevent nucleolytic degradation of telomeres, stabilize blunt ends in plants and suppress C-NHEJ on telomeres.

2 Aims of this thesis

The overall aim of my thesis was to investigate the role of DNA interaction of Ku heterodimer in telomere protection.

Objective 1: To determine whether human and *A. thaliana* Ku complexes differ in DNA binding properties

Human and Arabidopsis Ku complex show similar primary sequence and function. However, some distinctions in telomere phenotypes associated with Ku deficiency in *A. thaliana* and human suggest that these complexes may slightly differ in their biochemical properties. Using *in vitro* assays with recombinant proteins I aim to investigate differences in DNA interaction between human and Arabidopsis Ku.

Objective 2: To engineer Ku complexes with altered DNA binding properties

It has been shown that in budding yeast Ku directly binds telomeres and sliding is important for regulation of resection. There is no evidence for the importance of Ku/DNA interaction in telomere protection in human and Arabidopsis. I aim to create human and Arabidopsis Ku proteins with altered DNA binding/sliding properties using structure guided mutagenesis.

Objective 3: To examine how altered Ku/DNA binding properties affect telomere metabolism and DNA repair

Previously, complementation of Ku deficient *S. cerevisiae* with mutant complexes helped to investigate its role in telomere protection and maintenance. I therefore aim to investigate the impact of the Ku complexes with impaired DNA interaction on telomere biology *in vivo* using human cells and *A. thaliana*.

Objective 4: Identification of plant telomere binding proteins

Binding and sliding of Ku on telomeres might be influenced by presence of telomere binding proteins. Plant Shelterin complex has not yet been described. Therefore, I aim to characterize a putative telomere binding protein in *C. reinhardtii*, single-cellular green algae related to land plants.

3 Results

3.1 Ku-DNA interaction plays a role on telomeres in *A. thaliana*

3.1.1 The HsKu and AtKu exhibit differences in DNA binding properties

3.1.1.1 AtKu shares structural similarity to HsKu

The protein subunits of Ku complex are conserved through evolution and form homo- or heterodimers in all domains of life including some viruses (Bowater and Doherty 2006; d'Adda di Fagagna et al. 2003). Although, human (Hs) and *A. thaliana* (At) are evolutionary very distant, the respective Ku proteins (HsKu and AtKu) are structurally and functionally conserved. The AtKu70 and AtKu80 subunits share 31 % and 24 % protein sequence identity with their respective human counterparts (Blast, NCBI; or 28,6 and 22,5 % identity and 40,7 and 37,6 % similarity as reported previously (Tamura et al. 2002)). HsKu and AtKu are involved in NHEJ and act as important regulators of DSB repair pathway choice (F. Fattah et al. 2010; Qi et al. 2013). Furthermore, Ku suppresses the formation of t-circles and is important for telomere protection (Kazda et al. 2012; Wang et al. 2009; Zellinger et al. 2007). However, AtKu is important for integrity of blunt-ended telomeres and unlike in other organisms acts as a negative regulator of telomerase (Gallego et al. 2003).

The different functions of Ku proteins might be explained by differences in their biochemical properties. To better understand the structural similarity between the Ku complexes, we predicted structure of AtKu using the crystal structure of HsKu (1JEY, PDB). AtKu subunits were overlaid with HsKu bound to DNA in PyMol (Figure 7). The structure of both complexes is very similar. AtKu encircles DNA and therefore it might be able to bind and slide in similar manner as HsKu. The differences in DNA channel might lead to altered DNA binding/sliding properties of the complex. In *S. serevisiae* the direct binding of Ku to DNA and restricted inward translocation is necessary for it's telomere protection (Balestrini et al. 2013; Lopez et al. 2011). In *A. thaliana* AtKu protects telomeres from exonucleolytic degradation. We hypothesized that restriction of sliding of AtKu might be the underlying reason for formation of blunt-ended telomeres.

Therefore, we decided to analyze the differences in DNA binding/sliding of HsKu and AtKu *in vitro*.

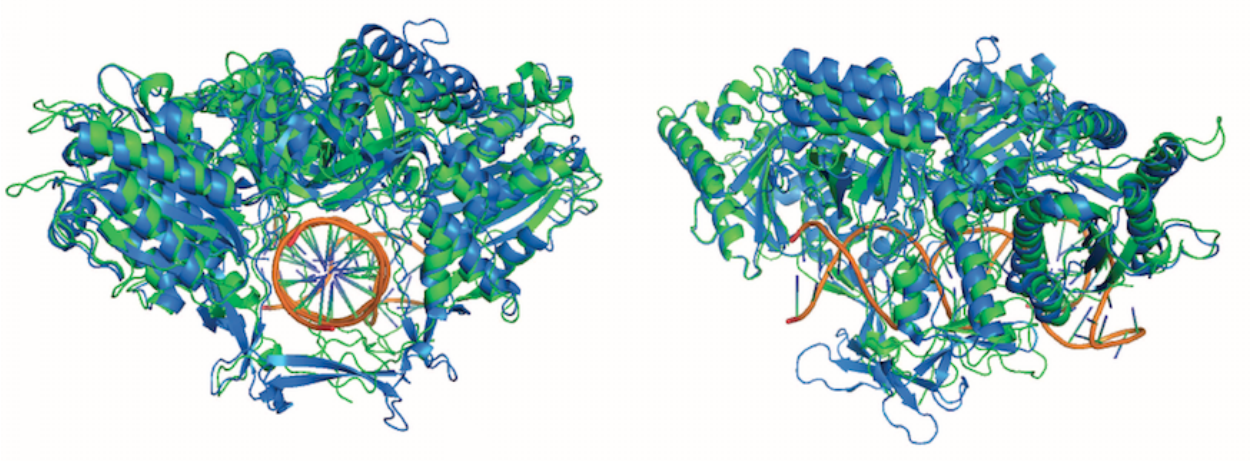

Figure 7: A model of HsKu and AtKu bound to DNA.
The crystal structure of HsKu (shown in blue, 1JEY PDB) was used to predict secondary structure of AtKu (shown in green). Both structures were overlaid using PyMol to show overall structural similarity and minor differences.

3.1.1.2 Coexpression of HsKu and AtKu in insect cells allows purification of dimers

Ku has been shown to bind and slide on the DNA *in vitro* in ATP and sequence independent manner (Arosio et al. 2002; Dynan and Yoo 1998; Walker et al. 2001). To analyze the properties of HsKu and AtKu proteins *in vitro* we needed to establish expression and reconstitution of recombinant complexes. The expression and purification of functional HsKu complex have been previously described using either baculovirus system or *Escherichia coli* (Arosio et al. 2002; Hanakahi 2007). Our earlier attempts to express AtKu in *E. coli* led to the production of insoluble AtKu70 subunits and heavily degraded AtKu80. Furthermore, coexpression from neither polycistronic nor monocistronic vector gained any improvement. Therefore, we decided for coexpression in insect cells using baculovirus system provided by Campus science support facilities (CSF, Vienna).

The cDNA of Ku subunits were inserted into the expression vector pFastBac Dual (Life Technologies). Technician in CSF transfected Hi5 cells with *E. coli* generated bacmids. Pellet of Hi5 cells containing Ku protein was obtained from CSF either fresh or

frozen. Storage of the pellet prior purification had no negative influence on the quality of the protein.

The cDNA of AtKu70 and AtKu80 was amplified from plasmids present in our laboratory (pCBJ02, pCBJ01). Sequencing revealed presence of four mutations in AtKu70: R117K (AGG->AAG), A155A (GCA->GCG), Q256Q (CAA->CAG) and V462V (GTA->GTG). The R117K was corrected using *in vitro* mutagenesis. Human Ku cDNA was amplified from HeLa cDNA (kindly provided by Johannes Popow). Sequence of HsKu80 contained one silent mutation T524T (ACA->ACG).

For purification of functional complexes we decided to place 6xHis tag on the N' terminus of Ku80 subunit. This terminus contains 5 amino acid residues that are not present in the crystal structure probably due to flexibility. Placing the tag in this flexible region reduces the probability of negative influence on the function of the protein. Furthermore, this terminus is localized on the loading face of the complex (Figure 8) and therefore is less likely to interfere with sliding.

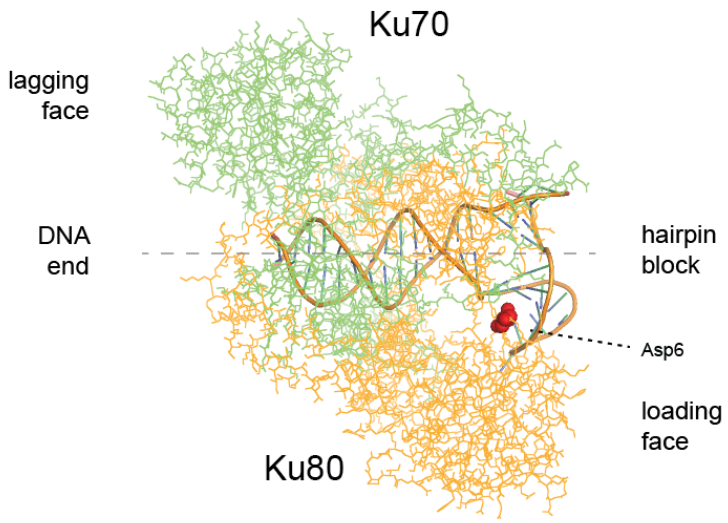

Figure 8: N' terminus of Ku80 subunit of HsKu.
The crystal structure of HsKu bound to DNA (1JEY, PDB). The N' terminal Asn6 (red) of Ku86 (orange) is located on the loading face of the complex. The amino acids HsKu80 1-5 are not present in the crystal structure.

The expression vector pFastBac Dual contains two promoters: Polh and P10. The HsKu80 or AtKu80 were first cloned into pFastBac HTA vector to introduce the N'terminal 6xHis tag. Whole cDNA with the tag was then cloned under the Polh

promoter using restriction digest. The cDNA of AtKu70 or HsKu70 subunits was cloned under the P10 promoter (Figure 9).

Figure 9: Scheme of baculovirus expression vector pFastBacDual for Ku expression

Both subunits of either HsKu or AtKu were cloned in pFastBacDual expression vector under Polh and P10 promoters. N' terminal 6xHis tag was introduced to HsKu80 or AtKu80 for purification.

For purification of multiple Ku complexes in parallel we used "His mag Sepharose Ni" (GE Healthcare). Magnetic beads allowed us to process proteins rapidly with no risk of cross-contamination and to control the elution volume. In single purification step we obtained AtKu or HsKu dimers (Figure 10). Purification via the single 6xHis-tag on Ku80 subunit allows us to monitor dimerization. Both AtKu and HsKu subunits were purified in equimolar concentrations and migrated in expected size (AtKu70 = 70,3 kDa, AtKu80 = 79,8 kDa, HsKu70 = 69,9 kDa, HsKu80= 86,0 kDa) demonstrating that both complexes efficiently dimerize when co-expressed in insect cells. Proteins were stable for at least one week at +4°C in elution buffer.

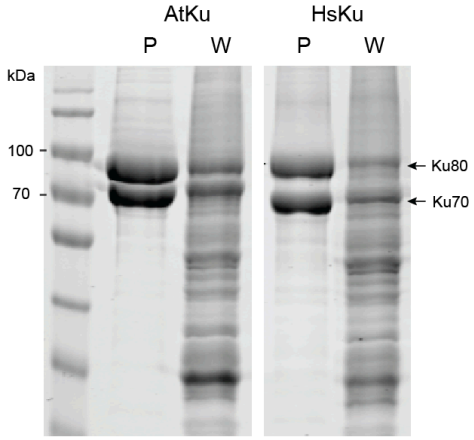

Figure 10: AtKu and HsKu purified from insect cells

Ku proteins AtKu and HsKu were expressed in Hi5 cells and purified using magnetic beads. Eluted protein (P) and the whole cell extract (W) were loaded on SDS PAGE gel in equal volume and stained using Coomassie staining. AtKu subunits migrate closer together due to the protein size differences: AtKu70 = 70,3 kDa, AtKu80 = 79,8 kDa, HsKu70 = 69,9 kDa, HsKu80 = 86,0 kDa.

3.1.1.3 AtKu has lower affinity to multi-site oligonucleotides

The thermodynamics of the HsKu-DNA interaction has been described previously using fluorescence anisotropy (Arosio et al. 2004). Fluorescently labeled DNA duplexes were excited by beam of polarized light. Free motion of fluorophores causes depolarization of emitted light. Upon protein binding the amount of polarized light in the emission increases and is recorded as increasing anisotropy. A series of different protein concentrations allows plotting an association curve and calculating Kd.

We used fluorescence anisotropy (FA) to compare DNA binding properties of HsKu and AtKu. The measurements were done in collaboration with Ctirad Hofr and Eliska Janouskova from CEITEC (Brno, Czech Republic). For binding assay we used short (25bp) and long (75bp) dsDNA oligonucleotides (Arosio et al. 2004). The ssDNA oligonucleotides (Sigma Aldrich) were annealed to obtain dsDNA. Only one 5' end was labeled using fluorescein. Upon mixing with Ku protein, each measurement was done in three technical replicas. The measurements were repeated 5 and 3 times for 25 bp and 75 bp oligonucleotide. The association curve and Kd were calculated and average values were plotted using SigmaPlot.

Association curve for the 25 bp dsDNA (one binding site) is similar for HsKu (Kd = 15 ± 1 nM) and AtKu (Kd = 23 ± 1 nM). AtKu has 1,5-fold increased Kd. However, the association curves visibly differ for the 75 bp dsDNA when Ku must translocate inwards to fill all three binding sites: HsKu (Kd = 39 ± 6 nM) and AtKu (Kd = 100 ± 10 nM). The Kd of AtKu has 2,5-fold increase (Figure 11).

Also, the shape of the association curve suggests more rapid binding of HsKu to 75 bp dsDNA. A possible explanation for this difference is a difference in sliding kinetics, as slower sliding of the AtKu complex onto DNA would make DNA association less efficient. Therefore, we decided to examine sliding of HsKu and AtKu using electrophoretic mobility shift assay (EMSA, gel shift assay) and electron microscopy.

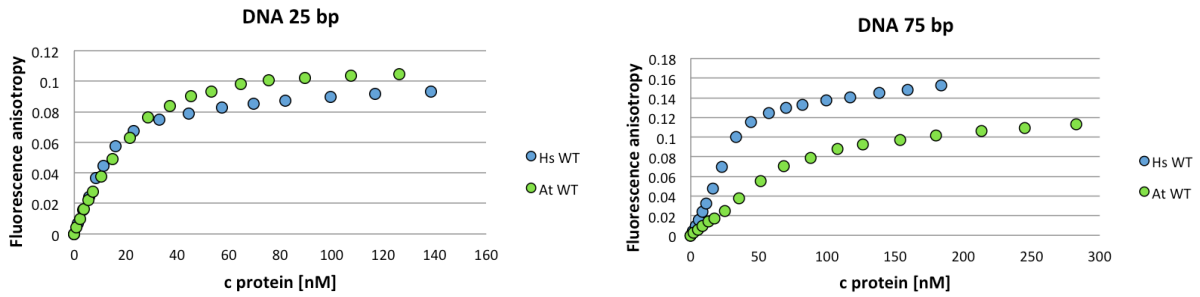

Figure 11: Fluorescence anisotropy of wild type HsKu and AtKu

HsKu and AtKu were expressed and purified from Hi5 insect cells and fluorescence anisotropy was measured using 5 nM 25 bp (left) and 75 bp (right) dsDNA oligonucleotides 5' end-labeled with fluorescein. The measurements were done with increasing protein concentrations. Measurements were repeated 5 and 3 times respectively, each point with 3 technical replicates. Average values were plotted and Kd values were calculated from the association curve using SigmaPlot. The average Kd values are 15 ± 1 nM (HsKu), 23 ± 1 nM (AtKu) for 25bp and 39 ± 6 nM (HsKu), 100 ± 10 nM (AtKu) for 75 bp oligonucleotide.

3.1.1.4 AtKu shows different kinetics of binding/sliding on DNA

EMSA is widely used method for analysis of Ku-DNA association (Arosio et al. 2002; Arosio et al. 2004; Balestrini et al. 2013; Lopez et al. 2011). Ku can bind DNA only from the free end (Walker et al. 2001). Therefore, inward translocation must occur to form complexes of 3 and more Ku per DNA. To analyze DNA interaction (binding, sliding) properties of the HsKu and AtKu we used 98 bp dsDNA PCR product that can accommodate up to 4 Ku molecules. DNA was end-labeled using ^{32}P-γATP that allowed us to detect free DNA and 4 shifted bands corresponding to 1-4 Ku/DNA (Figure 12).

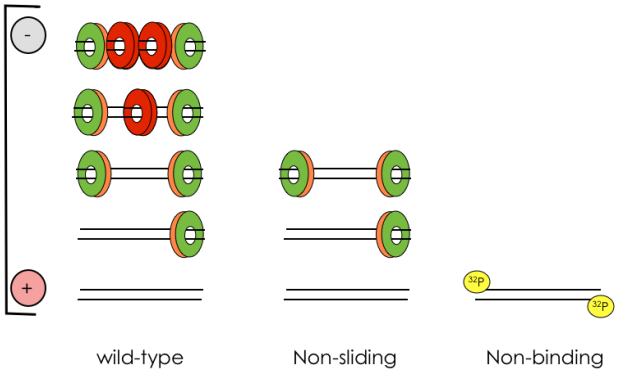

Figure 12: Scheme of the EMSA strategy

To observe the sliding ability of Ku we mixed the protein with 98 bp dsDNA with 4 Ku binding sites. After separation in electric field under native conditions we detected ^{32}P-DNA. Shifts can be observed upon binding the protein. Because Ku needs a free end to bind DNA, the two shifts corresponding to 3Ku/DNA and 4Ku/DNA can only occur when Ku is able to slide inwards.

With increasing protein concentration we observed change in the abundance of different Ku/DNA complexes. The products of sliding were visible already with 2 nM of HsKu. However, 5 nM of AtKu was necessary to reach 3 Ku/DNA. These data corroborate finding by FA suggesting slower sliding of AtKu onto DNA. Surprisingly, 40 nM of AtKu seems to be sufficient for all DNA to be bound by 4 Ku proteins, but 50 nM of HsKu was needed for the same effect. Although the accuracy of this observation might be influenced by the diffused character of AtKu bands. These differences are subtle but reproducible and suggest that AtKu slide with a different kinetics on the long DNA. Furthermore, the HsKu proteins form very sharp bands. In case of AtKu, the bands are smeared. Altering the running properties and the gel concentration did not to resolve this issue. The smeared banding might reflect more dynamic association of the protein (Figure 13).

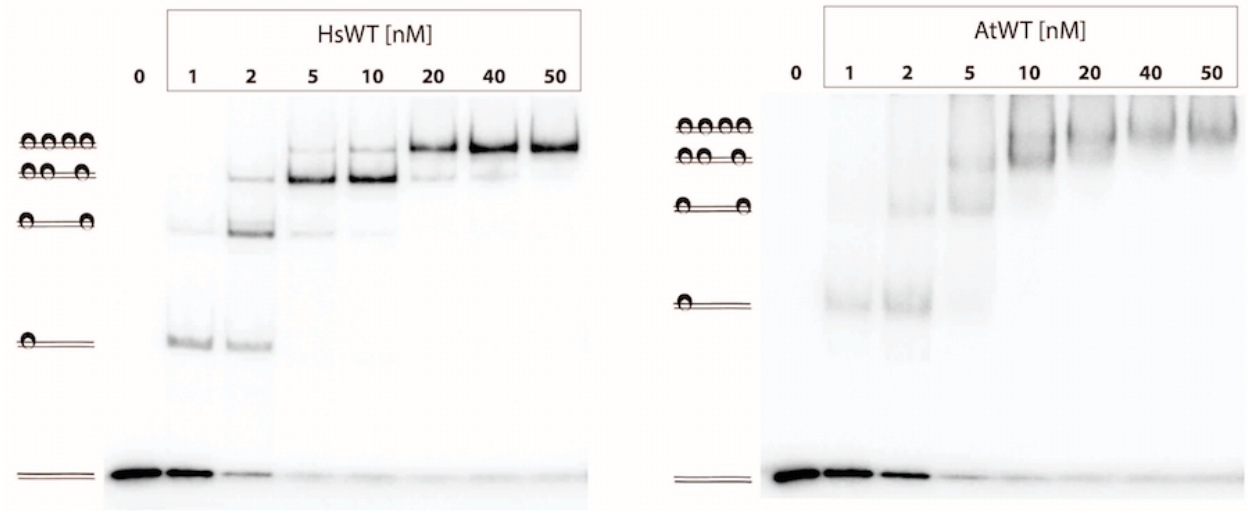

Figure 13: Binding and sliding properties of HsKu and AtKu.
To analyze binding/sliding we performed EMSA using Hi5 purified wild type protein complexes HsKu (HsWT, left) and AtKu (AtWT, right). Blunt radioactively labeled 98 bp dsDNA (0,3 nM) was used to observe how Ku proteins bind DNA depending on the protein concentration. With increasing protein concentration we observed how free DNA (bottom) is bound by Ku proteins and formed shifted bands corresponding to 1 Ku/DNA, 2 Ku/DNA, 3 Ku/DNA and 4 Ku/DNA (bottom to top).

HsKu has been reported to be able to transfer from one DNA molecule to another when the two DNA molecules shared complementary ends. For two Ku proteins present on the DNA, the transfer happened on “first in, first out” basis, suggesting inequality of proteins in multimeric Ku/DNA complexes. Internally bound Ku might behave differently

from DNA-end bound Ku (Bliss and Lane 1997). It has been previously shown that HsKu binds to 45 bp dsDNA (2 binding sites) in cooperative manner, but not to 60 bp or 90 bp (Ma and Lieber 2001). However, another studies showed no cooperative binding for 42 bp, 50 bp or 75 bp (Arosio et al. 2002; Arosio et al. 2004). To investigate possible differences between HsKu and AtKu in multimeric complexes we chose electron microscopy for direct observation of the molecules.

3.1.1.5 AtKu associates rapidly with long DNA and might exhibit cooperative binding

Ku protein thanks to its ring shape loads onto DNA via its free end. Once bound, it can diffuse in ATP independent manner along DNA. The sliding is a limiting factor for formation of multimeric complexes and it is time and temperature dependent (de Vries et al. 1989). The fluorescence anisotropy and EMSA methods show the behavior of population of molecules. Previously, atomic force microscopy and electron microscopy have been used to examine binding/sliding of single Ku proteins (Balestrini et al. 2013; Cary et al. 1997; de Vries et al. 1989).

To examine possible differences in sliding between HsKu and AtKu we used electron microscopy (CSF, Vienna). HsKu or AtKu (3620 nM) were mixed with 1100 bp dsDNA (1,53 nM) that is able to accommodate 40 complexes and were allowed to bind for 10 minutes at room temperature. The objective was to observe the early DNA end-binding and sliding of Ku. Samples were aerosolized and vacuum dried droplets were covered with Pt and C by rotary shadowing. Transmission electron microscope as used and images were acquired by Eagle 4k HS CCD camera.

Due to drying of droplets the molecules were not homogenously distributed. In the center of the droplet was electron dense deposition of glycerol and higher density of free proteins surrounded this area. On the outer edge of the droplet we observed entangled free DNA molecules. In the submarginal area were DNA-protein complexes with relatively low background of free proteins. Only DNA-protein complexes from the submarginal area were analyzed.

Due to short incubation period we expected enrichment of Ku proteins near the DNA ends and only a few proteins located in the center of DNA molecules. Surprisingly,

the distribution of the proteins along the DNA seemed random suggesting rapid sliding. The number of HsKu bound to DNA was lower (4,9 ± 2 per DNA) in compare to AtKu. DNA was almost completely covered by AtKu proteins (Figure 14). However, we could observe a fraction of free DNA in both samples. Unfortunately, it was not possible to estimate the amount of free DNA due to its entanglement on the edges of droplets. The decrease of AtKu protein amount to half did not reduce the amount of proteins on the DNA. This observation might suggest that the sliding of AtKu is more rapid in compare with HsKu, but it could also be a result of cooperative binding. The presence of free DNA in sample supports the possibility of cooperative binding of AtKu.

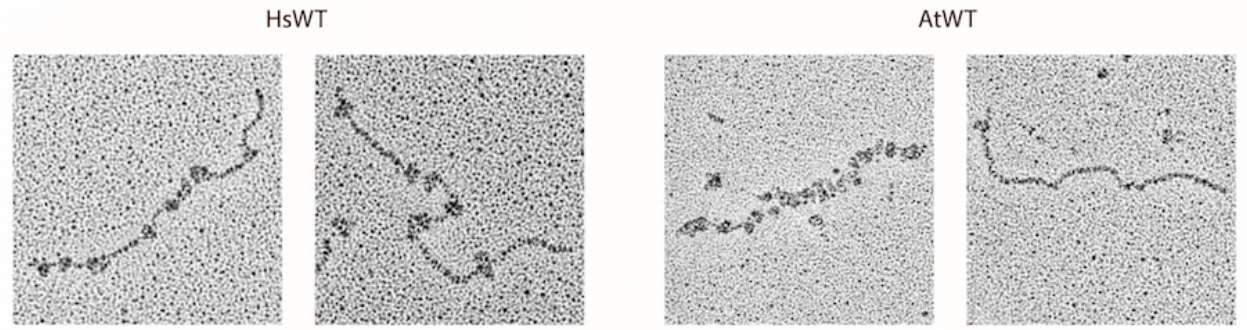

Figure 14: Electron microscopy of HsKu and AtKu
Purified HsKu (HsWT, left) and AtKu (AtWT, right) protein complexes (3,62 μM) were mixed with of 1100 bp dsDNA (1,53 nM), aerosolized and vacuum dried on mica chips, where using rotary shadowing covered by Pt and C layers. Layers were visualized by transmission electron microscope. Pictures of Ku/DNA complexes were taken from submarginal area of sample droplets.

The affinity of AtKu and HsKu to short dsDNA oligonucleotides is very similar. However, the association curve for longer oligonucleotide that requires sliding of molecules differs. The observations may imply that the sliding of AtKu on DNA is decreased and limit binding of free molecules. Surprisingly, the electron microscopy showed that sliding of AtKu might be more rapid than HsKu and could exhibit cooperative binding. The ability to recruit more molecules to DNA end *in vivo* might provide a possible explanation for presence of blunt ended telomeres in *A. thaliana*. Protein clustering could inhibit the exonucleolytic degradation of DNA ends.

It has been shown that direct binding of Ku to telomeres is important for telomere protection in yeast (Lopez et al. 2011) and increased sliding reduces the ability of Ku to protect DNA from nucleolysis (Balestrini et al. 2013). Reduced sliding could phenocopy clustering and protect from nucleases. Therefore, we decided to modify HsKu and

create complexes with reduced ability to slide and bind. Such complexes would provide a useful tool for analysis of importance of binding/sliding in telomere protection. It has not been shown whether direct binding of Ku to telomeres is also important in human cells. Based on the available crystal structure we identified residues that interact with DNA, mutated these residues and produced recombinant mutant proteins. Using EMSA, fluorescence anisotropy and electron microscopy we selected mutant complexes with altered binding/sliding. Because Ku protein is essential in human cells and complementation is not easily done, we also created, analyzed and complemented AtKu.

3.1.2 Conserved residues in DNA channel of Ku are important for DNA interaction

3.1.2.1 DNA binding channel contains positively charged residues

Electrostatic interactions play a major role in binding of Ku to DNA (Arosio et al. 2004). Several residues of Ku70 and Ku80 are localized in DNA channel and have been shown to interact with DNA backbone (Walker et al. 2001). The charged residues in this region were therefore considered a good target when designing Ku deficient in DNA binding/sliding. Previously, substitutions of residues in DNA channel led to DNA binding defects of ScKu from *S. cerevisiae* (Lopez et al. 2011).

We analyzed the DNA-protein interface of the HsKu crystal structure. We found high density of positively charged residues in the DNA binding channel (Figure 15). Some of these residues interact directly with DNA. Although, there are no obstructions to DNA at either end, overall it was suggested that they might constrain the movement to a helical path (Walker et. al, 2001). Our aim was to modify the charge of some residues or constrict the channel diameter in order to reduce binding or sliding of the complex. To reduce, but not completely abolish, sliding of Ku we decided to find conserved residues present on lagging face of the complex that is less critical for initial Ku/DNA interaction.

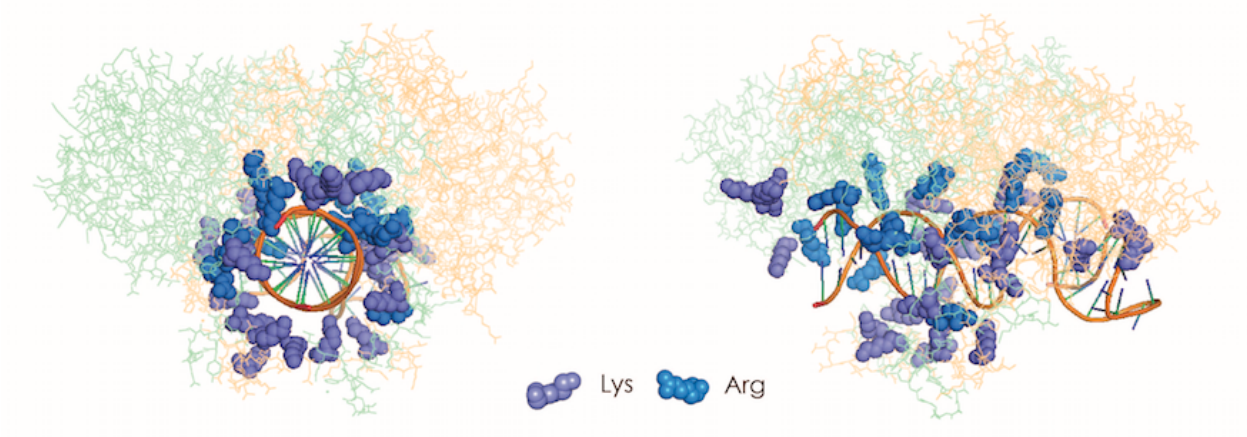

Figure 15: Positively charged residues in HsKu DNA binding channel
DNA channel of HsKu (HsKu70 in green, HsKu80 in orange) contains positively charged residues. Some of the Lys and Arg residues (blue) were highlighted in 1JEY crystal structure of Ku/DNA (PDB) using PyMol 1.3.

3.1.3 Lagging face of HsKu harbors conserved residues

Ku proteins are conserved in evolution (Bowater and Doherty 2006; d'Adda di Fagagna et al. 2003). Residues that are essential for DNA binding should therefore be shared among different organisms. We performed multiple protein alignment (CLC Main Workbench 6) and identified residues that are evolutionarily conserved. We focused also on their position in crystal structure and selected the residues from lagging face of the complex (Figure 16 and 17). Loading face of the HsKu is most likely responsible for the initial DNA association (Walker et al. 2001).

We found 6 residues on HsKu70 (HsKu70-R35, R80, K160, R254 and R258) that are positively charged, evolutionary conserved and localized in the DNA binding channel on the lagging face. The residue HsKu70-R444 was previously published to be essential for binding in budding yeast (ScKu70-R456) and we included it in our study (Lopez et al. 2011). We also found an interesting cluster of two negatively charged residues on HsKu80 (HsKu80-D299, D300) that might cause DNA repulsion. Another cluster of three lysine residues on HsKu80 (HsKu80-K543-K545) does not show direct DNA interaction in the crystal, but that might be due to the short length of DNA in the solved structure. Projection of longer DNA onto structure indicates that DNA might be in contact with these residues (Figure 16 and 17).

To alter binding/sliding of the complexes we substituted arginine and lysine residues with glutamine acid and aspartic acid with arginine. Deletion within a DNA-

binding loop of ScKu80 showed also reduction in association of ScKu to DNA in budding yeast (Pfingsten et al. 2012). Reduction of diameter of the DNA channel might lead to molecular friction and decrease the sliding efficiency. However, ScKu80 contains additional amino acid resides in the DNA-binding loop (Figure 17). We therefore decided to remove only 2 (HsKu70-K301, T302) and 4 (HsKu70-K299-T302) residues from the beta bridge of HsKu (Figure 16 and 17).

We assigned identification numbers to these residues or loci for simplification (mutation ID # in Table 1). Using *in vitro* mutagenesis we introduced mutations into expression vectors (Figure 9). To enhance effect of substitutions we also combined several mutations into one complex (Table 1).

In addition, we also wanted to analyze the effect of selected residues on AtKu complex. Therefore we introduced selected substitutions of evolutionary conserved residues in the AtKu complex as well (Figure 17, Table 1). However, some of the conserved residues, mainly the lysine cluster on Ku80 (HsKu80-K543-K545; AtKu80-K518E-K520) is present in different position within the crystal (Figure 17). These residues are not very well conserved in ScKu. Also, the residue ScKu70-R265 did not align with the HsKu70-R254 in our protein alignment (Figure 10). However, it is present in similar position in predicted structure and was published as homologous to HsKu70-R254 (Figure 11, Table 1) (Lopez et al. 2011). Some residues adjacent to the conserved residues lie on DNA interaction surface and could be potentially used for mutation analysis (ScKu70-R24, R25, R73, K161, K261, Figure 11 and Table 1).

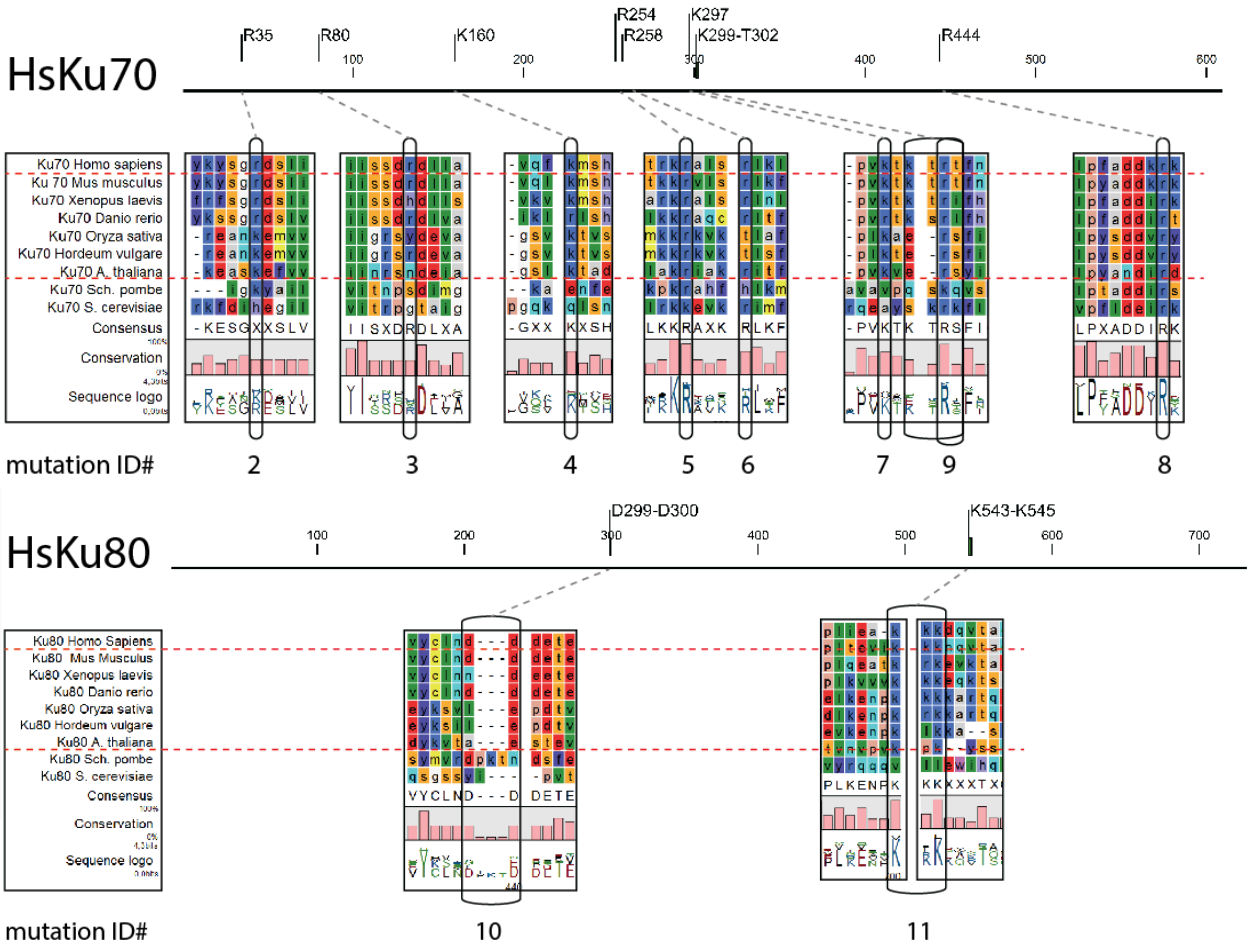

Figure 16: Selected regions of multiple protein alignment of Ku70 and Ku80 subunits.

A multiple protein alignment of Ku70 (upper panel) and Ku80 (lower panel) subunits from 9 species was created using CLC Main Workbench 6 software. Ten conserved regions were localized in the DNA binding channel (based on the crystal structure of HsKu). The residues were highlighted and position of corresponding residues is indicated on scheme of human Ku protein subunits. Identification numbers (mutation ID #) were assigned to selected regions/residues and can be seen in Table 1. ID #2-8 and #11 are positively charged residues that were substituted with glutamine acid, ID #10 is a negatively charged region substituted with arginine and ID #9 with adjacent region forms bottom of the DNA binding channel bridge and was deleted.

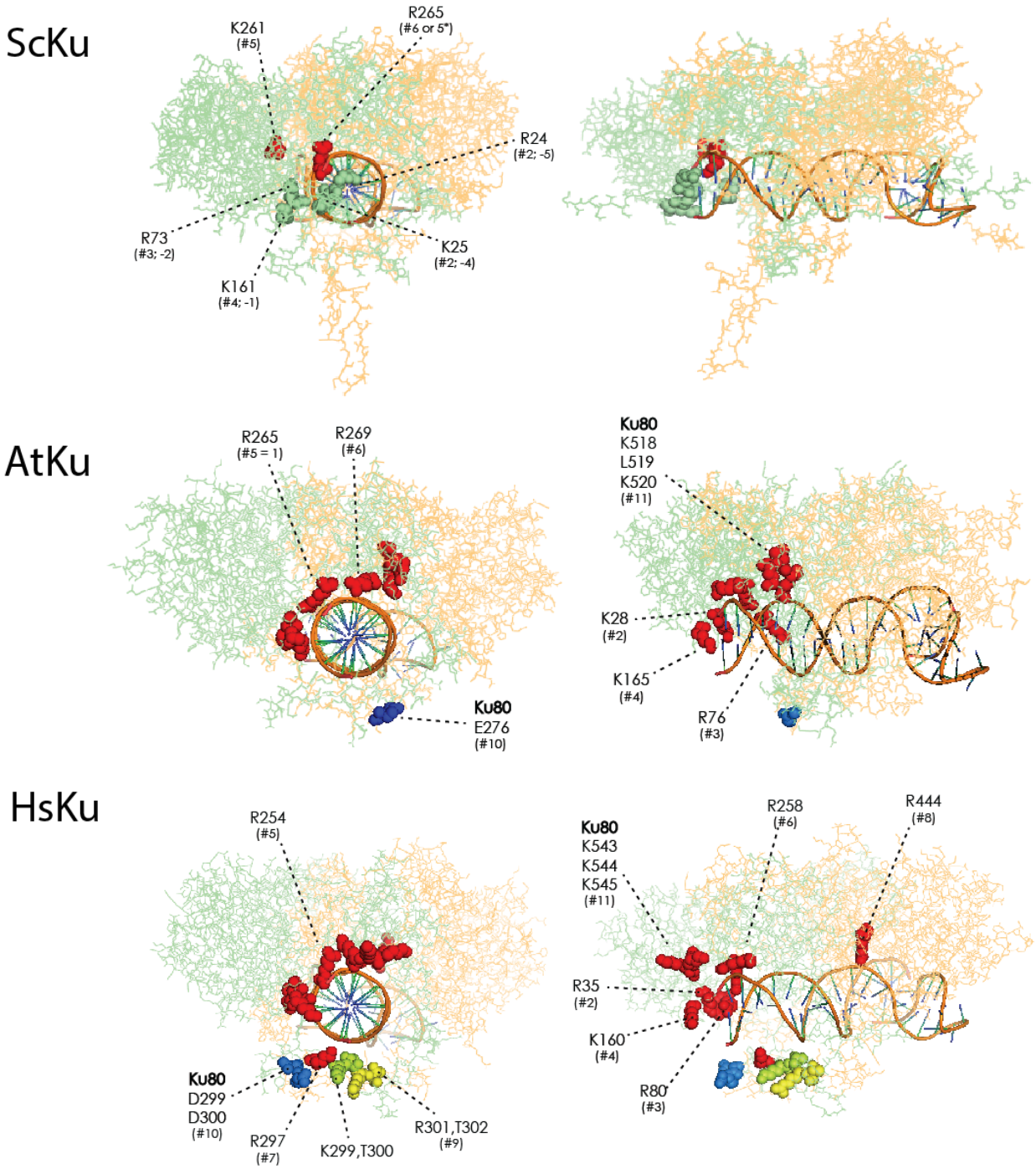

Figure 17: Position of selected residues in the HsKu crystal structure and predicted models of AtKu and ScKu

Selected conserved residues with their mutation identification numbers (#) are shown in the structure of HsKu (bottom, green = Ku70, orange = Ku80). Models of AtKu and ScKu (green = Ku70, orange = Ku80) were created using the Modeller and Pymol software and the relevant homologous residues were indicated. In ScKu we indicated residues that were adjacent to conserved residues of HsKu and interacted with DNA. The distance in amino acid sequence from the conserved position is indicated in the bracket after the mutation identification number. The "-" represents upstream position and "number" the

number of residue from the conserved region (position zero). The important residues are shown as spheres and colored according to type of substitution they were designed for: positively charged residues to negative (red), negative residues to positive (blue), minor deletions (yellow and lime green). The green residues in ScKu represent residues adjacent to conserved amino acids.

Table 1.: List of residue substitutions and their identification numbers

Conserved residues were chosen based on human crystal structure and substitutions were designed. Identification numbers were assigned to allow better orientation in loci across species. Only relevant residues of AtKu and ScKu are listed. (*) = not analyzed complexes; (**) = published mutations (Lopez et al., 2011); (***) = unsuccessful expression and purification; (§) position of residue according to alignment in this work, (§§) residue adjacent to conserved residues.

Mutation ID #	ID # combination	Subunit	HsKu	AtKu	ScKu
1		Ku70	R265E (#5)***	R265E	
2		Ku70	R35E	K28E*	R24E*§§ (K25E*§§)
3		Ku70	R80E	R76E*	R73E*§§
4		Ku70	K160E	K165E*	K161E*§§
5		Ku70	R254E***	R265E (#1)	R265E** (K261E*§)
6		Ku70	R258E	R269E*	R265E*§
7		Ku70	K297E		
8		Ku70	R444E		R456E**
9		Ku70	ΔK301,T302		
10		Ku80	D299R, D300R	E276R	
11		Ku80	K543E, K544E, K545E	K518E, L519E, K520E	
12	9+10	Ku70 Ku80	ΔK301-T302 D299R, D300R		
13	10+11	Ku80	D299R, D300R K543E, K544E, K545E	E276R K518E, L519E, K520E	
14	2+3+4	Ku70	R35E, R80E, K160E		
15	2+3+4+11	Ku70 Ku80	R35E, R80E, K160E K543E, K544E, K545E		
16	9+	Ku70	ΔK299,T300, R301,T302		
17		Ku70	R254A		
18	2+3+4+5+6	Ku70	R35E, R80E, K160E, R254E, R258E	K28E, R76E, K165E, R265E, R269E	
19	13+18	Ku70 Ku80	R35E, R80E, K160E, R254E, R258E D299R, D300R, K543E, K544E, K545E		

3.1.4 Mutant HsKu and AtKu complexes have altered DNA binding/sliding *in vitro*

3.1.4.1 Conserved residues on lagging face of Ku are important for DNA binding/sliding

EMSA has been used previously to describe DNA binding of mutant ScKu complexes (Balestrini et al. 2013; Lopez et al. 2011; Pfingsten et al. 2012). We used the same experimental setup as described for wild type complexes (Figure 12). The pFastBac dual expression vectors carrying WT HsKu and AtKu for insect cell expression were modified using *in vitro* mutagenesis protocol to introduce mutations. Purification was carried out via 6xHis-tag on the N' terminus of Ku80 using "His mag Sepharose Ni" (GE Healthcare). Purified proteins were loaded with equal volume to SDS PAGE gel and stained with Coomassie (Figure 18). Both subunits of wild type AtKu or HsKu complexes (At WT, Hs WT) were coexpressed in Hi5 cells and subunits were purified in equimolar concentrations. However, the first set of mutant HsKu complexes (mutation ID #1- #11) seemed to have higher amount of HsKu70 subunit. Because the purification tag was on the Ku80 subunit, decreased amount of Ku80 was likely due to degradation of the protein after complex purification. AtKu mutant #1 contained additional band migrating below AtKu70, which may result from partial protein cleavage of ~10 kDa from C' terminus of Ku80. This was confirmed by western blotting. The degradation but did not present a major problem for preliminary screening. Further optimization revealed that degradation was due to a low titer of virus used for infection of Hi5 cells and this problem disappeared when a higher titer of virus was used for expression.

In the first round of mutagenesis none of the residue substitutions or deletion (mutation ID# 1-11) disrupted dimerization as I could purify entire complex via tagged Ku80. The partial cleavage of Ku80 subunits resulted in formation of a light Ku complex that showed altered migration in EMSA. For different complexes we could observe a different ratio of heavy (full length Ku80) and light (cleaved Ku80) Ku. Both forms did bind and slide on the DNA (Figure 18). Complexes with light Ku80 migrated faster than heavy Ku80 and the combination of light and heavy complexes resulted in ladder of shifted bands. Nevertheless, the obtained data was sufficient to conclude that there was

no apparent disruption of DNA binding/sliding in Ku complexes with single amino acid substitutions.

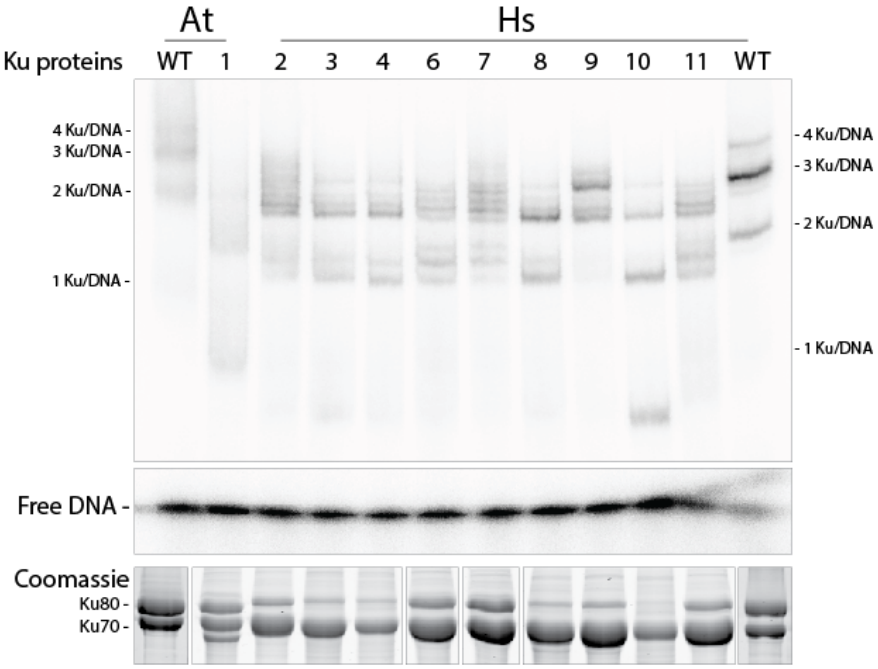

Figure 18: EMSA analysis of the first round of mutagenesis of HsKu and AtKu.
Purified wild type proteins (first and last lane) and mutant AtKu and HsKu were analyzed as previously by EMSA (upper panel). Unfortunately, mutant complexes contained light Ku80 subunit that arose as a consequence of protein degradation due to low virus titer. Degradation is seen on SDS PAGE gel stained with Coomassie (lower panel). Presence of heavy (full length) and light (cleaved) Ku80 resulted in increased speed of migration and presence of ladder of bands. Nevertheless, all mutant proteins were able to bind and slide on DNA.

Therefore, in the second round of mutagenesis, we modified several residues within a single Ku complex (mutation ID #12-19, Table 1). The deletion of 2 amino acids (ID #9) did not influence DNA binding. We further deleted two more residues (#16). Unfortunately, this did not lead to DNA binding/sliding defect. We were not able to purify HsKu70-R254E (#5). The milder substitution of this residue (Ku70-R254A (#17)) did not influence DNA binding/sliding.

Only HsKu complexes with mutation ID #10, #13, #15, #18 and #19 did exhibit a quantitative decrease in DNA interaction. All complexes were expressed and purified in parallel with AtKu homologues of #13, #18 and #19 and wild type HsKu and AtKu (HsWT, AtWT). The HsKu #15 was expressed separately in parallel with HsWT

(HsWT2). All purified proteins were analyzed with EMSA and were used for subsequent fluorescence anisotropy and electron microscopy experiments.

1) Hs#10

Substitution of two negatively charged residues in HsKu80-D299R, D300R (ID HsKu #10) exhibits similar DNA retardation as HsWT. However, with 5 nM protein concentration the 1 Ku/DNA complex was still detectable unlike in HsWT where majority of signal was in 2 and 3 Ku/DNA complexes (Figure 19). This suggests potential problem with binding/sliding. Higher protein concentrations were comparable to HsWT.

2) Hs#13, At#13

HsKu #13 was created as combination of HsKu #10 and HsKu #11 (HsKu80-D299R, D300R, K543E, K544E, K545E, Table 1). With 5 nM protein concentration the amount of 1 Ku/DNA complex was higher that HsWT, but lower than HsKu #10. However, with 50 nM of HsKu13 we could observe a significant portion of the signal in 3 Ku/DNA, while most of the HsWT signal was in 4 Ku/DNA complexes. This effect was reproducible and could suggest problem with sliding (Figure 20).

When we mutated homologous residues in the AtKu (Table 1), we could not observe any difference from the AtWT complex (Figure 21).

3) Hs#18, At#18

HsKu #18 combines 5 substitutions of positively charged residues in HsKu70 (HsKu70-R35E, R80E, K160E, R254E, R258E, ID # 2-6, Table 1). The mutations in this complex resulted in reduced binding/sliding that was even more pronounced than in HsKu #13. Two-fold increase in protein concentration (2 nM) was necessary to get equal amount of 1 Ku/DNA and 2 Ku/DNA as in HsWT (1 nM). Decrease in DNA binding might be responsible for this observation. However, we could not observe 4 Ku/DNA with Hs #18. DNA was only bound by 3 Ku in 20-50 nM concentrations what suggests defect in sliding (Figure 22).

AtKu #18 (Table 1) also exhibited decrease in DNA binding, but we detected complexes of 4 Ku/DNA with the 40 nM concentration (Figure 23).

4) Hs#19, At#19

To analyze whether combination of mutations #13 and #18 will have synergistic effect, we combined both subunits to create mutant complex Hs #19 (Table 1). Five-fold increase (5 nM) was necessary to reach same amount of 1 Ku/DNA as with HsWT. The

DNA binding is worse in compare to the #18. Complexes of 4 Ku/DNA were not observed. Therefore, sliding might be also impaired (Figure 24).

AtKu #19 (Table 1) showed slight improvement in binding/sliding in compare with AtKu #18. This observation is surprising, because AtKu #13 did not exhibit any difference from AtWT (Figure 25).

5) Hs#15

Furthermore, we wanted to understand how the residues contribute to the effect of decreased binding/sliding on the DNA. We did not detect binding/sliding defect of HsKu #11 and HsKu #14. When combined with additional residues, the binding/sliding of Ku decreased (HsKu #13, HsKu #18). We therefore combined the HsKu #11 and HsKu #14 into single complex Hs #15. Interestingly, we observed similar effect on DNA association as with the HsKu #18 (Figure 26). In both complexes we changed the local positively charged region into negatively charged. This observation suggests, that the effect we observed previously is not residue specific, but rather an effect of the overall change of charge in the channel that might reduce the affinity of Ku to DNA and its ability to translocate.

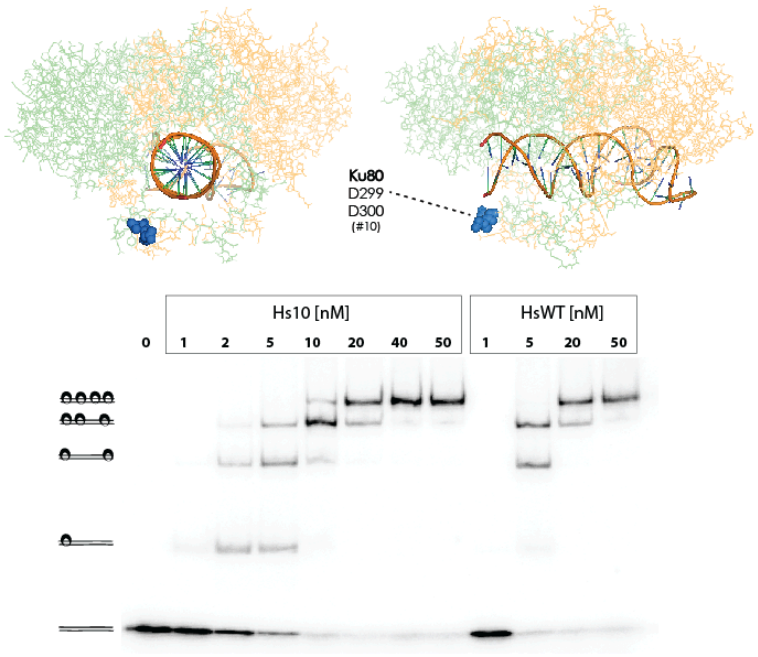

Figure 19: Mutation #10 position and EMSA

Position of HsKu80-D299R, D300R (#10) mutation in HsKu structure (above) and EMSA using HsKuWT (right) and HsKu#10 (left) complex with increasing protein concentration. The 98 bp DNA concentration was constant 0,3 nM.

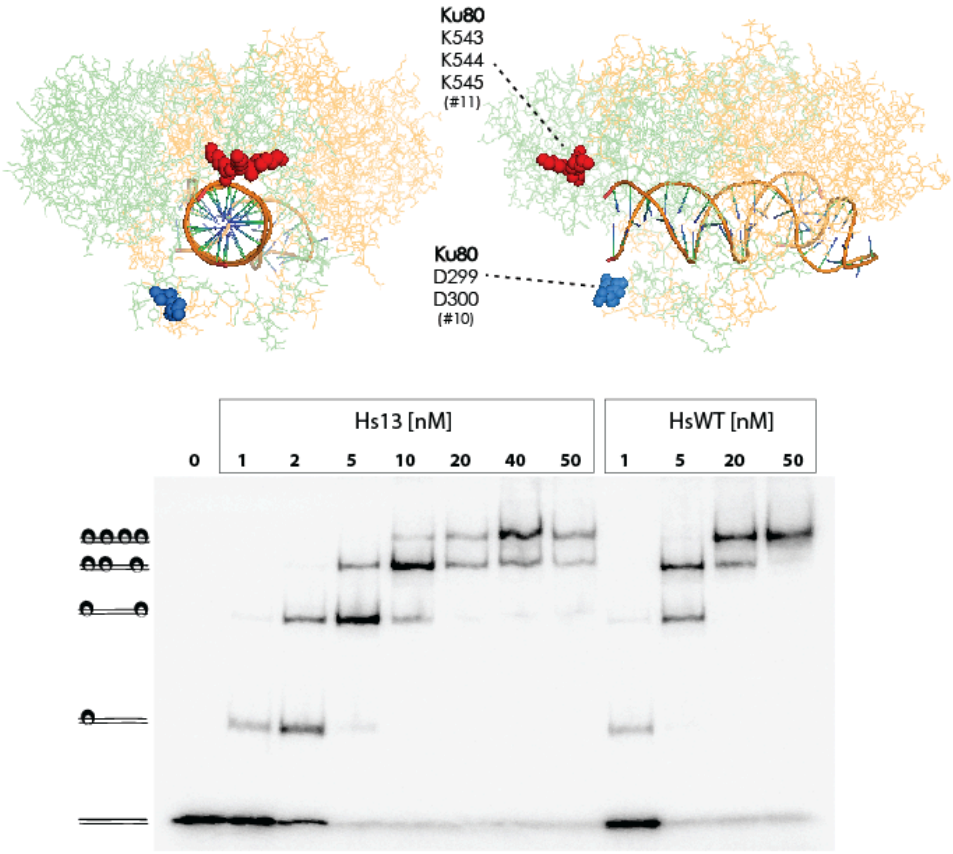

Figure 20: Mutation Hs#13 position and EMSA

Position of Ku80-D299, D300, K543, K544, K545 (#13) mutation in HsKu structure (above) and EMSA using HsKuWT (right) and HsKu#13 (left) complex with increasing protein concentration. The 98 bp DNA concentration was constant 0,3 nM.

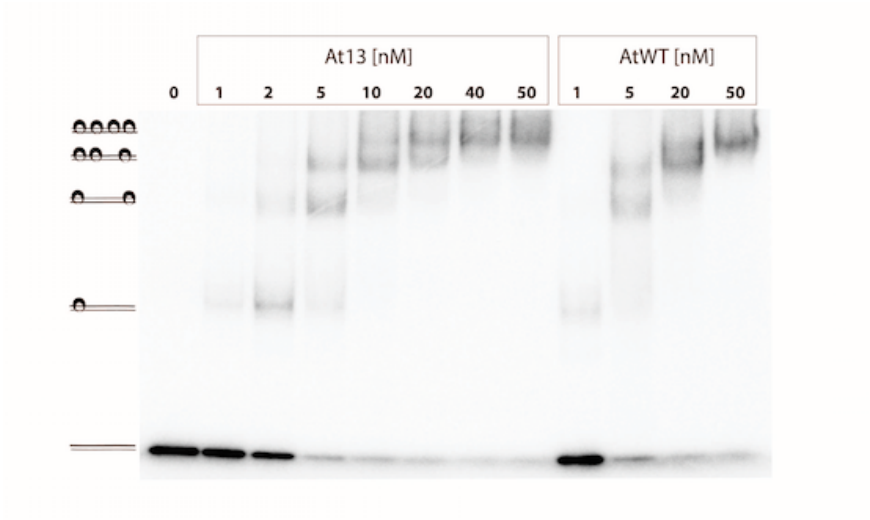

Figure 21: Mutation At#13 EMSA

EMSA using AtKuWT (right) and AtKu#13 (left) complex with increasing protein concentration. The 98 bp DNA concentration was constant 0,3 nM.

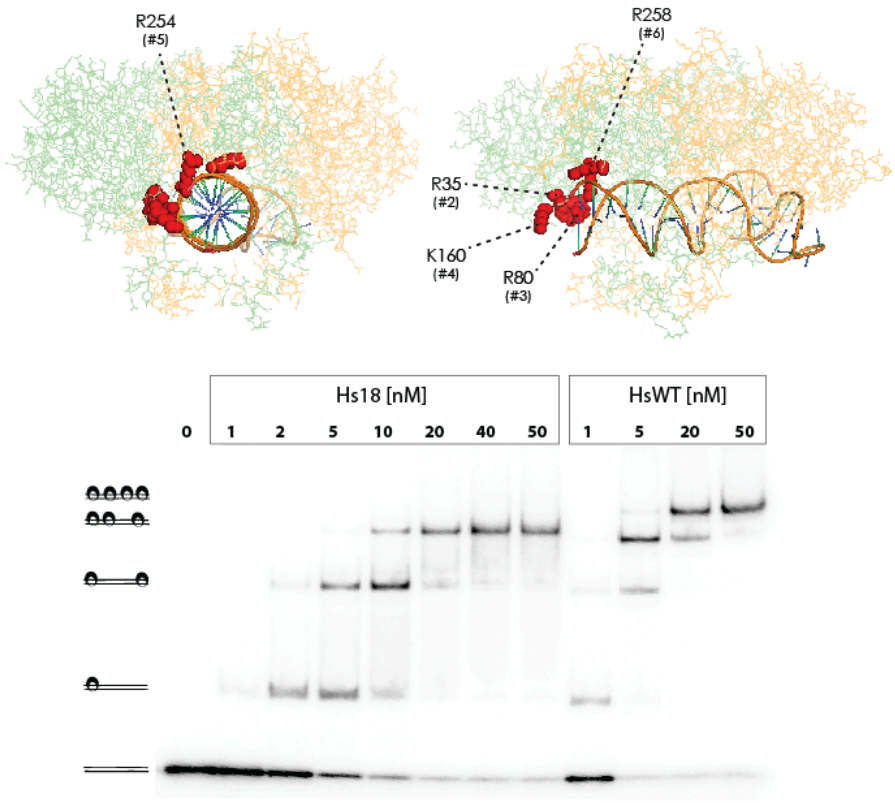

Figure 22: Mutation Hs#18 position and EMSA

Position of Ku70-R35, R80, K160, R254, R258 (#18) mutation in HsKu structure (above) and EMSA using HsKuWT (right) and HsKu#18 (left) complex with increasing protein concentration. The 98 bp DNA concentration was constant 0,3 nM.

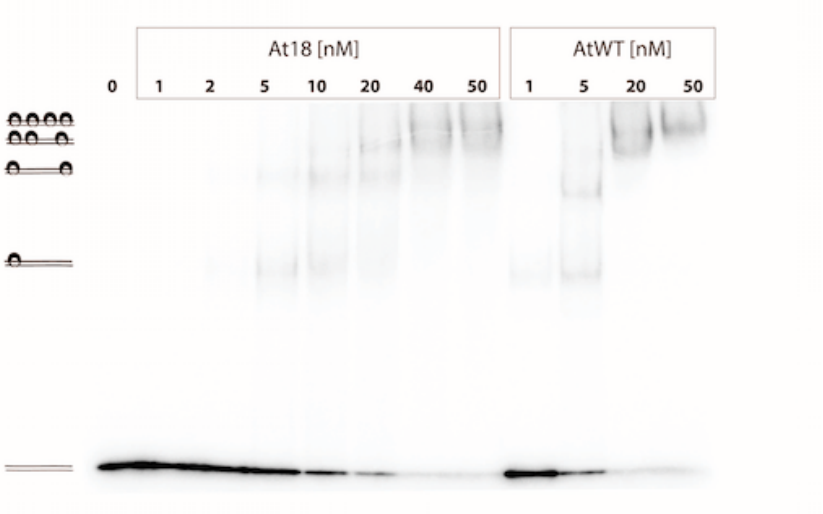

Figure 23: Mutation At#18 EMSA

EMSA using AtKuWT (right) and AtKu#18 (left) complex with increasing protein concentration. The 98 bp DNA concentration was constant 0,3 nM.

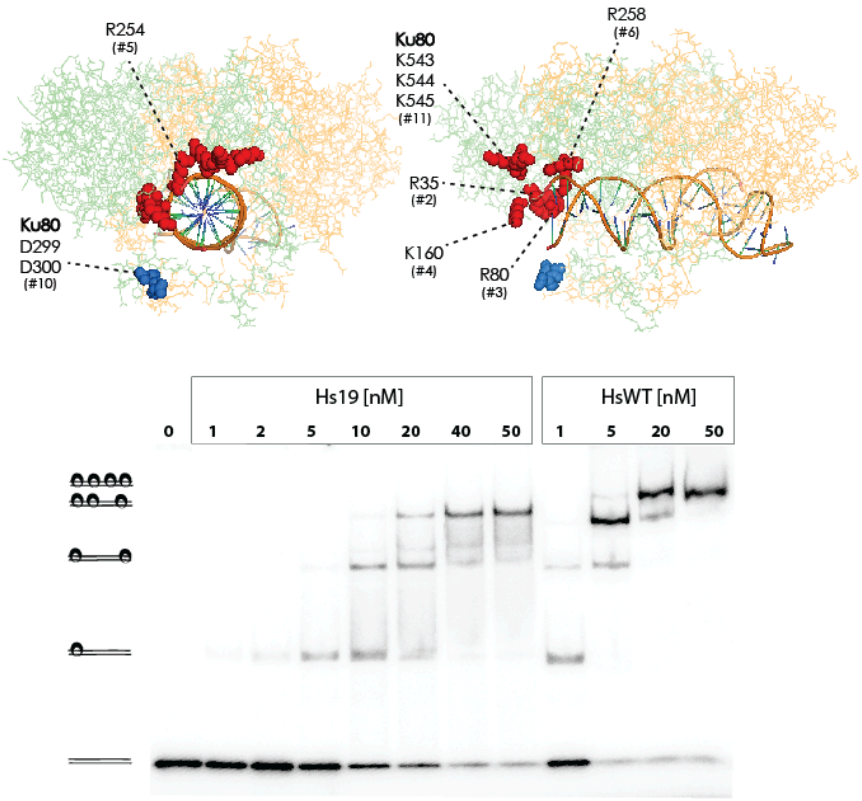

Figure 24: Mutation Hs#19 position and EMSA

Position of Ku70-R35, R80, K160, R254, R258, Ku80-D299R, D300R, K543E, K544E, K545E (#19) mutation in HsKu structure (above) and EMSA using HsKuWT (right) and HsKu#19 (left) complex with increasing protein concentration. The 98 bp DNA concentration was constant 0,3 nM.

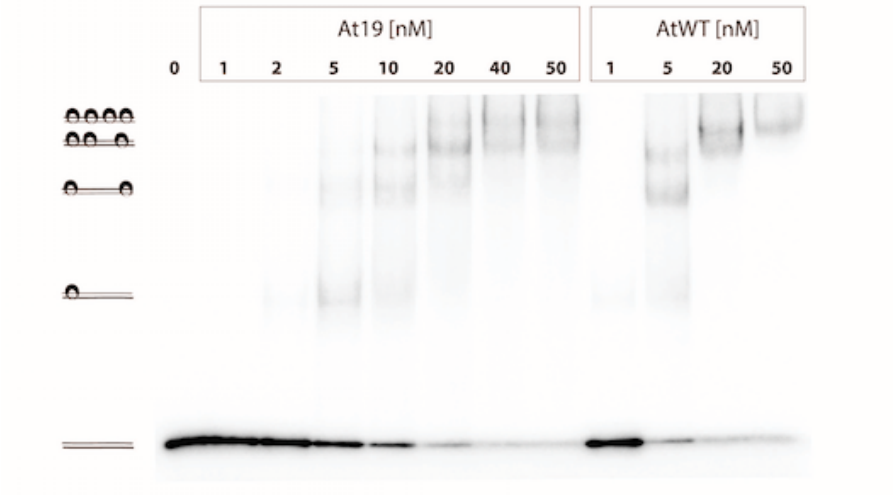

Figure 25: Mutation At#19 EMSA

EMSA using AtKuWT (right) and AtKu#19 (left) complex with increasing protein concentration. The 98 bp DNA concentration was constant 0,3 nM.

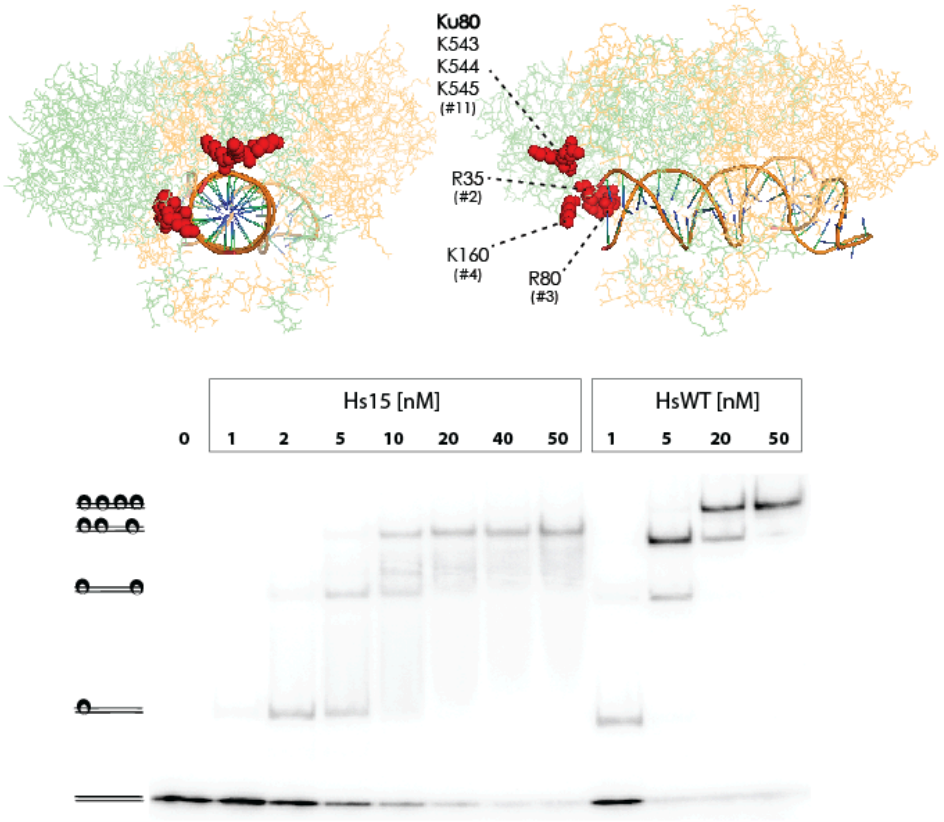

Figure 26: Mutation Hs#15 EMSA

Position of Ku70-R35, R80, K160, Ku80- K543E, K544E, K545E (#15) mutation in HsKu structure (above) and EMSA using HsKuWT (right) and HsKu#15 (left) complex with increasing protein concentration. The 98 bp DNA concentration was constant 0,3 nM.

In conclusion, EMSA analysis of mutant Ku complexes revealed that modification of a charge of the conserved residues at the lagging face of the Ku complex led to decrease in DNA interaction. These mutations did not disrupt dimerization or fully abolished binding. Previously published mutation in budding yeast ScKu70-R456E is homologous to HsKu-R444E (ID #9). It was reported to be DNA binding deficient (Lopez et al. 2011). We did not observe the same effect in HsKu #8. The minor deletions of 2 and 4 residues (#9 and #17) from the DNA binding loop also did not cause defect in DNA binding.

EMSA provided evidence that selected mutant Ku complexes exhibited reduction of binding or sliding. To quantify and verify this observation we decided to use fluorescence anisotropy (Arosio et al. 2004) in collaboration with Ctirad Hofr and Eliska Janouskova (CEITEC, Brno, Czech republic).

3.1.4.2 Selected mutant Ku complexes have decreased Kd

Fluorescence anisotropy was previously used to quantify DNA binding of HsKu (Arosio et al. 2004). As described for the wild type HsKu and AtKu before, we used short (25 bp) and long (75 bp) dsDNA oligonucleotides tagged with fluorescein. Mutant complexes were measured in concentration range 5 times for 25 bp and 3 times for 75 bp dsDNA. Each concentration was measured in three replicates. The average values were plotted using SigmaPlot ad Kd was calculated using one site saturation formula. Some of the complexes did not reach saturation and therefore the Kd values are only approximate (Table 2). The shape of the curve was analyzed

HsKu #10 and HsKu #13 had slightly increased Kd for both oligonucleotides. The difference in Kd for 75 bp oligonucleotide is not significant between HsKu #10 and #13 (P value = 0,2617) (Figure 28, Table 2). The AtKu #13 had slightly increased Kd in compare with AtWT for 25 bp (P value = 0,0016). There was no significant difference for 75 bp (Figure 27).

HsKu #18 and HsKu #19 did not reach saturation. The DNA binding is dramatically reduced. HsKu #19 association with 25bp DNA is lower, but not significantly different from HsKu #18 for 75bp (P $value_{25bp}$ = 0,224; P $value_{75bp}$ = 0,1235). AtKu #18 and AtKu #19 also did not reach saturation. Although the curves seem to indicate, that AtKu #19 binds better than AtKu #18, the difference in Kd values was not significant for both oligonucleotides.

HsKu #15 showed similar fold decrease in DNA affinity as mutants #18 and #19. The Kd of HsWT2 was lower in compare with the HsWT from previous purification (Figure 28).

The data from fluorescence anisotropy correlate with the results of EMSA. It is hard to conclude from either method whether the differences are due to impairment in sliding. Because of the ring-shape nature of Ku, it might be hard to distinguish these two processes on the level of population of molecules. We therefore decided to use the electron microscopy to visualize the single DNA/Ku complexes.

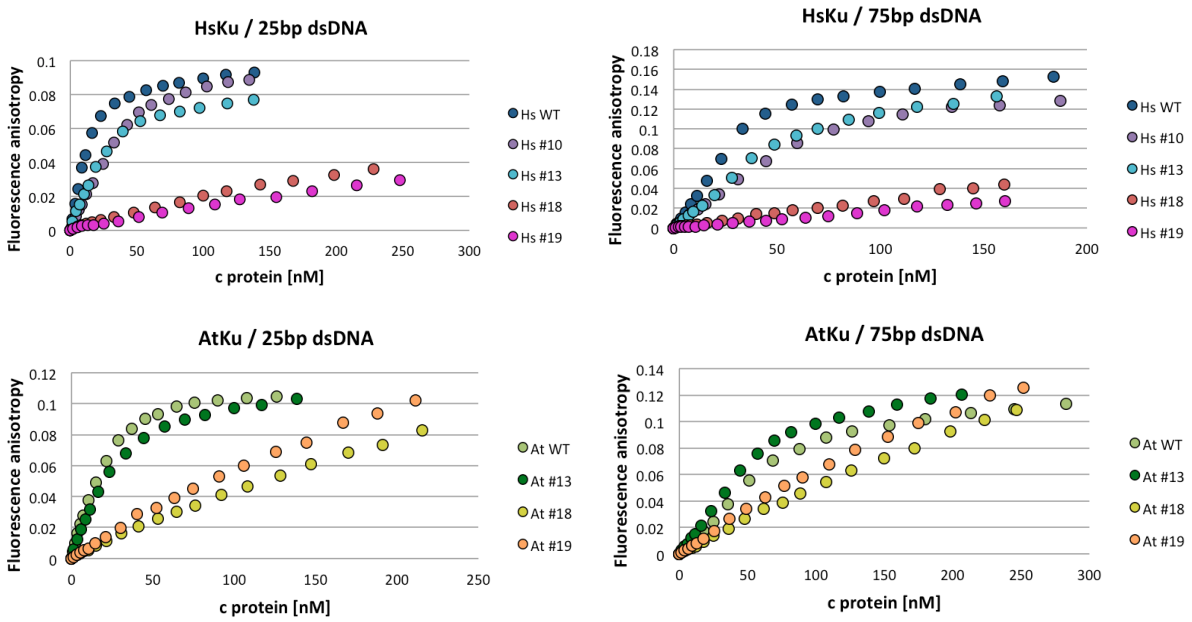

Figure 27: Mutant Ku complexes increase FA upon binding 25bp and 75bp dsDNA

The HsKu (top) and AtKu (bottom) complexes were expressed and purified from Hi5 insect cells in parallel. Fluorescence anisotropy was measured using 5 nM 25 bp (left) and 75 bp (right) dsDNA oligonucleotides 5' end-labeled with fluorescein. The measurements were done with increasing protein concentration 5 and 3 times respectively, each point with 3 technical replicates. Average values were plotted to form association curves.

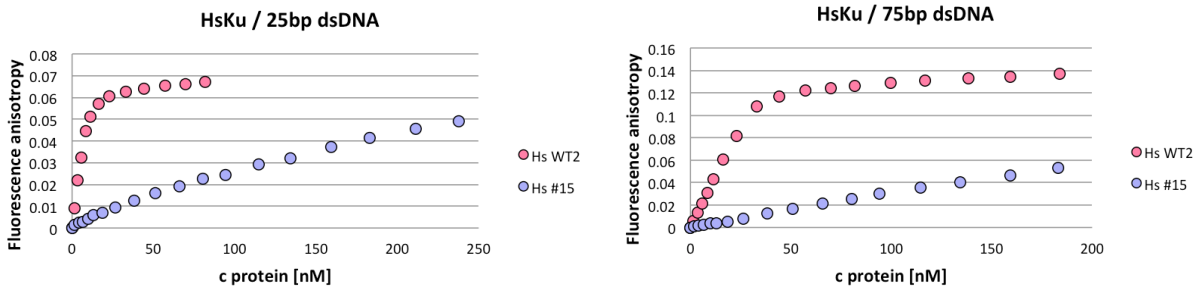

Figure 28: FA of HsKu #15 complex using 25bp (left) and 75bp (right) oligonucleotide

The HsKu mutant complex #15 was expressed and purified from Hi5 insect cells in parallel with a wild type control (HsWT2). Fluorescence anisotropy was measured using 5 nM 25 bp (left) and 75 bp (right) dsDNA oligonucleotides 5' end-labeled with fluorescein. The measurements were done with increasing protein concentration 5 and 3 times respectively, each point with 3 technical replicates. Average values were plotted to form association curves.

Table 2: Kd values for 25bp and 75bp oligo calculated from Fluorescence anisotropy

The fluorescence anisotropy measurements (Figures 21 and 22) were done with increasing protein concentration 5 and 3 times respectively, each point with 3 technical replicates. Average values were plotted and Kd values were calculated from the association curve using SigmaPlot. For each measurement was Kd calculated separately from 3 technical replicates and average Kd was calculated from all measurements (grey total rows). For mutant complexes Hs#18, Hs#19, At#18, At#19 and Hs#15 we could not reach saturation and therefore the Kd values are only derived from approximately fitted curve. Mutant complex Hs#15 was expressed and purified in different time with its own wild type control (HsWT2) and is therefore presented separately.

Oligo	Hs WT	Hs #10	Hs #13	Hs #18	Hs #19	At WT	At #13	At #18	At #19
25bp	16±2	47±6	25±2	500±100	600±200	23±1	28±2	470±50	340±10
	12±1	37±5	31±3	700±200	800±200	22±1	28±1	440±50	340±20
	15±1	42±5	35±2	500±100	800±200	20±2	32±2	470±40	410±40
	18±1	33±4	33±2	700±300	800±100	25±1	34±1	410±10	500±50
	16±1	43±5	29±2	500±100	800±100	26±2	33±1	400±100	450±50
	15±1	**40±5**	**31±2**	**600±200**	**800±200**	**23±1**	**31±1**	**440±50**	**410±30**
75bp	41±7	79±7	77±8	800±90	1500±300	100±10	90±10	900±100	520±60
	41±5	89±7	90±10	1100±500	1400±400	100±10	78±7	710±50	690±80
	35±5	110±10	65±8	900±300	1000±200	90±10	90±10	1100±100	340±20
	39±6	**93±8**	**77±9**	**900±300**	**1300±300**	**100±10**	**86±9**	**900±80**	**520±50**

oligo	Hs WT2	Hs #15
25bp	10±2	240±30
	6±1	320±30
	7±1	330±40
	6±1	380±40
	4±0,3	360±40
	7±1	**330±40**
75bp	34±6	800±200
	32±5	700±100
	20±3	1000±200
	29±5	**800±200**

3.1.4.3 Mutations alter Ku distribution on DNA when using Electron microscopy

Scanning force microscopy was used in previously to analyze sliding of ScKu (Balestrini et al. 2013). However, electron microscopy can be also used to visualize the DNA/protein complexes (Cary et al. 1997; de Vries et al. 1989). We used rotary shadowing technique and TEM to visualize mutant complexes associated with DNA as before described for wild type HsKu and AtKu. Due to high protein density, we were not able to quantify AtKu WT complexes. Therefore, only the HsKu complexes were quantified. However, also without extensive quantification we could observe that AtKu #13 formed less dense complexes. AtKu #18 and AtKu #19 show major decrease in DNA association and could be compared to human counterparts (Figure 29).

DNA/HsKu complexes present in submarginal region were selected according to criteria assuring quality (see Materials and Methods). In general, fraction of free DNA was not analyzed due to technical difficulties. DNA bound by at least one Ku was measured using ImageJ software in pixels and recorded.

Average number of HsKu per DNA molecule was calculated (Table 3, Figure 30). HsWT and HsKu #13 associate with equal amount of Ku (4,9 ± 2 and 4,9 ± 1,8 respectively). HsKu #18 shows 2,2-fold decrease in DNA association while the decrease is 3,5-fold for HsKu #19. Decrease indicates that association with DNA is impaired for HsKu #18 and #19.

Table 3: Quantification of HsKu/DNA interaction from electron micrographs

A number of images from submarginal area of electron micrographs were taken. High quality Ku/DNA complexes with at least one Ku per DNA (column 2, see materials and methods) were analyzed. To ensure the quality of analyzed complexes a total DNA length of analyzed complexes was kept in the range of 800-1000 px and it was monitored (column 3). Number of Ku proteins (column 4) and their position was recorded and average number of Ku/DNA was calculated (column 5). Because it was not possible to calculate number of free DNA, this number does not represent the whole DNA population in sample, only the subset of high quality Ku/DNA molecules.

Ku complex	Number of DNA/Ku complexes	Average DNA length in px	Total number of Ku proteins	Average number of Ku/DNA
Hs WT	103	896,8 ± 29	506	4,9 ± 2
Hs #13	103	897,0 ± 37	507	4,9 ± 1,8
Hs #18	102	895,1 ± 47	225	2,2 ± 1,3
Hs #19	103	897,0 ± 31	143	1,4 ± 0,6

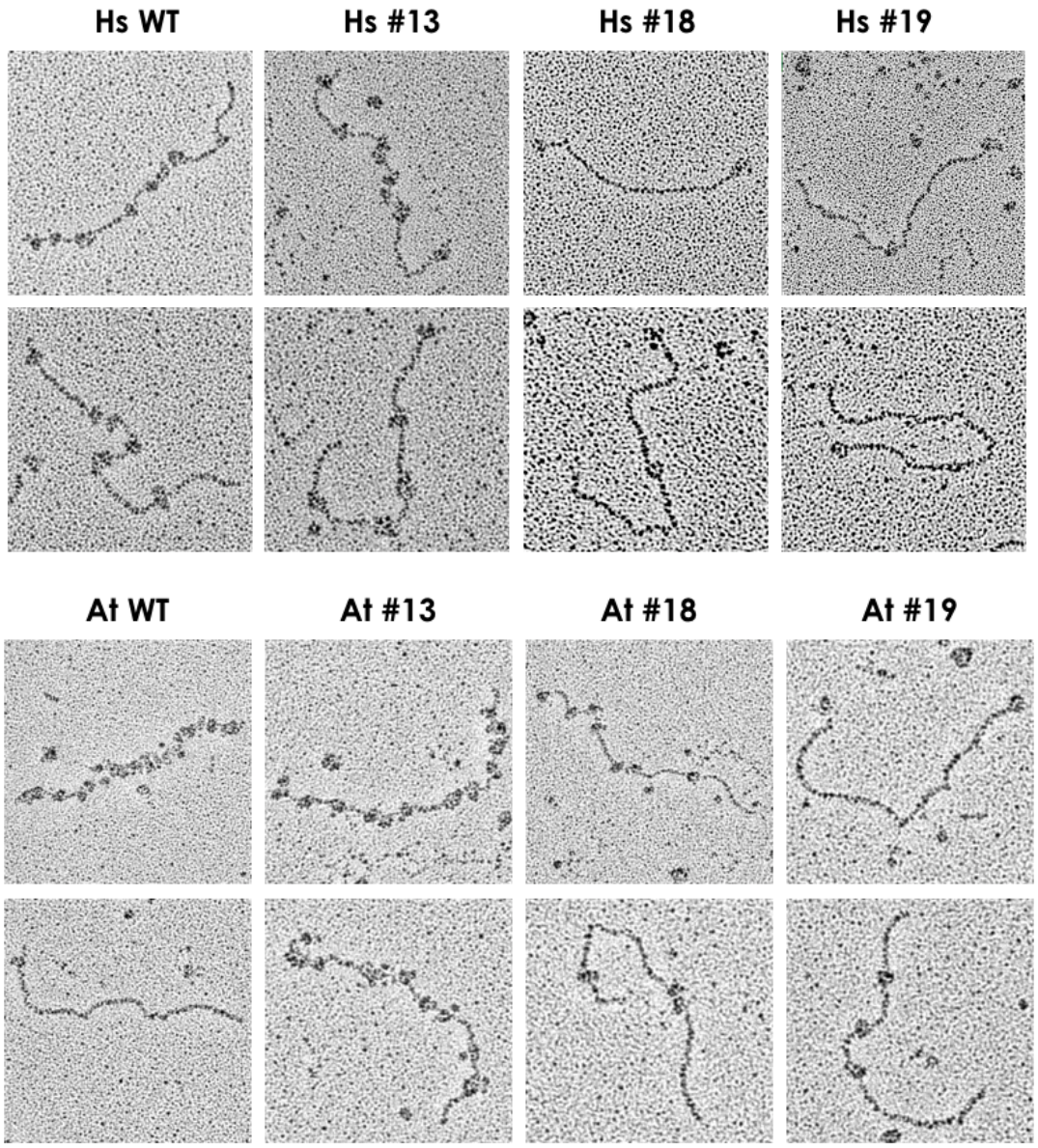

Figure 29: Electron microscopy of HsKu and AtKu

Purified mutant and wild type Ku complexes of 3,62 μM HsKu (top) and AtKu (bottom) were mixed with 1,53 nM of 1100 bp blunt dsDNA, aerosolized and vacuum dried on mica chips, where using rotary shadowing covered by Pt and C layers. Layers were visualized by Tecnai 20 transmission electron microscope. Pictures of Ku/DNA complexes were taken from submarginal area of sample droplets and the representative images are shown above.

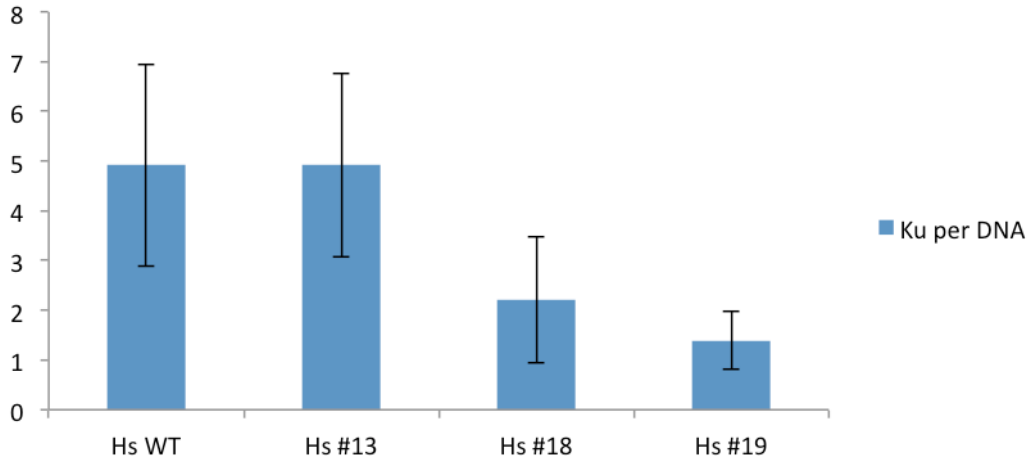

Figure 30: Average number of Ku proteins bound to the DNA
A graphical representation of the average number of Ku proteins bound to high quality Ku/DNA complexes. These complexes were chosen to have at least one Ku per DNA and were found in submarginal area of electron micrographs.

Sliding of Ku along the DNA is time dependent and binding requires free DNA ends (de Vries et al. 1989). Protein binding could be influenced by the extent of sliding. To investigate sliding of complexes we looked at the distribution of Ku complexes along the DNA. In ImageJ we measured the distance of single Ku proteins from the DNA end and grouped Ku proteins into 4 categories: Terminal, Subterminal, Medial and Central (Figure 31). We expected that Ku with impaired sliding would be more prevalent in the Terminal or Subterminal region. HsKu #13 did not have significant increase in terminally or subterminally localized Ku. However, we observed a significant (P value < 0.001 in two-tailed t-test, corrected for total protein) increase in number of terminal proteins for HsKu #18 and HsKu #19. Surprisingly, the difference in Ku abundance in Subterminal or other regions was not significant (P value > 0.05 in two-tailed t-test, corrected for total protein). This suggests that the progression from the early stages of DNA association towards diffusion is affected (Figure 32). The complex HsKu #18 is therefore interesting for *in vivo* analysis. Decreased sliding and increased association on DNA ends might provide a protection from nucleases. We would expect that cells with such Ku are proficient in telomere protection, but deficient in NHEJ, where is sliding necessary for repair (Turchi et al. 2000). Therefore, we decided to complement human cells with HsKu70 harboring mutations for HsKu #18 (Table 1). Because it is not clear whether

direct DNA binding of Ku to telomeres is required for telomere protection, we also decided to complement human cells with HsKu #13 that showed decrease in DNA binding in EMSA and fluorescence anisotropy study.

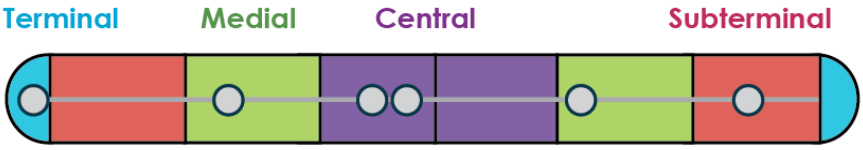

Figure 31: Scheme of DNA zones used to categorize Ku positions

For analysis of DNA translocation we divided DNA molecules into zones to obtain positional information. Zones are symmetrically organized around the center of DNA (grey line). Zones were defined as a distance of Ku (grey circles) from DNA end in pixels. Terminal: no DNA protruding from Ku, Ku was not further than 10 px from DNA end; Subterminal: ⟨1-155) px; Medial: ⟨155-310) px; Central: ⟨310-465⟩ px. In DNA >930 px all complexes in central region outside defined boundaries were considered part of left central region.

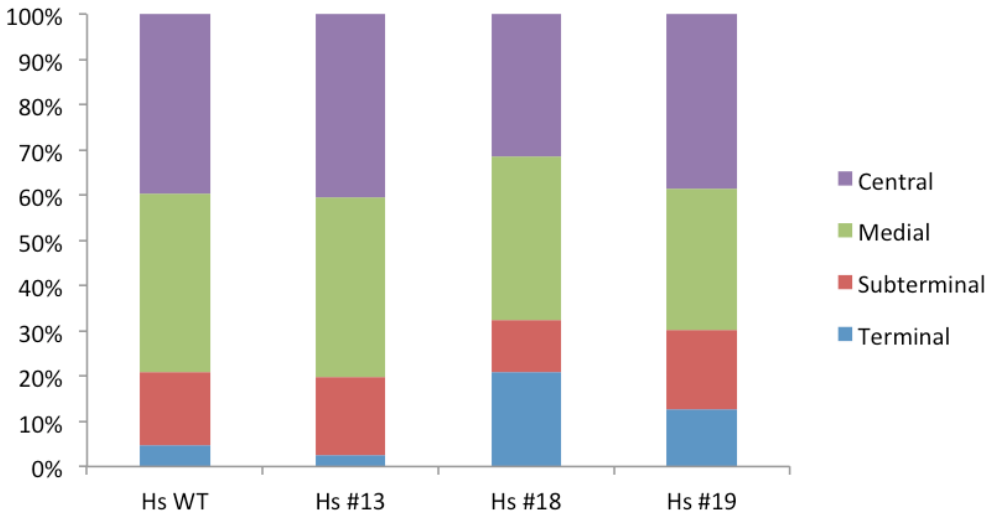

Figure 32: Distribution of Ku proteins along the DNA

For wild type and mutant Ku complexes we calculated the numbers of Ku proteins per different DNA zones (Figure 25). Here we show the graphical representation of what fraction each zone represents from the total Ku protein.

3.1.5 Human complementations

Ku is an essential protein in human cells. Therefore, we established collaboration with laboratory of Eric Hendrickson that previously generated conditional knock-out HCT116 cell lines for HsKu70 and HsKu80 (F. J. Fattah et al. 2008; Wang et al. 2009). We were able to work with cell lines having only a single functional allele with LoxP sites flanking the third exon (Ku70 F/-, Ku80 F/-). These cell lines also contained integrated

expression cassette producing Cre recombinase fused to estrogen receptor (CreER). Upon adding 4-hydroxytamoxifen (4-OHT), the Cre recombinase enters nucleus and causes inactivation of remaining endogenous allele. Substitutions in HsKu #18 are present only on Ku70 and in HsKu #13 only on Ku80 subunit. For complementation, double mutant cell lines were not necessary.

We cloned cDNA of both human Ku subunits (Ku70 and Ku80) into PiggyBac complementation vectors using Gateway cloning under chicken B-actin promoter. For each subunit we prepared wild type (70WT, 80WT) and mutant (7018, 8013) vectors. We transfected the conditional lines and generated stable cell lines. HCT116, Ku70 F/-, Ku80 F/- and complemented cell lines were grown for 4 days in presence or absence of 4-OHT. By western blotting we analyzed the level of HsKu80 protein. Ku80 F/- in presence of 4-OHT lost most of the HsKu80 protein due to recombination. Residual protein comes probably from cells where Ku did not undergo recombination. We can observe decrease in HsKu80 also for Ku70 F/- cell line. It is known, that Ku subunits are stable only in heterodimer. Complemented lines showed protein expression that was not at all or only mildly affected by 4-OHT (Figure 33).

Although, we could detect protein expression after 4 days post 4-OHT treatment, no viable cells were recovered after 14 days. We repeated the transfection using complementation constructs and we selected approximately 200 colonies for each WT and mutant Ku. After 4-OHT treatment none of the colonies survived. We were not able to complement Ku deficiency using this approach.

Ku is responsible for NHEJ, inhibition of recombination and suppression of t-circle excision in human and *A. thaliana* (F. Fattah et al. 2010; Kazda et al. 2012; Qi et al. 2013; Wang et al. 2009). This suggests a similar role and studying Ku in *A. thaliana* could help shed light on the role of Ku/DNA interaction in telomere biology. Therefore, next we decided to study DNA binding/sliding impaired Ku complexes in Arabidopsis.

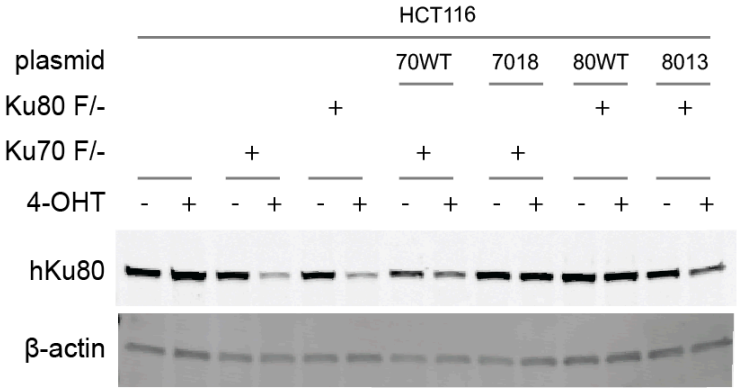

Figure 33: Western blot of cells after 4 days in the absence and presence of 4-OHT

Cells were plated in 6-well plates and grown for 4 days in presence or absence of 4-OHT. The whole cell protein extracts were prepared and analyzed by western blot using anti Ku80 antibodies Cell lines with stable integrated plasmid harboring with wild type (70WT, 80WT) of mutant (7018, 8013) were analyzed. Conditional cell lines (F/-) in response to 4-OHT lost endogenous allele and the HsKu80 (hKu80) protein levels, regardless of Ku70 or Ku80 depletion, declined. Complemented lines did not show similar decrease in HsKu80.

3.1.6 Mutant complexes #13 and #18 have different separation of function phenotypes in *A. thaliana*

3.1.6.1 Heterozygosity has no effect on telomeres or DSB repair

Loss of one allele of HsKu80 causes haploinsufficiency in human cells (Li et al. 2002). Complementation in *A. thaliana* could potentially lead to altered protein levels. Therefore, we decided to examine the effect of heterozygosity on telomere length and sensitivity to DSB inducing agent bleocin.

Segregating T-DNA insertion lines of *A. thaliana* for both Ku subunits (*ku70-2* SALK_123114; *ku80-7* SALK_112921) were obtained from NASC collection. Ku is a negative regulator of telomerase (Riha and Shippen 2003). Telomere length is therefore a good indicator of telomere protection by Ku. Telomere restriction fragment analysis (TRF) was performed with Ku +/- plants as well as Ku +/+ and Ku -/- plants segregated from the same parent. For Ku70 and Ku80, lack of one allele did not result in telomere elongation. Inactivation of both alleles led to telomere elongation for both Ku70 and Ku80 genes (Figure 34).

DSB repair was analyzed in seedlings growing in presence of bleocin. DNA damage causes cell cycle arrest and Ku deficient plants show developmental defects

such as short roots and no or aberrant (single or asymmetric) true leaf formation. Seeds of Ku +/- parent were plated on 1/2 MS medium with 100 ng/ml of bleocin. Seedlings were analyzed after 11 days for suppression of true leaf development and genotyped. We did not observe a difference in bleocin sensitivity in the Ku +/+ and Ku +/- plants. Progeny of Ku80 +/- plants grew slower in than Ku70 (Figure 35).

Thus we conclude that a single allele of either Ku subunit provides amount of protein sufficient for telomere maintenance and DSB repair.

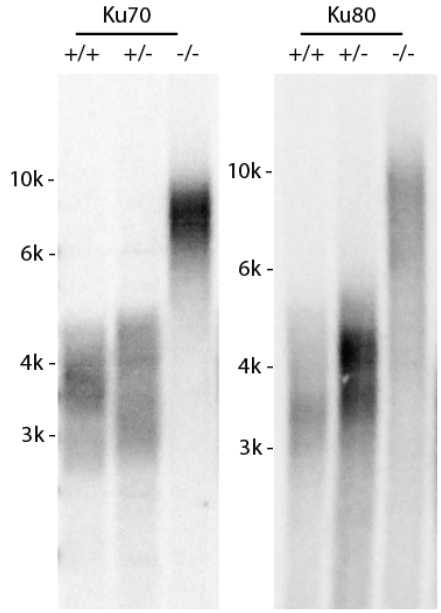

Figure 34: Telomere restriction fragment (TRF) analysis of *A. thaliana* gDNA from inflorescences.

Telomere restriction fragment (TRF) analysis of wild type (+/+), heterozygous (+/-) and mutant (-/-) Ku80 and Ku70 plants. The genomic DNA from inflorescences was digested with TruI1 and hybridized with a radioactively labeled (TTTAGGG)4 probe after gel electrophoresis.

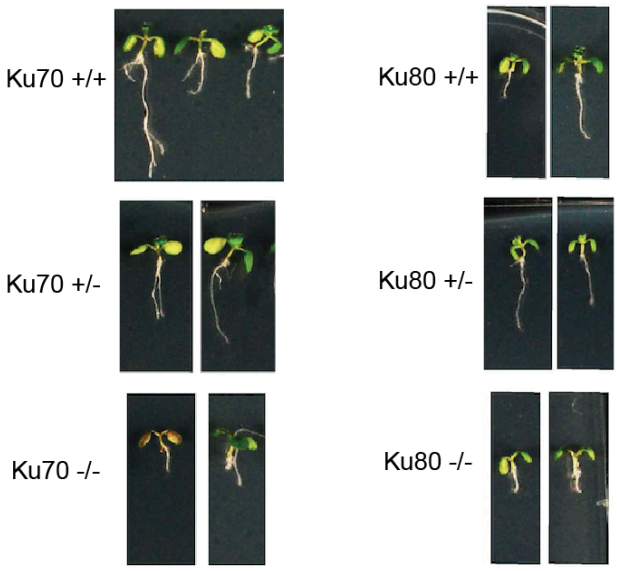

Figure 35: Bleocin (100ng/ml) assay to analyze DSB mediated developmental defects.

Seeds from self-fertilized heterozygous parent plants (Ku were plated on medium containing 100 ng/ml of bleocin. Seedlings were genotyped and grouped based on the genotype. Representative plants are shown above.

3.1.6.2 Cloning and mutagenesis of Ku for complementation

Constructs for complementation were derived from endogenous loci of *A. thaliana* Col0. Both subunits contained their respective endogenous promoters. AtKu70 construct contains only its first intron. AtKu80 lacks introns 6-9 and the C' terminus is fused to 12xMyc tag (Figure 36). Wild type constructs (70WT and 80WT) were used as controls for experiment. Mutations AtKu80-E276R, K518E, L519E, K520E (80#13) and AtKu70-K28E, R76E, K165E, R265E, R269E (70#18) were introduced from insect cell expression vectors into the respective constructs.

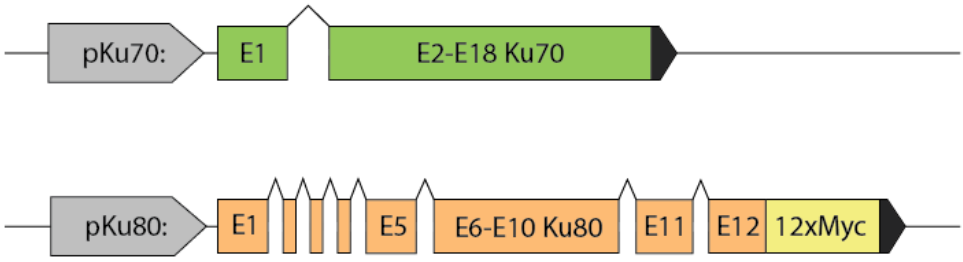

Figure 36: Scheme of complementation constructs

Complementation constructs were derived from sequences of endogenous Ku70 and Ku80 genes with upstream sequences containing promoters. For cloning purposes were some introns of Ku70 (I2-I17) and Ku80 (I6-I9) removed. Ku80 construct contains 12 C' terminal Myc tag repeats.

3.1.6.3 Complementation strategy

Complementation constructs were transformed to *Agrobacterium tumefaciens* and heterozygous plants were transformed by floral dip (80WT, 80#13 into Ku80 +/- and 70WT and 70#18 into Ku70 +/-). T1 transgenic plants were selected using BASTA selection marker. Plants homozygous for endogenous ku mutation containing transgenic constructs were identified by genotyping. Inflorescences from these plants were used to analyze telomere length (Figure 37 A). Seeds were collected and T2 population was analyzed (Figure 37 C). Seedlings were grown on BASTA to look for segregation ratio. Resistant seedlings were then analyzed for protein levels and telomere length (Figure 37 B). To get rough estimate of DSB sensitivity, seeds were plated on bleocin (100ng/ml) and number of plants that lacked true leaves or had aberrant true leaves was determined for several independent lines. Due to segregation, these numbers were only used for rough characterization. One line of Ku80 WT and 13 was taken to the next generation and T3 plants were analyzed for telomere length, DSB sensitivity and presence of G-overhangs (Figure 37 E, F). Conducted experiments are preliminary and further detailed study will follow.

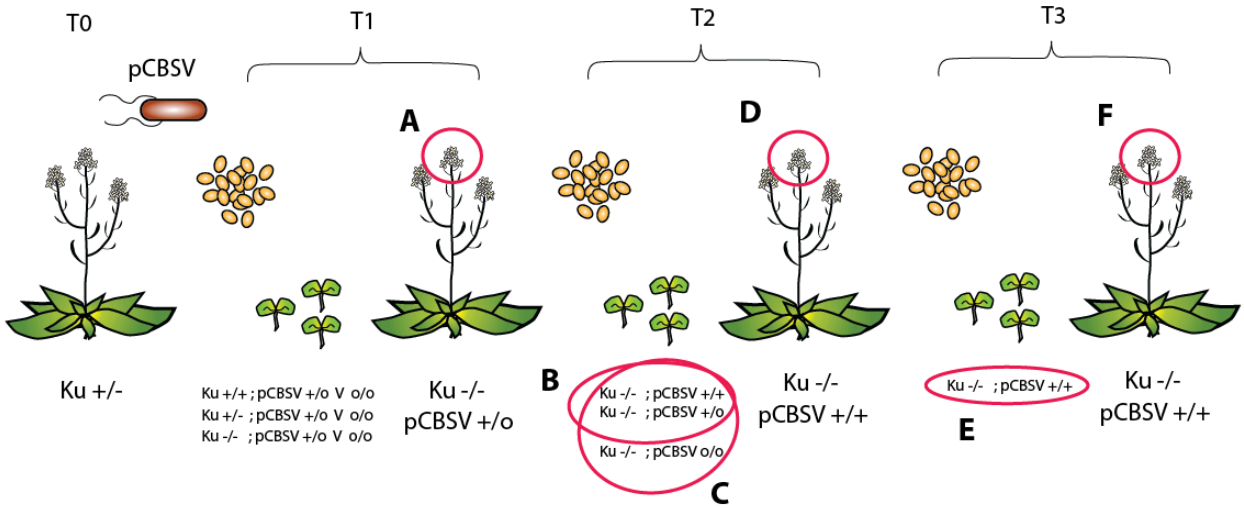

Figure 37: Scheme of complementation

Heterozygous plants of either Ku70 or Ku80 (Ku +/-) were transformed using agrobacterium harboring complementation plasmid carrying wild type or mutant allele of Ku70 or Ku80 respectively (pCBSV). Seedlings and plant material were analyzed from different generations and genotypes and are depicted using red circles (A-F).

3.1.6.4 AtKu70 #18 causes mild telomeric defect and strong DSB sensitivity

HsKu #18 mutant complex showed decreased affinity to DNA and increase in DNA terminus localization *in vitro*. AtKu #18 also exhibited decrease in DNA binding, but effect on sliding could not be determined.

DNA from inflorescences of 3 independent T1 plants mutant for endogenous Ku70 (Figure 37 A) was analyzed by TRF. The wild type construct AtKu70 (70WT) fully complemented telomere length. TRF of plants with AtKu70 #18 (70#18) protein complex seem more heterogeneous and longer than wild type (Figure 38). Mean telomere length was quantified using TeloTool software (Gohring et al. 2014). The difference between the average mean TRF length of complemented 70WT plants (3697 ± 247 bp) and 70#18 (4518 ± 477 bp) was not significant in two-tailed t-test (P value = 0,119).

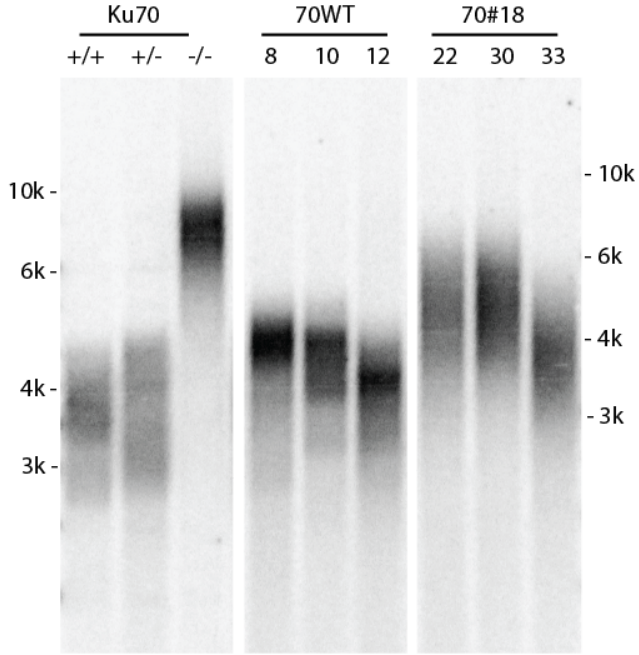

Figure 38: TRF of T1 generation Ku70

Genomic DNA was isolated from inflorescences of T1 generation (Ku70-/-; pCBSV+/o) and analyzed by TRF. Three independent plants were analyzed from complementation by wild type (70WT) or mutant (70#18) construct. The average mean TRF length in bp is 3697 ± 247 (70WT) and 4518 ± 477 (70#18) for complemented lines. The difference is not significant (in two-tailed t-test P value is 0,119).

Expression levels could influence the extent of telomere complementation. Therefore, we analyzed more insertion lines. T2 seedlings were grown on BASTA selection plates to select plants containing constructs (Figure 37 B). Based on BASTA

segregation ratio we identified lines with multiple insertion loci: 70WT: 10, 12 and 70#18: 11, 19, 33, 40, 49 (Figure 39 and 40).

Total protein extract from resistant seedlings was used for western blot analysis of AtKu70 protein levels. The seedling population consists of plants with hemizygous and homozygous insertions and it was used only as a rough estimate for telomere length and protein levels. The control heterozygous seedlings were a segregating population containing all three genotypes. The protein level in this seedling population is therefore slightly different than it would be from pure Ku +/- plants. Level of AtKu70 proteins was analyzed by anti-Ku70 antibodies (Figure 39).

The telomere length in different lines was similar to length from T1 generation. However, we observed a variation in telomere length between different insertion lines that partially correlated with protein levels (Figure 39 and 40). The average mean TRF length was calculated for all lines complemented with 70WT (3796 ± 320 bp) and 70#18 (4878 ± 719 bp). The difference was significant (Figure 41).

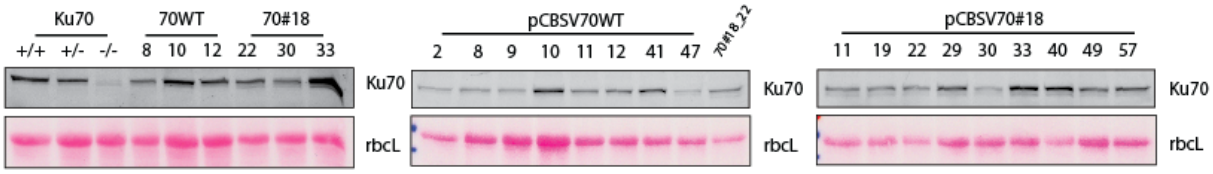

Figure 39: Western blot analysis of protein expression

Total protein from seedlings of T2 generation used for TRF analysis was analyzed by western blot. Protein loading was monitored by Ponceau staining. Antibodies against AtKu70 were used for protein detection. Protein from seedlings complemented by mutant Ku70#18 line #22 was loaded on all gels as reference. Protein concentration might reflect number of insertions. Based on BASTA segregation we detected lines with multiple insertion loci: p70WT: 10, 12; p70#18: 11, 19, 33, 40, 49.

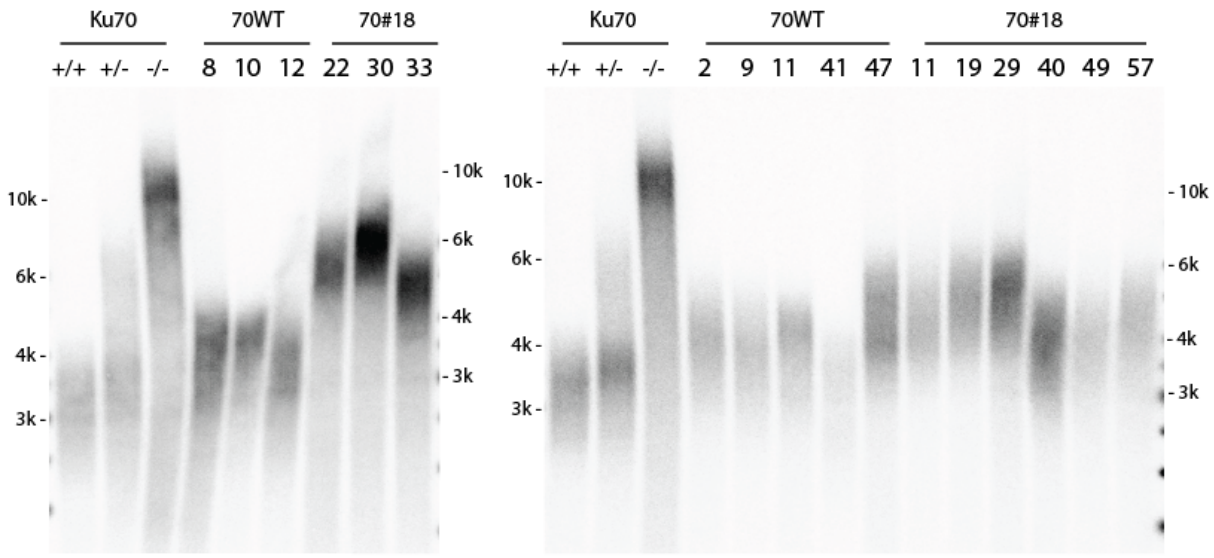

Figure 40: TRF analysis of T2 generation Ku70

Genomic DNA was isolated from seedlings of T2 generation and analyzed by TRF. Seedlings complemented with wild type (70WT) or mutant (70#18) plasmid were harvested from BASTA plates to ensure presence of construct (Figure 31 B). Control seedlings were grown without selection. Ku70+/- is a DNA from segregating population of +/- parent.

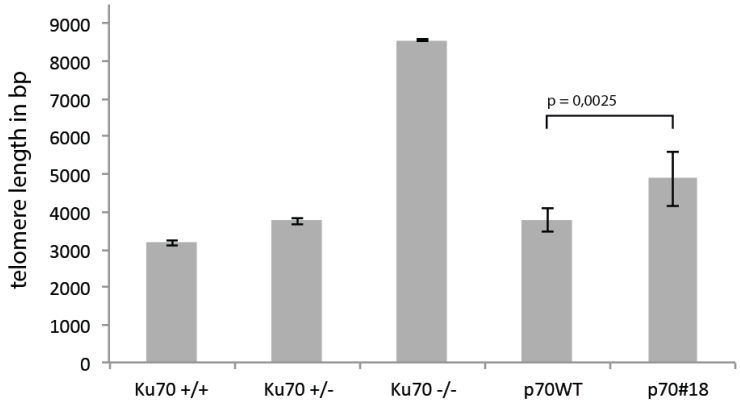

Figure 41: TeloTool analysis of TRF

TeloTool software was used to analyze mean telomere length from TRF analysis. Average mean TRF length was plotted from complemented (p70WT and p70#18) and control lines. The difference between p70WT and p70#18 is significant as determined by two-tailed t-test (P value < 0,05).

AtKu is involved in DSB repair and AtKu -/- plants do not develop true leaves on 1/2 MS medium with 100ng/ml bleocin (Figure 35). We plated T2 seeds onto 1/2 MS with 100ng/ml bleocin and G2 of non-transformed control plants. Plants with no or aberrant true leaves were considered sick. T2 is still segregating plants that lack insertion and these plants did not develop true leaves.

Control Ku70 +/+ plants showed no defect in true leaf development. Seeds from Ku70 +/- parent segregated all three genotypes and accordingly had approximately 25% of sick plants, as expected with 3:1 segregation of Ku -/-. Plants with Ku -/- had 100% plants with defect in true leaf development.

The average % of sick plants of 70WT (41 ± 24 %) was 2,4-fold lower than 70#18 (98 ± 3) and had greater variation. Plants complemented with AtKu #18 were extremely sensitive to bleocin suggesting deficiency in DNA repair (Figure 42).

Mild increase in telomere length suggested that substitution of five residues does not severely influence telomere protection. Surprisingly, DSB repair seems to be almost non-functional. However, further experiments will be done with non-segregating T3 generation and comparable protein levels.

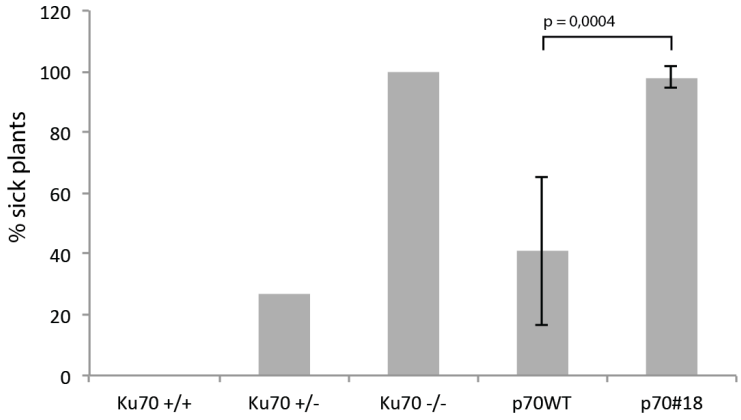

Figure 42: DSB sensitivity of seedlings using bleocin treatment

Seeds of segregating lines were plated on medium supplemented with 100 ng/ml of bleocin. Number of seedlings with impaired true leaf formation was calculated as a % of sick plants from total amount of seedlings. Control plants (Ku70 +/+ and Ku70 -/-) represent the G2 generation after segregating from Ku70 +/- parent. Ku70 +/- represents segregating population of heterozygous parent where 25% of plants are expected to be Ku -/- and sensitive to bleocin. Complemented lines represent segregating T2 generation, where lines with single insertion segregate 25% plants without insertion. The average % of sick plants from 8 wild type (p70WT: 2, 8-12, 41, 47) and 9 mutant (p70#18: 11, 19, 22, 29, 33, 40, 49, 57) complemented lines was plotted and the difference in not significant when using two-tailed t-test (P value > 0,05).

3.1.6.5 AtKu80 #13 causes pronounced telomeric defect and mild DSB sensitivity

The AtKu80 complementation was done in a similar way as AtKu70. T1 generation however showed already more pronounced telomere length defect. The

difference in average mean TRF length of complemented 80WT plants (3487 ± 239 bp) and 80#13 (5390 ± 180 bp) was significant. Telomeres of plants complemented with AtKu80 #13 were elongated and more resembled the telomere length of Ku -/- (Figure 43).

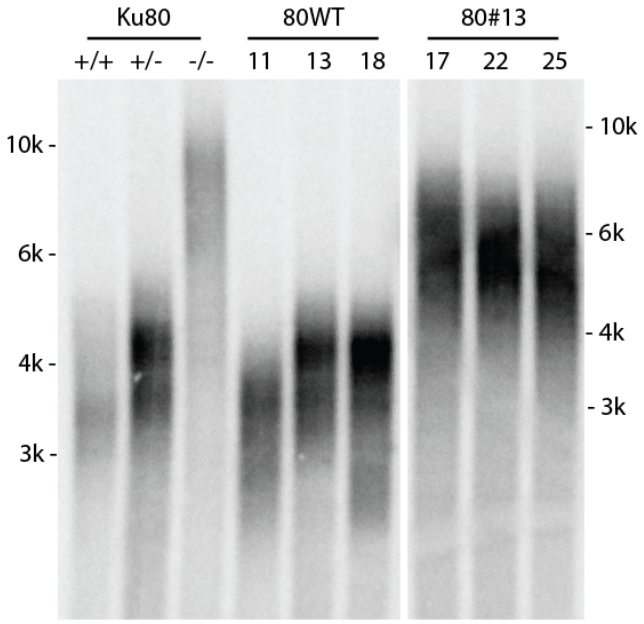

Figure 43: TRF of Ku80 generation T1 sample A.
Genomic DNA was isolated from inflorescences of T1 generation (Ku80-/-; pCBSV+/o) and analyzed by TRF. Three independent plants were analyzed from complementation by wild type (80WT) or mutant (80#13) construct. The average mean TRF length in bp is 3487 ± 239 (80WT) and 5390 ± 180 (80#13) for complemented lines. The difference is significant (in two-tailed t-test P value is 0,00118).

In T2 generation we observed higher variation in telomere length between different insertion lines that partially correlated with protein level (Figure 44 and 45). The protein level was influenced in some lines by presence of multiple insertions: p80WT: 18, 24; p80#13: 17, 22, 35#1 (Figure 44 and 45). For detection of Ku80 proteins from complementation construct we used anti-Myc antibodies. Levels of AtKu70 decrease in absence of AtKu80 what allodew us to use anti-Ku70 to observe protein levels in control samples.

The average mean TRF length was calculated for all lines complemented with 80WT (4594 ± 1276 bp) and 80#13 (6686 ± 1395 bp). The difference was significant (Figure 46).

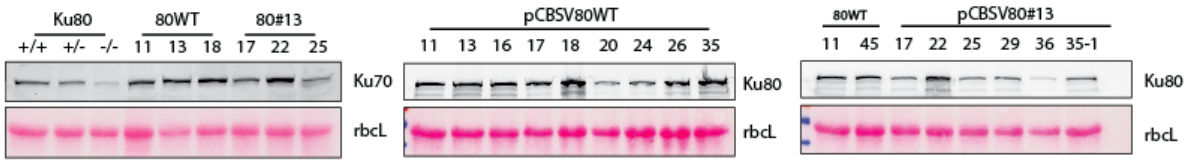

Figure 44: Western blot analysis of protein expression

Total protein from seedlings of T2 generation used for TRF analysis was analyzed by western blot. Protein loading was monitored by Ponceau staining. Antibodies against AtKu70 (left) and against Myc tag (middle and right, Ku80) were used for protein detection. Protein from seedlings complemented by wild type Ku80WT line #11 was loaded on all gels as reference. Protein concentration might reflect number of insertions. Based on BASTA segregation we detected lines with multiple insertion loci: p80WT: 18, 24; p80#13: 17, 22, 35#1.

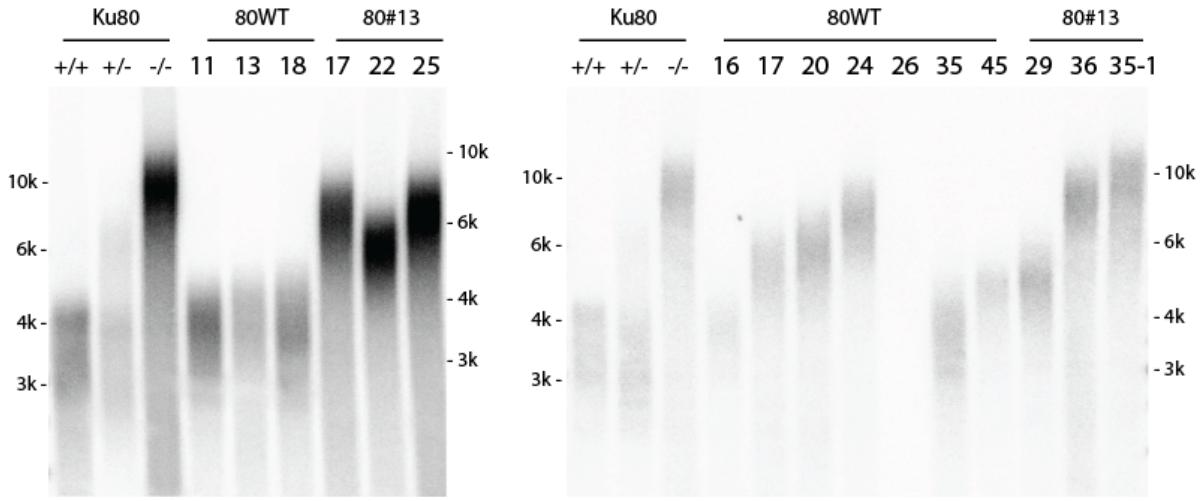

Figure 45: Generation T2 sample B.

Genomic DNA was isolated from seedlings of T2 generation and analyzed by TRF. Seedlings complemented with wild type (80WT) or mutant (80#13) plasmid were harvested from BASTA plates to esure presence of construct (sample B, Figure 37). Control seedlings were grown without selection. Ku80+/- is a DNA from segregating population of +/- parent.

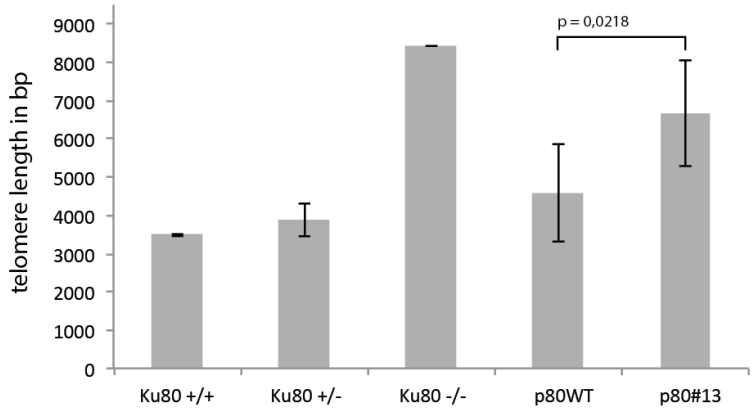

Figure 46: TeloTool analysis of TRF

TeloTool software was used to analyze mean telomere length from TRF analysis. Average mean TRF length was plotted from complemented (p80WT and p80#13) and control lines. The difference between p80WT and p80#13 is significant as determined by two-tailed t-test (P value < 0,05).

DSB sensitivity was tested for T2 seedlings on bleocin as it was done with Ku70. Control Ku80 plants seemed to be more sensitive to 100ng/ml of bleocin. Ku80 +/+ had increased % of sick plants.

The average % of sick plants in 80WT (80 ± 15 %) was not significantly different from 80#13 (72 ± 15 %). Plants complemented with AtKu #13 did not show DSB repair deficiency (Figure 47).

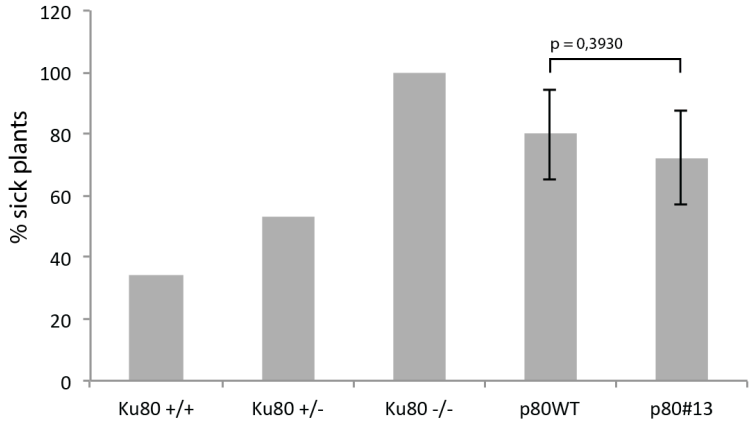

Figure 47: DSB sensitivity of seedlings using bleocin treatment

Seeds of segregating lines were plated on medium supplemented with 100 ng/ml of bleocin. Number of seedlings with impaired true leaf formation was calculated as a % of sick plants from total amount of seedlings. Control plants (Ku80 +/+ and Ku80 -/-) represent the G2 generation after segregating from Ku80 +/- parent. Ku80 +/- represents segregating population of heterozygous parent where 25% of plants are expected to be Ku -/- and sensitive to bleocin. Complemented lines represent segregating T2 generation, where lines with single insertion segregate 25% plants without insertion. The average % of sick plants from 10 wild type (p80WT: 11, 13, 16-18, 20, 24, 26, 35, 45) and 6 mutant (p80#13: 17, 22,

25, 29, 36, 35#1) complemented lines was plotted and the difference in not significant when using two-tailed t-test (P value > 0,05).

Segregation of T2 seedlings introduced minor error into analysis of telomeres and bleocin sensitivity. For more accurate results we analyzed T3 generation of from complemented lines Ku80WT_11 and Ku80#13_17. As control plants (Ku80 +/+ and Ku80 -/-) we used G3 generation after segregating from Ku80 +/- parent. Both lines show no growth defect in absence of DSB inducing agent (Figure 42). These two lines have different level of protein expression, however the Ku80 level is still above protein level of heterozygous plant (Figure 44 and 49).

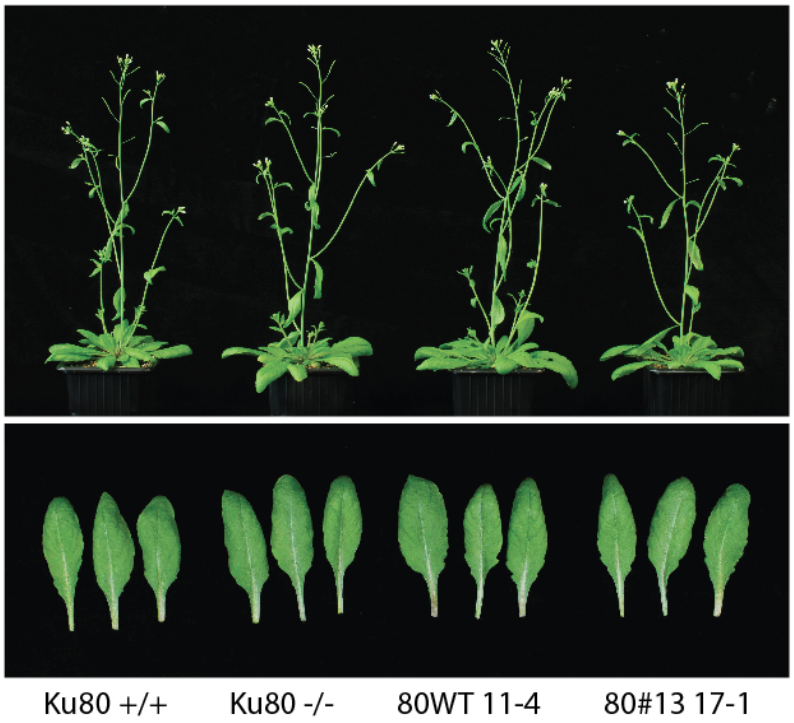

Figure 48: Morfology of a whole plant (upper panel) and leafs (lower pannel) in T3 generation for Ku80 complementation

Plants were grown in soil in absence of selection and photographs were taken from representative plants and leaves. Control plants (Ku80 +/+ and Ku80 -/-) represent the G3 generation after segregating from Ku80 +/- parent. Complemented lines represent marker non-segregating T3 generation of 80WT insertion line #11 and 80#13 insertion line #17 in Ku80 -/- background.

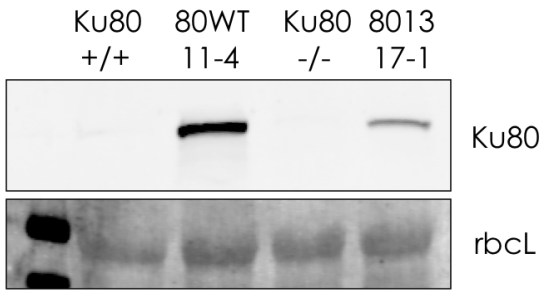

Figure 49: Protein levels in T3 generation Ku80

Total protein from seedlings of G3 generation of control plants (Ku80 +/+ and Ku80 -/-) and non-segregating T3 generation (Figure 31 E) of 80WT and 8013 was analyzed by western blotting. Protein loading was monitored using Odyssey (Li-Cor). Antibodies against Myc tag were used for detection of protein level of Ku80 in complementation lines.

Genomic DNA was purified from inflorescences (Figure 37 F) and the telomere length was analyzed for 3 different T3 plants. Telomere length of complemented 80WT lines was not significantly different from Ku +/+ plants. Plants complemented with 80#13 had telomeres indistinguishable form Ku80 -/- plants (Figure 50).

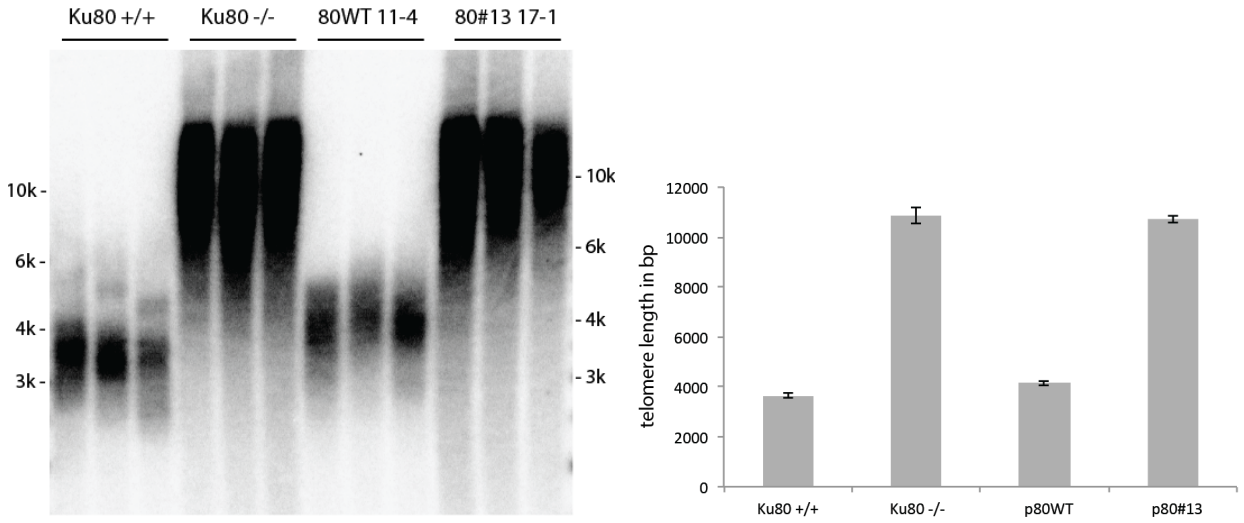

Figure 50: TRF of Ku80 generation T3

Genomic DNA was isolated from inflorescences of three independent plants and analyzed by TRF (left). Control plants (Ku80 +/+ and Ku80 -/-) represent the G3 generation after segregating from Ku80 +/- parent. Complemented lines represent marker non-segregating T3 generation of 80WT insertion line #11 and 80#13 insertion line #17 in Ku80 -/- background. TeloTool software was used to analyze mean telomere length from TRF analysis. Average mean TRF length was plotted from complemented control lines (right).

Ku protein controls resection of telomeres in A. *thaliana* (Kazda et al. 2012). We analyzed the G-overhangs using in-gel hybridization. Control sample was treated by T4 DNA polymerase and does not contain any G-overhang signal. Plants complemented with the wild type Ku80 (80WT) have comparable G-overhang signal to wild type plants. Mutant Ku80 (80#13) had increased G-overhang signal similar to Ku80 -/- (Figure 51). This indicates that AtKu80 #13 does not inhibit telomerase activity and fails to protect telomeres from resection.

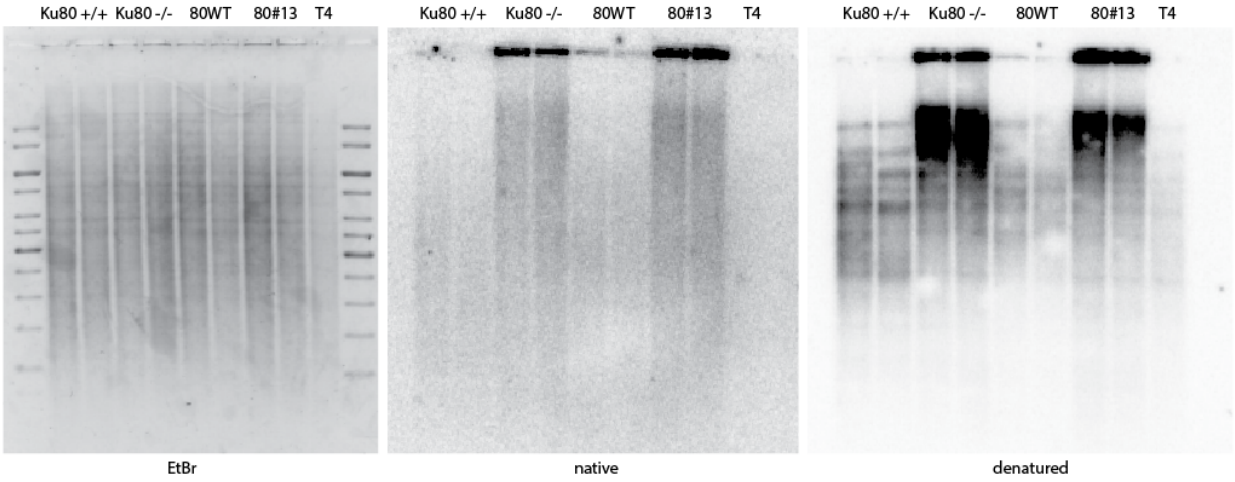

Figure 51: In-gel hybridisation of Ku80WT and Ku80#13 in T3 generation

Genomic DNA was isolated from inflorescences of three independent control plants (Ku80 +/+ and Ku80 -/-) in G3 generation and complemented lines (80WT, 80#13) in T3 generation. The In-gel hybridization assay was performed with untreated genomic DNA and with Ku80 +/+ DNA that was previously incubated with T4 DNA polymerase to remove telomeric G-overhangs. The digested DNA was separated on an agarose gel, stained with ethidium bromide (left) and hybridize with a ^{32}P labeled probe first under native (middle) and then under denaturing conditions (right).

To analyze the DSB sensitivity, T3 seedlings were plated on two different bleocin concentrations (50 and 100 ng/ml). Seedlings were scored for true leaf defects (Figure 52).

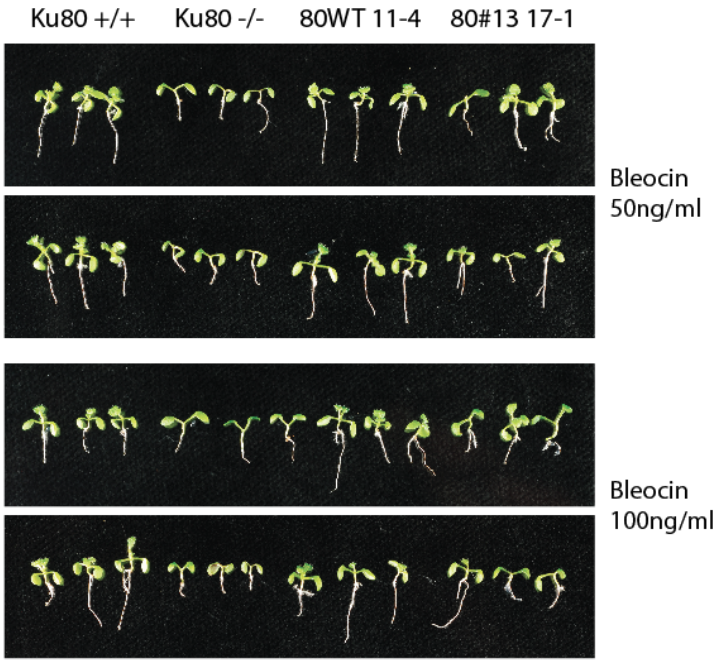

Figure 52: Selected seedlings from bleocin treatment to assay DSB sensitivity in T3 generation

Seeds of non-segregating lines (Figure 31 E) were plated on medium supplemented with 50 or 100 ng/ml of bleocin. Control plants (Ku80 +/+ and Ku80 -/-) represent the G3 generation after segregating from Ku80 +/- parent. Complemented lines represent marker non-segregating T3 generation of 80WT insertion line #11 and 80#13 insertion line #17 in Ku80 -/- background. Three representative plants from two independent plates were removed from plate and photographed.

The Ku80 +/+ seedlings did not show any defect on 50 ng/ml of bleocin. However, a few plants with defects were observed on 100 ng/ml of bleocin. All Ku -/- plants lacked true leaves in 50 ng/ml and 100 ng/ml. Ku80WT_11 showed defected plants only in 100 ng/ml and complemented DSB sensitivity as wild type. AtKu80 #13 exhibit increased % of sick plants on both concentrations of bleocin, however the effect was not as severe Ku80 -/- (Figure 53). In future we will analyze more independent lines to confirm the finding.

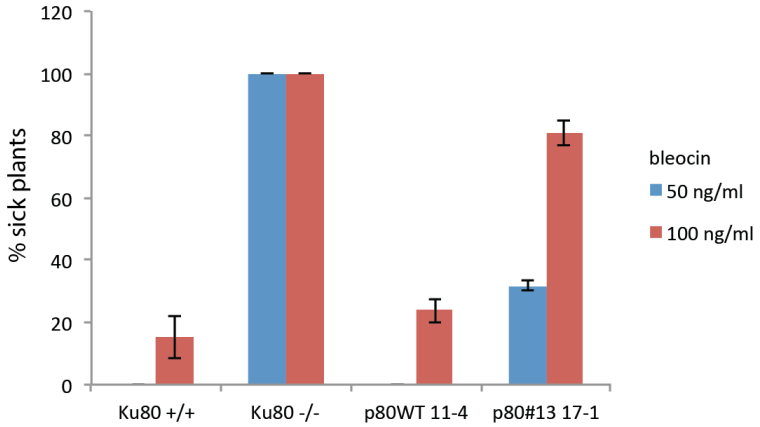

Figure 53: DSB sensitivity of seedlings using bleocin treatment

Seeds of non-segregating lines were plated on medium supplemented with 50 and 100 ng/ml of bleocin. Number of seedlings with impaired true leaf formation was calculated as a % of sick plants from total amount of seedlings on two different plates. Control plants (Ku80 +/+ and Ku80 -/-) represent the G3 generation after segregating from Ku80 +/- parent. Complemented lines represent marker non-segregating T3 generation of 80WT insertion line #11 and 80#13 insertion line #17 in Ku80 -/- background.

3.2 Telomere proteins in *C. reinhardtii*

Telomere DNA associates with proteins (de Lange 2005) that potentially modulate binding and translocation of Ku. In *A. thaliana* the telomere binding proteins (TBPs) undergone major gene duplication and there are two major TBP families (Karamysheva et al. 2004). The role of TBPs in formation of blunt-ended telomeres remains to be determined (Kazda et al. 2012). Using genetic approach it was not yet possible to confirm importance of TBP homologues. We decided to take a different approach to identify plant TBPs. *C. reinhardtii* is a unicellular green algae and I analyzed its telomeres and identified putative TBPs.

3.2.1 Telomeres of *C. reinhardtii* are similar to land plants

3.2.1.1 C. reinhardtii strains have diverse telomere lengths

Telomeric repeats in *C. reinahardtii* contain additional thymine in compare with other land plants: TTTTAGGG (Petracek et al. 1990), however the structure was not described. Telomere length varies across species. We analyzed 7 different strains of *C. reinhardtii* using TRF analysis. Telomere length was in the range of 350 - 2000 bp (Figure 54). We observed variation in the length between different strains.

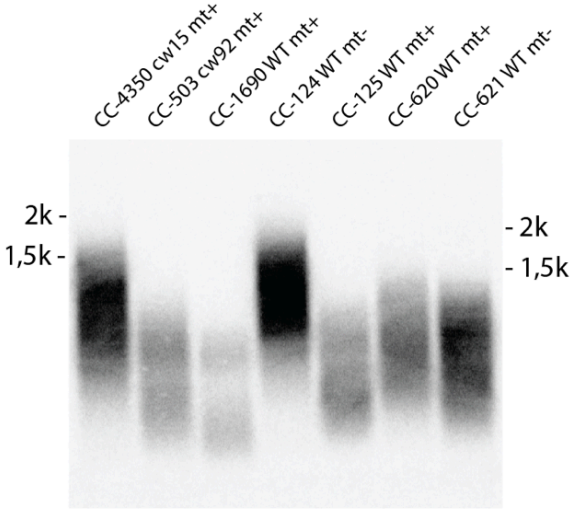

Figure 54: TRF of several strains of *C. reinhardtii*

Genomic DNA from different strains of *C. reinhardtii* was isolated, digested with AluI and hybridized with a radioactively labeled (TTTTAGGG)3 probe after gel electrophoresis.

3.2.1.2 Telomeres form a telosome structure

To investigate protection of telomeric DNA by proteins we performed digest by micrococcal nuclease (MNase). Isolated nuclei from cell wall deficient strain were treated with increasing amount of MNase (Figure 55). This allows us to look on the chromatin structure and analyze whether telomeric chromatin is nucleosomal. Purified DNA was separated in agarose gel and analyzed by ethidium bromide and southern blotting. Telomeric DNA was protected in non-nucleosomal pattern (Figure 56). Such structure is commonly referred to as a telosome (Figure 55). This structure could be protected in part by TBPs.

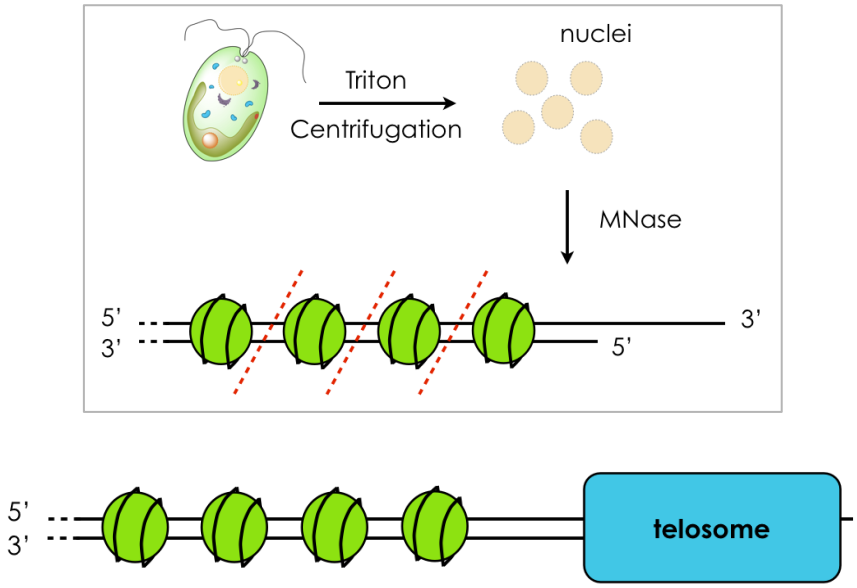

Figure 55: Scheme of the Micrococcal nuclease (MNase) digest.
Nuclei from cell wall deficient strain of *C. reinhardtii* were separated and subjected to DNA digest using MNase. MNase causes DNA degradation in protein-free parts of DNA and leads to nucleosome separation (middle). In some organisms a protein complex protects telomeric DNA in a non-nucleosomal manner (telosome, bottom).

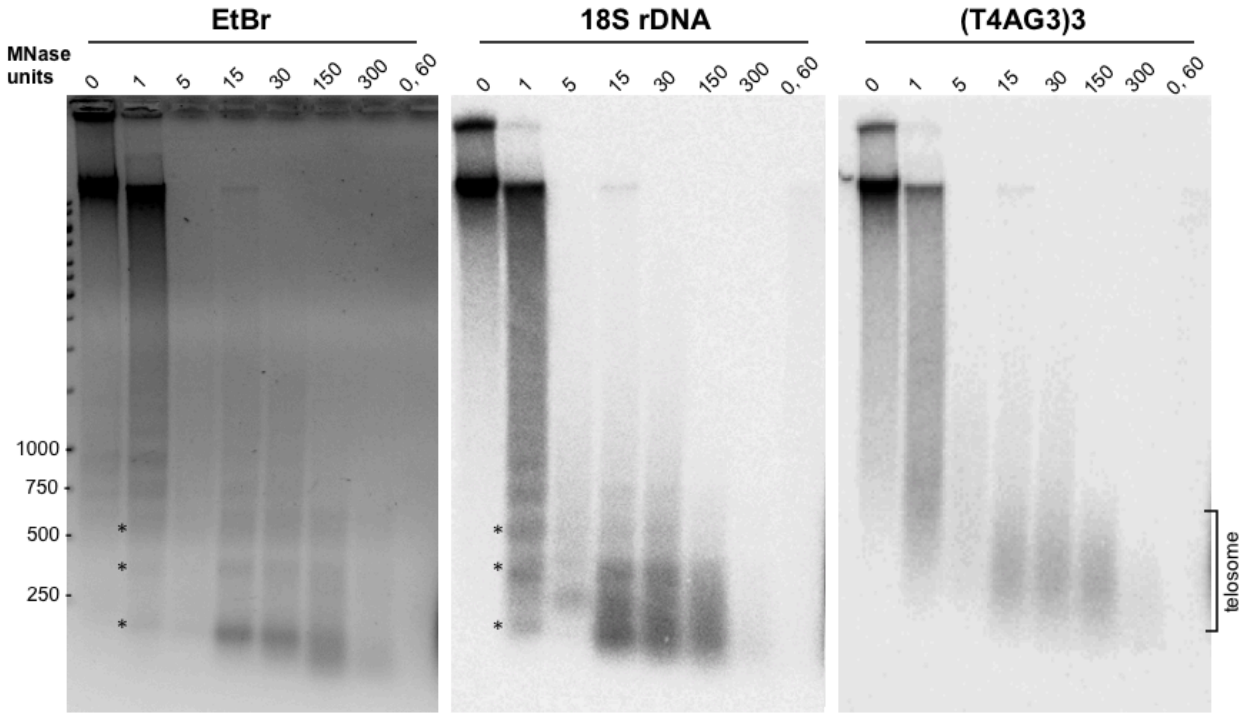

Figure 56: Micrococcal nuclease digest of *C. reinhardtii* nuclei.
Nuclei from CC-4350 strain were subjected to increasing amount of MNase units. After reaction inactivation DNA was purified, separated on an agarose gel, stained with ethidium bromide (left) and after southern blotting hybridized using radioactive labeled telomeric probe (right). Membrane was stripped and hybridized with probe against 18S rDNA (middle). Control nuclei were not subjected to nuclease digest in first step, but after protein removal, DNA was treated using 60 units of MNase (last lane). Nucleosomal DNA is highlighted with * for mono-, di-, and tri-nucleosomes. Telosome DNA is indicated.

3.2.2 *In silico* identification of telomere binding proteins

One of the main features of telomere binding proteins is presence of telobox sequence (Peska et al. 2011). Telobox is responsible for sequence specific binding to telomeric DNA. Because genome of *C. reinhardtii* is GC rich, AT rich sequence binding motives, such as telobox, should be rare. I identified two proteins containing telobox sequence: CrTBP1 (Cre02.g147550.t1.1) and CrTBP2 (Cre04.g221200.t1.1). CrTBP2 contains N' terminal telobox sequence and CrTBP1 contains C' terminal Myb-like domain with telobox. Due to similarity with mammalian TRF we focused on the CrTBP1.

3.2.2.1 Scheme of the crTBP1 and domains from HHpred

CrTBP1 sequence harbors homology with Myb-like domain of TRF proteins and TBP proteins from plants and also shares homology with central region of plant TBPs (Figure 57 an 58). Interesting feature of this protein is a stretch of 23 glutamines (Figure 57). In collaboration with Luis Valledor we analyzed nuclear proteome from isolated

nuclei of cell wall deficient *C. reinhardtii.* We were able to find 3 peptides from CrTBP1. We could not find them in whole cell proteomic data. This might suggest that these proteins are enriched in nucleus and not abundant.

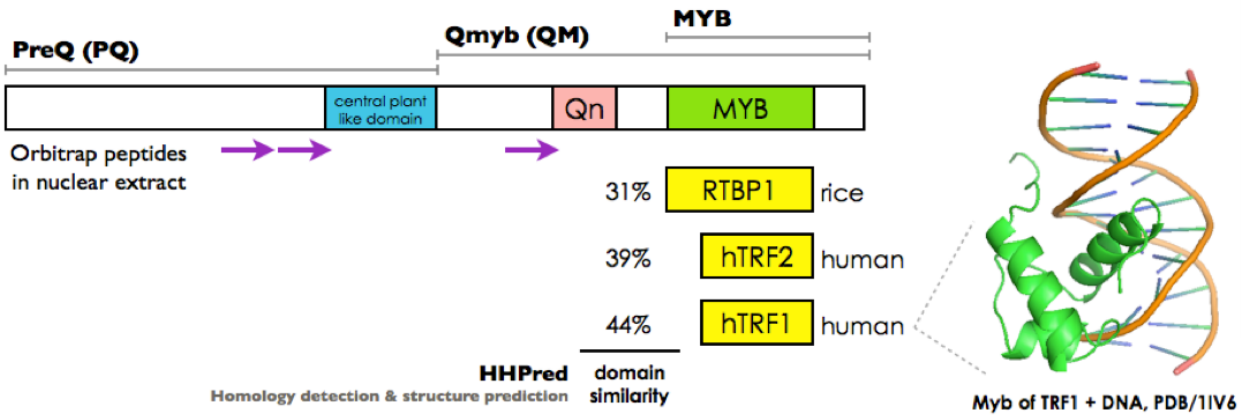

Figure 57: Scheme of CrTBP1

CrTBP1 protein contains C' terminal Myb-like domain with telobox sequence (MYB). Using the online HHPred domain prediction software we were able to identify similarity with RTBP1, hTRF2 and hTRF1 Myb-like domain that is responsible for sequence specific binding of telomeres. Upstream from MYB we identified a stretch of 23 glutamines (Qn). In the first half of the protein lies a sequence homologous to central domain of putative plant telomere binding proteins (central plant like domain). In collaboration with Luis Valledor we were able to identify three peptides using protein mass spectrometry from nuclei (magenta arrows, Orbitrap peptides). For dimerisation assay we split protein to three regions: PreQ, Qmyb and MYB.

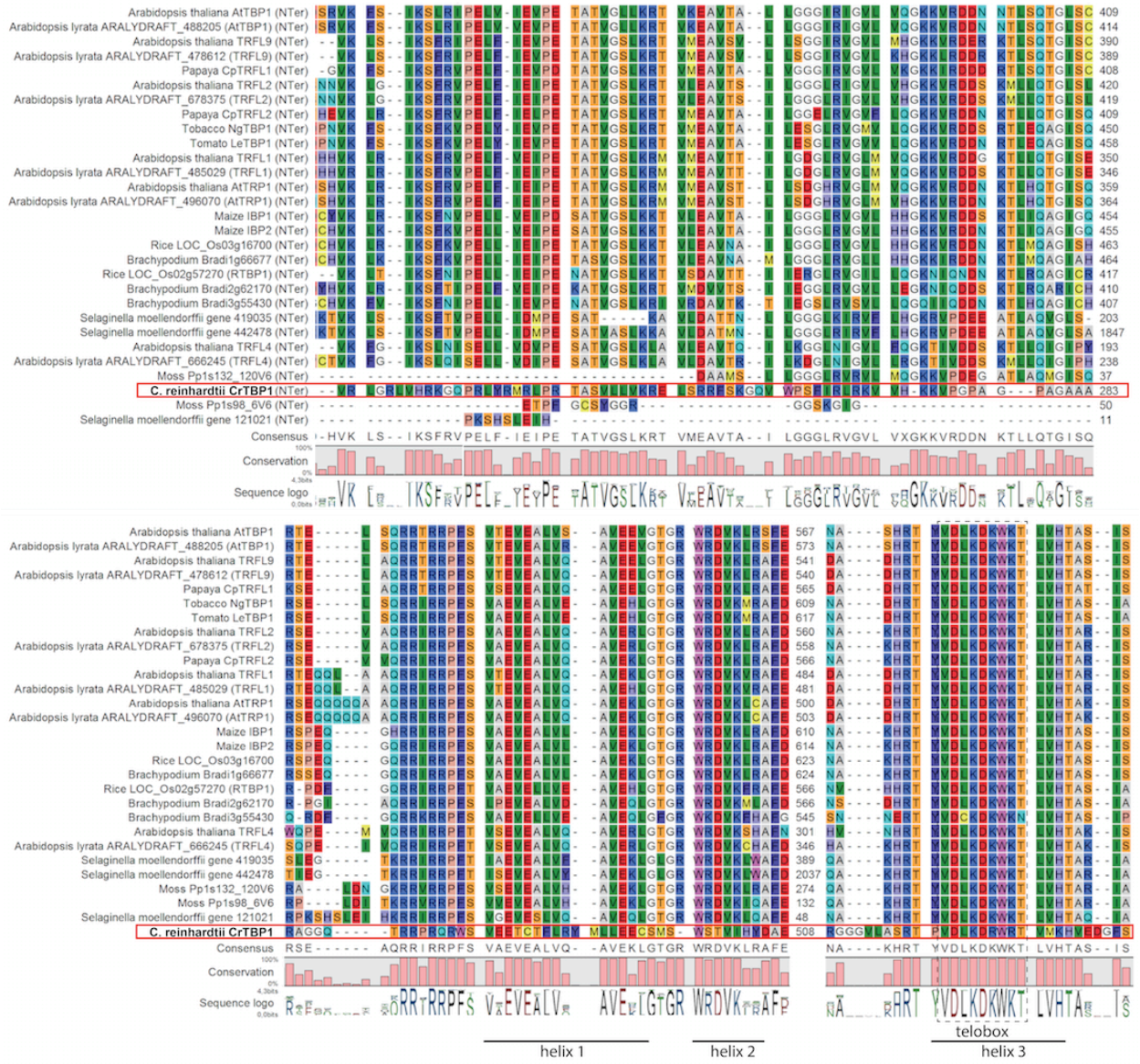

Figure 58: Multiple protein alignment

Multiple protein alignment was done by Nick Fulcher using N' terminal fragment 1-470 (top) or full-length 575 amino acids (bottom) of CrTBP1. When Myb-like domain was removed from telomere binding proteins (top) a centrally located homology was apparent in region of 216-272 amino acids of CrTBP1. When full-length proteins were aligned (bottom) a Myb-like domain homology can be observed in region 495-568 aa of CrTBP with its three helices and telobox sequence VDLKDRWRT in the helix 3.

3.2.3 CrTBP1 forms dimers *in vitro*

Another feature of TPBs is dimerization. Both subunits are required to bind telomere DNA. If one of the monomers lack Myb-like domain, such protein fragment serves as dominant negative peptide and would be a great tool to study CrTBP1 *in vivo*.

To study dimerization of CrTBP1 we used *in vitro* translation system (Promega) to express CrTBP1 and its fragments. We used T7 tag to generate bait protein fragments. These were incubated with prey CrTBP1 protein that was previously labeled using fluorescently labeled lysine (Figure 59). After immunoprecipitation we analyzed captured proteins using fluorescence scanner and western blot.

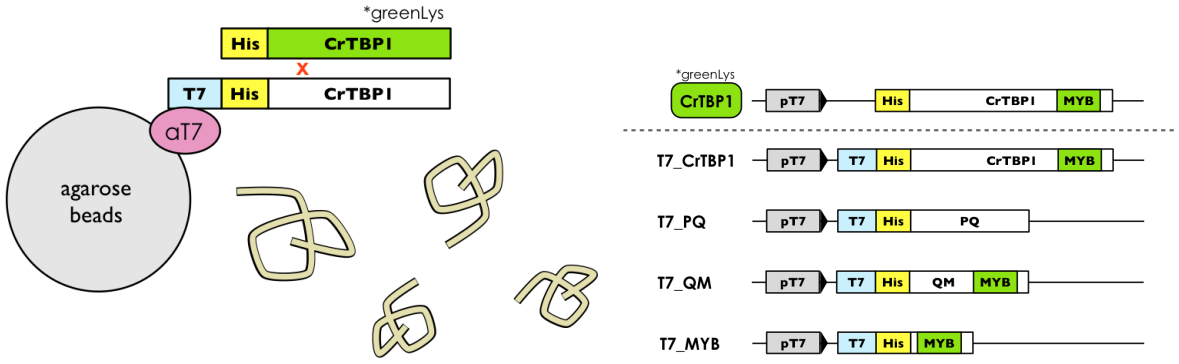

Figure 59: Scheme of dimerisation assay of CrTBP1 and bait protein fragments
To analyze possible homodimerization of CrTBP1 we expressed using *in vitro* translation system CrTBP1 using fluorescently tagged lysine (*greenLys). We expressed in parallel T7-tagged full length CrTBP1 as well as fragments PQ, QM and MYB (Figure 57). We mixed each fragment with labeled CrTBP1 and using antiT7 antibodies and agarose beads we pulled down proteins and analyzed presence of labeled CrTBP1.

When full-length bait CrTBP1 was used, we could detect fluorescence signal of prey protein. We used three different fragments as bait (Figure 59). All three fragments were able to bind the prey protein. However, the amount of fragments on the beads was higher than full length CrTBP1, but the amount of bound prey CrTBP1 was lower (Figure 60). This suggests that either there are two distinct dimerization surfaces or one large one. In any case, the entire dimerization surface seems necessary for the most effective binding. Based on the fluorescence signal versus bait protein on beads we suggest that the most effective in dimerization is the full length protein, the PreQ and Qmyb fragments have comparable binding and the MYB domain alone is the least effective (Figure 60).

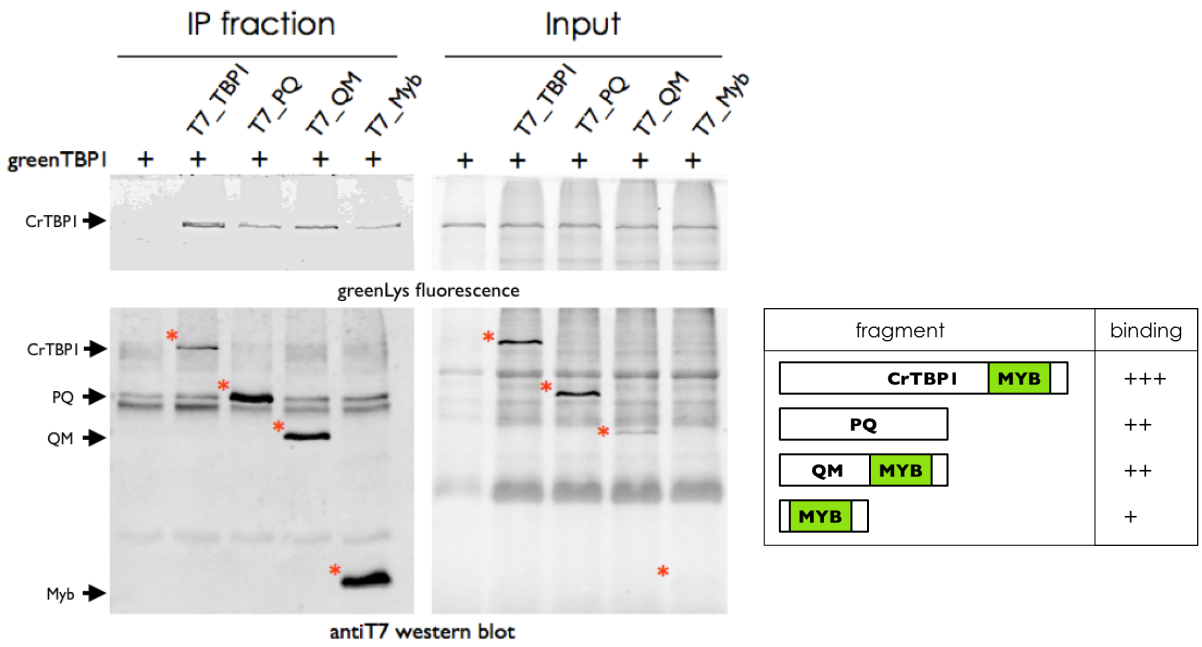

Figure 60: *In vitro* dimerisation of CrTBP1

Fluorescently tagged full length CrTBP1 was mixed with full length T7-tagged CrTBP1 or different T7-fragments, complexes were pulled down using anti-T7 antibodies loaded on PAGE gel. Proteins that did not bind to the anti-T7 antibodies were also analyzed (Input). Fluorescence was detected in the gel (upper panel) and the T7-tagged proteins were visualized by western blot using anti-T7 antibodies (lower pannel). The relative binding affinity of the fragments is reviewed on the right. "+" low binding, "+++" high binding.

3.2.4 CrTBP1 and its Myb-like domain bind telomeric DNA *in vitro*

Further, we wanted to investigate whether CrTBP1 binds to telomeric DNA. The earlier attempts to express full-length protein in *E. coli* were unsuccessful. We therefore expressed the Myb-like domain of the protein and purified it using the N' terminal 6xHis tag. The Myb-like domain bound 24bp dsDNA with telomeric sequence from *C. reinhardii*, *A. thaliana*, human as well as scrambled DNA sequence in unspecific manner. The complexes did not migrate into the gel. A clear shifted band was seen when using labeled oligo with *C. reinhardtii* telomeric sequence and cold scrambled oligonucleotide. When a cold competitor DNA was used, this decreased the signal of the shifted band. A faint broad band was observed when using human telomeric sequence and cold *C. reinhardtii* competitor (Figure 61).

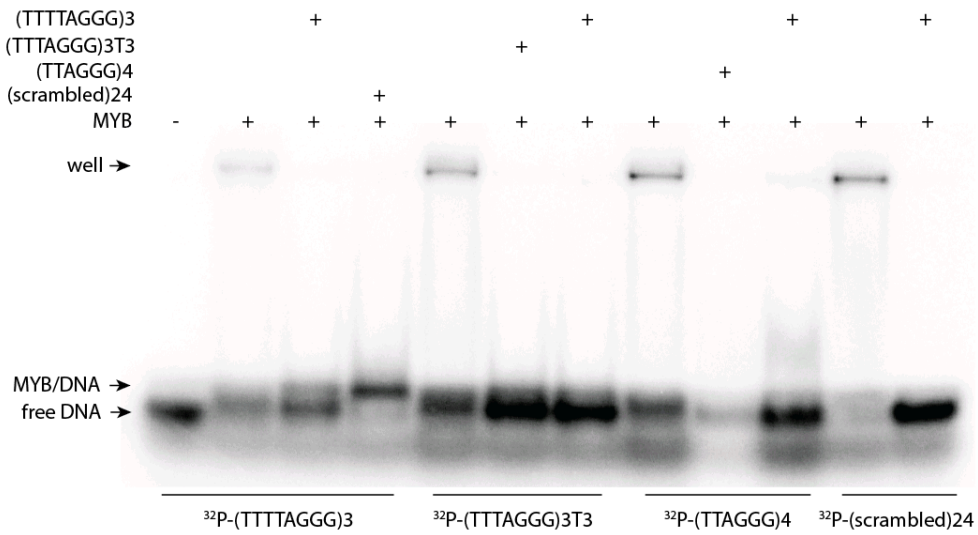

Figure 61: EMSA of Myb-like domain from CrTBP1
C' terminal fragment of CrTBP1 containing Myb-like domain (MYB) was expressed and purified from *E. coli*. Different ^{32}P-labeled oligonucleotides harboring telomeric repeats from *C. reinhardtii* (TTTTAGGG), *A. thaliana* (TTTAGGG) and human (TTAGGG) were used for gel shift assay. Unspecific binding resulted in signal accumulation in well, but was eliminated when using cold competitor oligonucleotides.

Using baculovirus system we were able to purify small amount of full-length N' 6xHis-CrTBP1. This protein was able to bind *C. reinhardtii* telomeric oligo that was labeled using fluorescent dye IRD 800 and scanned using Odyssey from Li-Cor. The product did not migrate as a clear band, but its migration was slower in compare with purified Myb-like domain (Figure 62). This evidence indicates that CrTBP1 is able to bind telomeric DNA of *C. reinhardtii in vitro* via its Myb-like domain. This supports the prediction that it might be a telomere binding protein.

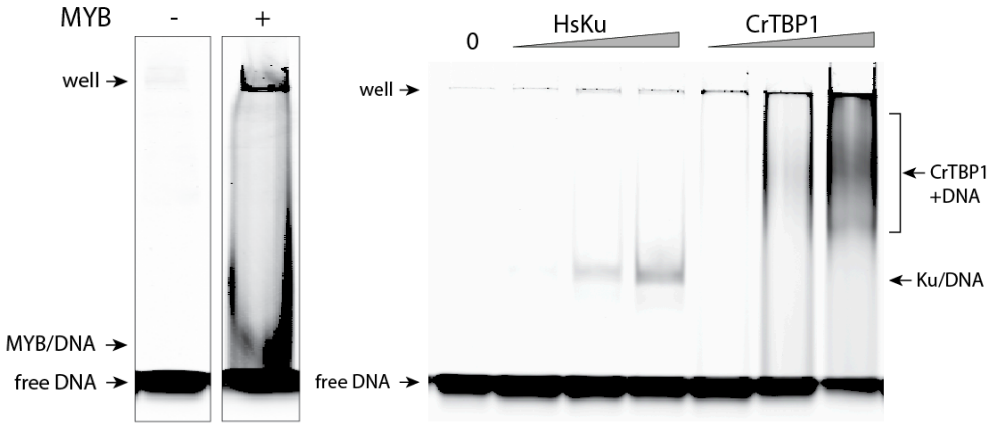

Figure 62: EMSA with CrTBP1 (right) and Myb-like domain (left)
Fluorescent 5'IRD800-(TTTTAGGG)3 oligonucleotide was used to investigate binding of CrTBP1 fragment containing Myb-like domain (MYB, left) expressed in *E. coli* and full length CrTBP1 (right) expressed in insect cells. Human Ku purified from insect cells was used as a positive control for DNA binding.

4 Discussion

4.1 Human and *A. thaliana* Ku complexes differ in DNA binding properties

Ku is a unique evolutionary conserved protein complex that tightly encircles DNA and exhibits strong affinity to DNA ends (Bowater and Doherty 2006; d'Adda di Fagagna et al. 2003). It is involved in important cellular processes such as DNA repair and telomere protection. Studies of mutants revealed slight differences in importance for these functions (Downs and Jackson 2004).

During DSB repair by NHEJ, Ku binds to broken DNA ends and suppresses alt-NHEJ, recombination and nuclease resection (Bombarde et al. 2010; Riha et al. 2006). However, similar mode of interaction and function has also been observed on telomeres (Kazda et al. 2012; Lopez et al. 2011; Wang et al. 2009). The mechanism of NHEJ suppression by Ku on telomeres is not well described. Based on the formation of blunt-ended telomeres in angiosperm plants we propose that limited sliding might provide necessary restriction of NHEJ on telomeres (Kazda et al. 2012). This model is supported by literature describing that sliding is important for NHEJ (Kysela et al. 2003) and enhanced sliding leads to telomere deprotection (Balestrini et al. 2013). We propose that sliding in *A. thaliana* might be limited by telomere binding proteins and by physical hindrance protect newly synthetized blunt ended chromosomes from nucleolytic resection. However, binding and sliding of Ku on DNA might be a result of its inherent structural properties and/or the interaction with proteins. We investigated the binding and sliding properties oh human and Arabidopsis Ku on free DNA. If inherent protein characteristics of AtKu would restrict resection of newly formed chromosome ends, modification of HsKu in this manner could result in formation of blunt-ended telomeres in human cells, assuming Ku needs to bind telomere ends in these organisms as in *S. cerevisiae* (Lopez et al. 2011).

Despite the low primary sequence identity of HsKu and AtKu, predicted structure showed similarity of both complexes. Structural similarity could explain the similar affinity to DNA as observed for short oligonucleotides. Interestingly, when sliding was required for filling all binding sites, Kd of AtKu to this substrate increased. This observation would suggest defect in sliding. However, EMSA showed no sliding defect

in higher protein concentrations. Moreover, it seemed as in higher concentrations of protein, the sliding was better for AtKu than HsKu. While in low protein concentrations there was retention of Ku in complexes that do not require sliding for formation. We also suggest a possibility of different dynamics of DNA/protein association based on the observation of smeared bands of AtKu/DNA. Increased sliding efficiency could explain observation from electron microscopy where AtKu covered most of the DNA, while HsKu was much less abundant. This observation is surprising, because it would suggest that AtKu binds multiple binding sites easier than HsKu what might lead to lower Kd. However, the Kd for 3 binding sites was higher for AtKu. Presence of free DNA in electron microscopy samples could be a sign of possible cooperative binding. If presence of bound protein increases the possibility of binding second protein, the affinity of Ku to free DNA would be the limiting factor for Kd derived from population of proteins. While if at least one Ku protein is bound to all DNA molecules, the filling of all binding sites would be easier for complex with enhanced sliding. Human Ku seems to bind DNA in non-cooperative manner (Arosio et al. 2002; Arosio et al. 2004; Ma and Lieber 2001). Cooperativity would be therefore unique for AtKu. Because enhanced sliding alone could lead to rather excessive exonucleolytic resection (Balestrini et al. 2013) cooperative binding could result in protein aggregation on DNA ends and might explain the presence of blunt-ended telomeres in *A. thaliana* (Kazda et al. 2012). However, involvement of other factors cannot be excluded.

4.2 Structure-based mutagenesis of Ku complexes alter DNA binding properties

Although in *S. cerevisiae* function of Ku at telomeres requires direct binding to telomeric DNA, such evidence is missing for animals and plants (Lopez et al. 2011). Presence of Ku-dependent blunt-ended telomeres and different biochemical properties of AtKu suggest possible involvement of Ku/DNA interaction in telomere biology of *A. thaliana*. To investigate the importance of DNA/Ku interaction in human and *A. thaliana* we decided to engineer Ku complexes with impaired DNA interaction. Previously such mutants were generated for *S. cerevisiae*. Altering charge of residues in DNA binding channel or deletions in bridge region led to disruption of binding between Ku and DNA. Interestingly, changes in residues without direct contact with DNA led to enhanced

sliding, probably due to allosteric changes (Balestrini et al. 2013; Lopez et al. 2011; Pfingsten et al. 2012).

Crystal structure of human Ku allowed us to perform structure-guided mutagenesis. Selected substitutions were later applied to the AtKu complex. Due to the electrostatic nature of Ku/DNA interaction (Arosio et al. 2004) we decided to focus on the charged residues in DNA binding channel. To create diverse mutants with not only abolished binding, we used the fact that Ku loads directionally. Loading face of the complex probably serves as the site of primary contact with DNA (Walker et al. 2001). Lagging face consisting of N-terminus of Ku70 and C-terminus of Ku80 was therefore primarily used to design mutations. Previously, substitution of arginine in this region ScKu70-R265E did not lead to disrupted binding, while residue ScKu70-R456E localized towards the loading face caused abolished binding (Lopez et al. 2011). We assumed that residues important for DNA interaction would be conserved throughout evolution and according to the protein alignment we chose residues that fit our criteria. Interestingly, ScKu70-R265 did not align with the residue HsKu70-R254 as previously published (Lopez et al. 2011). This might be attributed to different conditions of alignment. However, the position in predicted structure of ScKu was very similar to the HsKu70-R254. The alignment for the predicted structure was done by HHPred and might differ from our alignment.

As deletions in bridge region would lead to decrease in DNA channel diameter, we also considered this type of modification. In *S. cerevisae* only large deletions of more than 20 residues in ScKu80 abolished DNA binding (Pfingsten et al. 2012). This is surprising, because the bridge region in HsKu is relatively short (cca 100 residues). However, ScKu80 seem to have an insertion of residues in bridge region in compare with other species. This insertion is visible as loop of 20 residues in predicted structure. Therefore, we decided only for deletion of 2 and 4 residues. However, this deletion was probably too short and did not influence DNA binding of HsKu.

Although, single residue changes led to DNA binding defect in *S. cerevisiae*, we did not observe this extreme effect in HsKu or AtKu. Surprisingly, residue homologous to ScKu70-R456, when substituted in HsKu to HsKu70-R444E did not influence DNA

binding. These differences could be due to the differences in protein structure between ScKu and HsKu, different binding conditions or combination of both factors.

Substitution of several positively charged residues with glutamic acid seem to have additive effect on decreasing binding of Ku to DNA in both HsKu and AtKu. Rather than specific residues, probably the overall positive charge in the channel opposite the bridge has influence on DNA affinity as we observed similar effect in HsKu#18 and HsKu#15.

In the structure of HsKu with DNA we noticed a gap between DNA and the base of the bridge. We found a cluster of negatively charged residues in this region. We anticipated, that position of DNA in the channel near the Ku body might be supported by repulsion from the HsKu80-D299, D300 residues. We confirmed, that substitution HsKu80-D299R, D300R leads to decrease in DNA binding and is altered by additional substitutions in positively charged residues (HsKu80-D299R, D300R, K543E, K544E, K545E) localized on the opposite side of DNA. In AtKu this region contains only one negatively charged residue AtKu80E276 and the substitution was not sufficient to decrease DNA binding in combination with additional substitution of positively charged residues. However, despite unaltered DNA binding, in electron microscopy the mutant AtKu protein complexes appeared less dense in in compare with the wild type complexes. We hypothesize that formation of the dense complexes might be due to cooperative binding. The cooperativity might be partially disrupted in the mutant.

The most interesting observation was the increased amount of terminally located HsKu proteins when five positively charged residues were altered to negative charge (HsKu70-R35E, R80E, K160E, R254E, R258E = HsKu#18). This mutant protein complex had severely decreased DNA binding. Addition of further substitutions (HsKu80-D299R, D300R, K543E, K544E, K545E) led to further decrease in DNA binding, but it did not significantly alter the fraction of terminally localized Ku complexes. Ku was not enriched in subterminal region and was able to localize centrally on DNA. From this data, we conclude that these mutants may have affected the efficiency of sliding. In AtKu mutation of homologous residues also led to the decrease DNA binding. Unfortunately, it was not possible to analyze wild type complexes with electron microscopy in similar fashion as in HsKu and therefore sliding could not be analyzed.

We propose that Ku/DNA interaction probably consists of three stages: 1) initial contact of Ku loading face with DNA, 2) transitional docking of DNA into the channel 3) diffusion of Ku inwards (Figure 63). Binding of Ku to DNA leads to conformational changes (Lehman et al. 2008). Such changes might support the transition between steps 2 and 3. Conformational changes could lead to “locking” the Ku onto DNA and preventing from backwards diffusion. Such speculation leads to the question whether Ku is able to diffuse in both directions. Assuming Ku does not require ATP for its movement, thermal movement could provide necessary kinetic energy. Restricting the motion along the DNA can focus this energy to lateral movement. Restriction in backwards motion could further increase the efficiency of sliding. Such restriction could explain the rapid sliding that has been observed. Disruption of unidirectional motion block would lead to lower efficiency of sliding and would allow diffusion of Ku away from the DNA end. Furthermore, Ku that is not able to transition into the step 3 might appear as having lower affinity, because no stable DNA/protein complexes are formed. However, the transient association might prevent other proteins to associate and result in overall increase in Kd. Indeed, we observed increase in Kd of mutant complexes, while the number of terminally located Ku per DNA end was not lower than in wild type complex. This suggests that sliding of Ku might be influencing the observed DNA affinity.

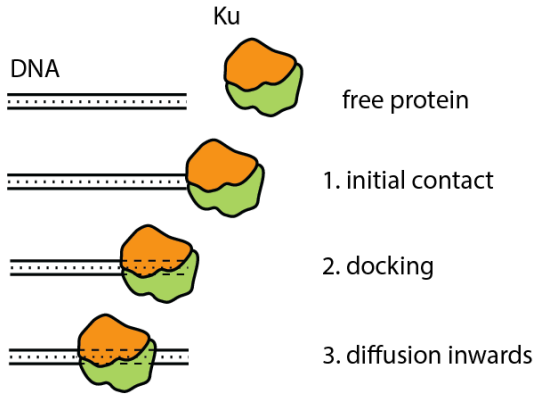

Figure 63: Proposed stages of Ku/DNA interaction
Ku/DNA interaction may consist of three stages: 1) initial contact of Ku loading face with DNA, 2) transitional docking of DNA into the channel 3) diffusion of Ku inwards (sliding).

The increase in sliding causes Ku to fail to inhibit ExoI nuclease degradation of DNA (Balestrini et al. 2013). Presence of Ku on the DNA terminus, even if transient,

might protect DNA from resection. If the association of Ku with telomeric DNA is necessary for its protective function, it might be linked to the sliding. Decreased sliding might be sufficient for telomere protection and even promote formation of blunt-ended telomeres regardless of the telomere chromatin. However, because inward translocation is important for NHEJ (Turchi et al. 2000), such mutant complex would cause increased sensitivity to DSB inducing agents. DSBs protected by Ku could mimic telomeres and lead to cell death due to chromosome fragmentation. Alternatively, transient association of Ku with DNA end might not be sufficient to promote C-NHEJ. Abolished binding of Ku to DNA led previously to decrease in DNA repair in *S. cerevisiae* (Lopez et al. 2011).

Investigation of the effect of HsKu#18 in human cells would be extremely interesting. Since telomeric protection by Ku is essential for cellular survival, such separation of function mutant would be extremely useful. We therefore established collaboration and attempted to complement human cells with mutant complex. Unfortunately, despite detectable protein expression, we were not able to complement Ku deficiency. Low protein expression could be a possible explanation. Even loss of one allele leads to haploinsufficiency (Li et al. 2002). *A. thaliana* does not exhibit haploinsufficiency and thanks to the available mutants and genetic tools presents a good alternative for studying the effect of Ku mutations. Although the complexes HsKu and AtKu differ, the effect of the mutations may give us hint about the role of DNA/protein interaction in telomere biology.

4.3 Altered Ku/DNA binding properties affect telomere maintenance and DSB repair in *A. thaliana*

Previous studies indicated that direct DNA binding and sliding of Ku on telomeres is important for telomere protection in budding yeast (Balestrini et al. 2013; Lopez et al. 2011). Presence of blunt-ended Ku-dependent telomeres might suggest necessity of Ku directly binding to telomere ends to mediate this protection also in Arabidopsis (Kazda et al. 2012). As in human cells, Arabidopsis Ku suppresses homologous recombination and excision of t-circles. It also negatively regulates telomere maintenance presumably by limiting formation of substrate for telomerase, single stranded G-overhangs (Kazda et al. 2012; Zellinger et al. 2007). Ku mutants therefore exhibit elongated telomeres, more ssDNA of G-overhangs and presence of telomeric circles accompanied by

transformation of blunt ended telomeres to G-overhang containing telomeres. Furthermore, plants mutant in Ku do not exhibit developmental defects unless treated with DSB inducing agents (Riha et al. 2002) suggesting that Ku depleted telomeres are fully functional and likely adopt an alternative capping state.

Most of the results of complementation studies presented in this work are preliminary. Further detailed investigation will follow to accurately describe the effect of the mutant complexes in clean background. However, we were able to analyze several independent insertion likes in mutant background. Although we could still observe segregation of insert in T2 generation, analysis of several lines gave us valuable information regarding the effect of mutations on telomere maintenance and DSB repair.

Extremely interesting separation of function was observed when analyzing T2 generation of Ku70 complemented with the AtKu70#18. This complex showed decrease in DNA binding *in vitro*, however the effect on sliding could not be investigated. The human counterpart did exhibit increase in number of terminally localized Ku. Telomere length varied between different insertion lines and although the average was significantly higher than wild type complex, the increase was only 1,3-fold. Variation in telomere length could be partially explained by different protein levels. Interestingly, the sensitivity to DSB induced by bleocin was very high and significantly higher than in wild type. This observation would support the hypothesis that sliding restriction is crucial for telomere protection, while its release is necessary for NHEJ. Further analysis of G-overhangs and blunt-ends need to follow to investigate this hypothesis.

Results of complementation of Ku80 with the AtKu#13 mutant complex were surprising. Based on EMSA and fluorescence anisotropy, the complex seemed to have similar affinity to DNA as wild type complex. The only evidence of possible defect comes from electron microscopy where we observed less dense occupation of DNA molecules. We suggested that it might be due to disruption of potential cooperative binding. We also suggested that enhanced sliding with cooperative binding could result in aggregates of Ku on telomeres protecting the ends from nucleases. Deprotection would lead to resection that might increase the amount of substrate for telomerase and increase telomere length. Further, resection would allow DSB repair by HR or alt-NHEJ. Extensive resection and homologous recombination would lead to accumulation of t-

circles. In T2 generation we could observe increase in telomere length greater that it was observed in Ku70 complementation (1,5-fold). This effect got more pronounced in T3 generation in single line that was analyzed. This might be attributed to a clean homozygozity of insertion and different level of expression. Other insertion lines need to be analyzed. However, the DSB sensitivity was not severely affected. In T2 generation DSB sensitivity was not significantly different from wild type complex. Although in T3 generation we could observe severe telomere phenotype and partial DSB sensitivity. In the single line form T3 generation we could detect also increased signal from G-overhangs indicating that telomeres are not sufficiently protected from nucleases. These findings would support that AtKu enhanced sliding ability when present without cooperative binding might lead to decrease in nuclease protection *in vivo*. In future will be these findings investigated in multiple insertion lines.

Finally mutations that alter DNA interaction of Ku can effect telomere protection, maintenance and DSB repair. This indicates that direct interaction of Ku might in *A. thaliana* play important role as observed in *S. cerevisiae*.

4.4 Putative telomere binding protein in *C. reinhardtii*

Telomeric DNA is present in complex with several telomere binding proteins. TBPs were previously implicated in suppression of NHEJ on telomeres in different organisms (Riha et al. 2006). It is possible that presence of telomere binding proteins could restrict sliding of Ku protein on DNA and provide a possible explanation for formation of blunt-ended telomeres and protection in *A. thaliana*. The TRF2 interaction with Ku has been implicated in regulation of NHEJ also via protein-protein interaction (Ribes-Zamora et al. 2007; Ribes-Zamora et al. 2013). Unfortunately, due to gene redundancy it is still unknown what proteins form the Shelterin complex in plants. To identify plant Shelterin complex we used *Chlamydomonas reinhardtii*, algae closely related to the plant lineage. *C. reinhardtii* is an excellent model organism for biochemistry thanks to its easy cultivation and availability of strains lacking a rigid cell wall.

We analyzed telomeres in *C. reinhardtii* to ensure that the telomeres are similar to land plants. Telomere length was shorter than in *A. thaliana*, but longer than in *S. cerevisiae* (Riha et al. 2006). And, similarly to other organisms, we could observe

variability in telomere length between analyzed strains. Although *C. reinhardtii* lacks nucleosomal structure in telomeric region, the absence of nucleosomes cannot be confirmed. Part of the telomeric sequence is protected from micrococcal nuclease in a telosome fashion and might be protected by telomere binding proteins (Dmitriev et al. 2003; Liu et al. 2004; Xin et al. 2008).

We identified putative TBP using *in silico* approach. We looked for the presence of telobox sequence (Peska et al. 2011) and identified two proteins. CrTBP1 harbor C-terminal Myb-like domain and CrTBP2 contain N-terminal telobox sequence. CrTBP1 was investigated in detail because it shares similarity with TRF1 and TRF2 proteins forming Sheltein in mammals. Unfortunately, our attempts to express tagged CrTBP1 in *C. reinhardtii* or miRNA knockdown were unsuccessful. We therefore tried to confirm presence of the protein in nucleus my mass spectrometry. Based on the mass spectrometry data of CC-4350 strain from Luis Valledor (unpublished) this protein is relatively low abundant and is only detectable in nuclear fraction. This finding suggests its possible nuclear localization. Furthermore we confirmed that CrTBP1 forms dimers *in vitro*. Dimerization domain could be used as dominant negative peptide to investigate telomeric function of CrTBP1 (van Steensel et al. 1998). However, we could not identify dimerization domain as the data suggests presence of two or one large domain. Point mutations in telobox might serve similar purpose as dominant negative allele, but it would require further biochemical confirmation.

We further wanted to investigate whether CrTBP1 can bind telomere sequence *in vitro*. The expression of recombinant CrTBP1 was difficult and therefore we expressed the Myb-like domain in *E. coli*. This domain successfully binds TTTTAGGG repeats *in vitro*. Affinity to TTAGGG cannot be excluded, however the slight shift that was observed could be also due to nonspecific binding. A small amount of full length CrTBP1 was obtained from insect cells. This protein was shown to form complexes with *C. reinhardtii* telomere sequence as well.

CrTBP1 is a nuclear protein with Myb-like domain containing conserved telobox sequence, forming homodimers and binding telomere sequence *in vitro*. It presents a good candidate for telomere binding protein in *C. reinhardtii*. However, the *in vivo* role in telomere protection needs to be investigated. With current advancement of

CRISPR/Cas9 technology (Jiang et al. 2013) or emerging insertional mutant library for *C. reinhardtii* (Zhang et al. 2014) it might be possible to analyze function of CrTBP1. However, expression of tagged protein and affinity chromatography would be invaluable for identification of Shelterin subunits.

5 Materials and Methods

5.1 Bacteria

5.1.1 Strains and growth conditions

Bacterial strains used in this study are shown in the Table 4. *E. coli* were grown at 37°C or 28°C on solid or liquid LB medium (10 g peptone, 5 g yeast extract, 25 g NaCl or commercially available Bertoni mix (10 g tryptone, 5 g yeast extract, 10 g NaCl)) while aeration. *A. tumefaciens* were grown at 28°C on solid or liquid LB medium. Medium was supplemented with appropriate antibiotics in concentrations ampicilin and kanamycin 50µg/ml. chloramphenicol 34 µg/ml, gentamycin 50 µg/ml.

Table 4. List of bacterial strains.

Species	Strain
Escherichia coli	DH5α
	Rosetta (DE3)pLys
Agrobacterium tumefaciens	CV3101

5.1.2 Transformation of competent *E. coli* cells

Chemically competent *E. coli* were thawed on ice and plasmid DNA was added. The cells were mixed gently and incubated on ice for 5 min. Heat shock (42 °C for 45 sec) was applied and after incubation on ice for 2-5 min, LB medium was added. Cells were incubated at 800 rpm for 30-60 min at 37°C. The cells were collected by centrifugation at 2700 g for 3 min and resuspended in 100 µl LB medium and plated on LB plates with appropriate antibiotic and grown overnight at 37°C.

5.1.3 Agrobacterium transformation by electroporation

Electrocompetent *Agrobacterium tumefaciens* (strain GV3103) cells were thawed on ice. 10 – 100 ng of a plasmid DNA was added and the mixture was transferred to a precooled cuvette. The cuvette was placed in the electroporation chamber and the cells were charged with the following paramerter: 400 Ω, 25 µF and 1,8 kV for a 1 mm cuvette or 2,5 kV for a 2 mm cuvette (GenePulser Xcell, BioRad). The length of the pulse was 5 – 8 msec. Quickly, 1 ml of LB media was added and the cells were transferred to a microcentrifuge tube. Cells were incubated for 1 hr without movement at

room temperature. 100 µl of transformation mixture was plated on LB medium with appropriate antibiotics and incubated for 2 - 3 days at 26°C.

5.1.4 Plasmid extraction

Bacteria were grown over night in LB medium or 8 hours in 2xTY at 180 rpm in a tube with appropriate antibiotics. 2-5 ml of overnight culture were spun down at 16100 xg for 15 sec. The pellet was resuspended in 250 µl resuspension buffer (50 mM Tris-HCl pH 8,0, 10 mM EDTA pH 8,0, 200 µg/mL RNaseA) and mixed gently by inverting 3-5 times with 250 µl lysis solution (200 mM NaOH, 1% SDS). The lysis reaction was neutralized by gentle mixing with 300 µl neutralization buffer (3M KOAc pH 5,5). The debris was spun down at 16100 g for 6 min, and the plasmid DNA in the supernatant was precipitated by adding 600 µl isopropanol, vortexed for 1 min and pelleted by centrifugation at 16100 g for 1 min. The pellet was washed with 500 µl 70 % ethanol, pelleted at 16100 g for 2 min, dried at 37 °C for 10 min, and resuspended in 50 µl dH20.

5.2 Chlamydomonas reinhardtii

5.2.1 Strains and growth conditions

Strains used in this study are listed in Table 5. *C. reinhardtii* was grown in liquid TAP media (Gorman and Levine 1965; Hutner 1950) at 100-120 RPM, supplied with L-arginine (100 µg/ml) for strain CC-4350, under constant illumination at 22°C. For solid medium 1% agar was added to TAP media. Strains were stored at +4°C and passaged on solid media monthly.

Table 5. List of strains of *C. reinhardtii*

Strain	Source
CC-4350 cw15 arg 7-8 mt + (X302)	Miroslava Slaninova Prif UK, Slovakia
CC-1690 WT mt+ (21gr)	
CC-124 WT mt-	
CC-125 WT mt+	
CC-620 WT mt+	
CC-621 WT mt-	
CC-503 cw92 mt+	Luis Valledor, Austria

5.2.2 Genomic DNA extraction from *C. reinhardtii*

Liquid TAP medium was inoculated and cells were grown for three days while aeration. Biomass was pelleted and 7 mL of 2xCTAB DNA extraction buffer (2 % w/v CTAB (hexadecyltrimethylammonium bromide, Fulka), 1,4 M NaCl, 100 mM Tris-HCl pH 8,0, 20mM EDTA pH 8,0) per 100ml of culture was added and the samples were incubated at 65°C for 30-60 min. DNA was extracted with an equal volume of phenol:chlorophorm:isoamylalcohol (50:49:1). DNA was precipitated from aqueous phase with 0,8x isopropanol and centrifugation for 10 – 30 min at 16100 xg. The pellet was washed with 800 µl 70 % ethanol and resuspended in 200 µl TE (10 mM Tris-HCl, 1mM EDTA, pH 8,0). 10-20 mg/ml RNase A was added during the to isolated DNA and removed by equal volume of phenol:chlorophorm:isoamylalcohol (50:49:1) followed by chlorophorm:isoamylalcohol (49:1) and next round of DNA precipitation.

5.2.3 RNA isolation and reverse transcription

For total RNA extraction 1-5 ml of three-day liquid culture was pelleted. Pellet was resuspended in 0,5-1 ml of TRI RNA extraction reagent (Sigma) and incubated for 10 min at room temperature. RNA was extracted with 100-200 µl chloroform, vortexed, and incubated for 10 - 15 min at room temperature followed by centrifugation at 16100 xg for 10 min at +4°C. The RNA in the aqueous phase was precipitated by addition of 0,8x isopropanol and incubated for 10 – 15 min at room temperature, followed by centrifugation at 16100 xg for 10 min at +4°C. The pellet was washed with 70 % ethanol, air dried, and resuspended in 50 µl nuclease free water. For storage RNA was frozen at -80°C.

5.2.4 Isolation of nuclei

Nuclear fraction was prepared from cell wall mutant CC-4350. Exponentially growing cells (2 days in liquid culture) were gently spun and thoroughly resuspended in 90 ml Buffer A per 1 L of culture (25 mM Hepes-NaOH, pH 7,5, 20 mM KCl, 20 mM MgCl2, 600 mM sucrose, 10% (v/v) glycerol, 5 mM DTT). Triton X-100 was added to a final concentration of 0.5%. It was first diluted in 10 ml of Buffer A per 1 L of culture and subsequently added drop-wise to the cells while swirling them gently. Nuclei were pelleted at 800 xg 2-4 minutes. Using a paintbrush, pellet was gently resuspended in

fresh Buffer A without Triton X-100. After centrifugation integrity of nuclei (1-5 ul) was checked using DAPI/vectashield (5 ul) and fluorescent microscope. Nuclei were resuspended in Buffer B (2,5% (w/v) Ficoll 400, 0, 5M sorbitol, 0.008 % spermidine (w/v), 50 % (v/v) glycerol, 1 mM DTT), 1-2 ml per 200 ml of original culture volume. For storage, nuclei were frozen in liquid nitrogen and stored on -80°C.

5.3 Arabidopsis thaliana

5.3.1 T-DNA insertion lines and growth conditions

T-DNA insertion lines used in this study are listed in Table 6. Plants were grown at 22°C, with 16 hrs light on soil (ED 63) mixed 3:1 with vermiculite. Alternatively, sterilized seeds were sown on 1/2 MS plates (2,21 g/l Murashige and Skoog complete salts incl. vitamins and MES buffer (Duchefa), 10 g/l sucrose, 8 g/l agar, pH 5,7) and grown at 25°C with 16 hrs light.

To synchronize germination, seeds were stored at +4°C for 1-3 days.

Table 6. List of used T-DNA insertion lines of *A. thaliana*.
Seeds of segregating line were obtained from SALK.

Allele	Ecotype	AGI code	Insertion line
ku70-2	Columbia 0	At1g16970	SALK_123114
ku80-7	Columbia 0	At1g48050	SALK_112921

5.3.2 Seed sterilization

Seeds for soil cultivation were washed for a few seconds with 70 % ethanol and rinsed 3 times with sterile water or let dry on filter paper in laminar flow hood.

Seeds for medium cultivation were washed several seconds with 70 % ethanol and then sterilized with freshly made 50 % bleaching solution (Clorox bleach ~ 6 % sodium hypochloride; DanKlorix) containing a few drops of Triton X-100. After incubation in rotational shaker for 7 min seeds were washed 3 times with sterile water.

5.3.3 Floral dip transformation of plants with *Agrobacterium tumefaciens*

Single colony of *A. tumefaciens* containing complementation plasmid DNA was inoculated in 5 ml LB medium supplemented with 50 µg/ml gentamycin and 50 µg/ml kanamycin and grown at 28°C overnight while aeration. 1ml of the inoculated culture

was added to 500 ml LB medium and the culture was incubated at 28°C overnight. Culture was centrifuged at 1500 xg for 10 min and the pellet was resuspended in 250 ml 5 % sucrose containing 200 µl/l SilwetL 77 (Lehle seeds). For transformation, flowering plants were dipped in the solution for 30 sec and then grown under normal conditions. Infection was repeated after 5 days.

5.3.4 Basta selection

For selection of seedlings on soil, sterilized and dried seeds were evenly spread and germinated on soil. Seven days old seedlings were sprayed with Basta® solution (40 µg/ml Basta glufosinat ammonium; Bayer). Spraying was repeated after 1-2 days. Alternatively, seedlings were selected on 1/2 MS plates supplemented with 20 µg/ml Basta. Resistant seedlings were transferred to 1/2 MS plates without selection prior transferring on soil.

5.3.5 Bleocin treatment

1/2 MS plates were supplemented with 50 or 100 ng/ml bleocin (Calbiochem). Sterilized seeds were germinated and grown for 11-15 days. The effect of the DNA DSB inducing agent on formation of true leaves was examined. Plants with no true leaves, one true leaf or asymmetric true leaves were categorized as sick and and % of sick plants was calculated.

5.3.6 Protein isolation

Total protein was extracted from two leaves, inflorescences or seedlings. Material was homogenized with blue pestle in 2x extraction buffer (100 mM Tris-HCl pH 7,5, 20 % glycerol, 0,2 % NP-40, 2 mM EDTA pH 8,0, 1 mM DTT, 1x protease inhibitors (Complete Mini, Roche) were added just before use). The cell lysate was cleared by centrifugation at 16100 xg for 10 min. The supernatant was stored at -80°C.

5.3.7 High throughput PCR grade DNA extraction from *A. thaliana*

One metal bead (3 mm) was added to 1-2 leaves and 200 µl DNA extraction buffer (200 mM Tris-HCl pH 8,0, 250 mM NaCl, 0,5 % SDS, 25 mM EDTA pH 8,0) in microtiter tubes. Leaves were disrupted with two runs with the Schwingmühle Retsch® MM400 at 30 Hz for 4 min. The tubes were inverted between the two runs in order to treat all samples equally. The samples were centrifuged at 2500 g for 15 min and the DNA in

the supernatant was precipitated with an equal volume of isopropanol and centrifugation at 2500 g for 15 min. The pellet was washed with 500 µl 70 % ethanol, dried at 56°C for at least 30 min and resuspended in 100 µl TE buffer. 2 µl were used per PCR reaction. DNA was stored at -20°C.

5.4 Human cells

5.4.1 Cell lines and growth conditions

Cell lines used in this study are listed in Table 7. All were obtained from the laboratory of Eric Hendrickson, University of Minnesota. Cells were grown in McCoy's 5a (Corning) growth medium at 37°C, 5 % CO_2 and humidity. Growth medium was supplemented with 10 % Fetal bovine serum (Corning), 1 % L-Glutamine (Gibco 200mM), 1 % Penicillin-Streptomycin (10 000 U/ml, Gibco). For selection were used 0,5 mg/ml G418-sulphate (Corning) and 1 µg/ml Puromycin (Gibco). For activation of Cre recombinase 5 nM 4-Hydroxytamoxifen (Sigma) was used.

Table 7: List of used cell lines

Cell line	Genotype	Organism	Origin tissue	**Growth medium**
HCT116		human	colorectal carcinoma	McCoy's 5a
HCT116	Ku70 Flox/- CRE-ER T2 12-6	human	colorectal carcinoma	McCoy's 5a
HCT116	Ku86 Flox/- CRE-ER T2 #19	human	colorectal carcinoma	McCoy's 5a

5.4.2 Transfection and selection of stable lines

6,25 x 10^5 cells were plated per well in 6-well plate and grown overnight. Medium was replaced with 2 ml of fresh media. Transfection reaction (500 µl OptiMEM, 1,25 µg of helper plasmid pPBTS, 1,25 µg donor plasmid pDEST-CG-Ku (70WT, 7018, 80WT, 8013), 10 µl LipoLTX) was incubated RT for 30 min and added drop wise to respective cell line. Next day, media from cells was replaced it with 2 ml of fresh media and after 24 hours TrypLE (Gibco) was used to detach cells and Countess (Invitrogen) with trypan blue was used to determine viable cell number. Different cell numbers ($5x10^3$, $10x10^3$, $20x10^3$, $50x10^3$, $100x10^3$) were plated per 10 cm Petri dish in selection media (0,5 or 1,0 mg/ml G418). After two weeks, colonies were picked with pipette tip and

transferred into 50 µl of trypsin. Spread cells evenly and add medium to inactivate trypsin.

5.4.3 Isolation of proteins

Trypsinized cells were washed in PBS buffer (137 mM NaCl, 2,7 mM KCl, 8 mM Na_2HPO_4, 2 mM KH_2PO_4). After centrifugation at 500 g for 2-4 minutes, pellet was resuspended in lysis buffer (10 mM Tris pH7,4, 150mM NaCl, 1 % NP-40, 0,5 % Sodium Deoxycholate, 1 mM EDTA, 1 mM DTT, Complete mini (Roche) protease inhibitors). Debris was spun down at 16100 xg at 4°C for 15 min and supernatant was stored at -80°C.

5.5 DNA protocols

5.5.1 cDNA synthesis

RNA was treated using the TURBO DNA-free Kit (Ambion) according to the manufacturer's instruction. DNA-free RNA was used to synthesize cDNA with the ThermoScript™ Reverse Transcriptase (Life technologies) according to the manufacturer's instruction.

5.5.2 PCR

PCR was used for cloning and genotyping of *A. thaliana*. For cloning, Phusion or Phusion Hot start (New England Biolabs) was used according to manufacturer's instructions.

For genotyping, GoTaq with Green reaction buffer (Promega) was used. Total volume of 20 µl contained 1 x GoTaq reaction buffer (Promega), 0,2 mM dNTPs, 0,5 µM right primer, 0,5 µM left primer, 0,5 U Go Taq DNA polymerase and 2 µl template. The PCR program was the following: 95°C for 3 min; 35 cycles of 95°C for 30 s, 55°C for 30 s, 72°C for 60s; and finally 72°C for 7 min.

Primers used for genotyping are shown in Table 8. Complementation constructs lack several intron sequences and special primer combinations were used to detect wild type allele, T-DNA insertion and complementation construct (Table 9). For Ku80 complementation constructs, primer combination LP/RP was used. This pair amplifies also wild type allele, but due to competition only in absence of insert. Further, product from complementation construct is shorter than wild type.

Table 8: Primers used for genotyping *A. thaliana*

Primer name	sequence
AtKu70_LP	TTACTTTGTTGTTTCGGGTGC
AtKu70_RP	CTCTTGGCAAGTACACGCTTC
AtKu70_B	GAAAAAGAGGCTTCCAAAGAATTTGTAGTC
AtKu80_LP	ACCAAAGATCCATTTGAAGGG
AtKu80_RP	CGTGGATTTCGATTTCAACTC
AtKu80_B	ATTTCATCAGTATGAGTTGAC
Left border primer LBb1.3	ATTTTGCCGATTTCGGAAC

Table 9: Primer combinations for genotyping

gene	wild type allele	T-DNA insertion	complementation construct
AtKu70	LP/RP	RP/LBb1.3	RP/B (728 bp)
AtKu80	LP/B (LP/RP)	RP/LBb1.3	LP/RP (shorter than WT)

5.5.3 Cloning

5.5.3.1 Restriction cloning

Primer pairs were designed to amplify target sequence containing necessary restriction sites flanked with ATAT sequence to allow direct restriction digest of amplified PCR product. Usually PCR product was first separated on agarose gel and extracted using Nucleospin Extract II kit (Macherey Nagel) or Qiaex II (Qiagen). Restriction digest was performed according to manufacturer's instructions and another round of purification was performed.

When digesting vector, restriction digest was followed by treatment with 1 µl shrimp alkaline phosphatase (SAP; Fermentas) at 37°C for 30-60 min. SAP was inactivated by incubation at 65 °C for 10 min. When necessary, correct fragment was purified from agarose gel.

For ligation reaction a 3:1 ratio of insert : vector was used. Usually 50 ng of vector was used. 10 units of T4 DNA ligase (Fermentas) was used in 1x T4 DNA buffer (400 mM Tris-HCl, 100 mM MgCl2, 100 mM DTT, 5 mM ATP pH 7,8) for at least 1 hour. The entire reaction volume was used for transformation of chemically competent cells.

5.5.3.2 Site-directed mutagenesis in vitro

For generating point mutations and small deletions or insertions two complementary oligonucleotides were synthetized (Table 10, Sigma) containing the mutation with approx. 15 bases on each side. Template plasmid (100-150 ng) was purified from DH5α cells. 5 U of Pfu polymerase (Promega) was used to perform oligonucleotide extension. The polymerase reaction was performed in 1x Pfu Buffer supplied with $MgSO_4$ (20 mM Tris-HCl (pH 8,8 at 25°C), 10 mM KCl, 10 mM (NH4)2SO4, 2 mM MgSO4, 0.1 % Triton® X-100 and 0,1 mg/ml nuclease-free BSA), 200 µM each of dATP, dGTP, dCTP, dTTP (Fermentas) and 1 µM of each oligonucleotide in a final volume of 40 µl. Program: 95°C 1', [95°C 30'', 55°C 40'', 71°C 7'30''] 20x, 71°C 15'. After polymerization 5 µl TANGO buffer (Fermentas) was added to the reaction and the template DNA was digested using 20 U DpnI (Fermentas) for 2 hours on 37°C. Reaction was inactivated 20' on 80°C. 5-10 µl were used for transforming chemically competent cells. Two colonies were sufficient for analysis in most cases. At least one contained the mutation. In 1 of 29 colonies an additional mutation was detected in gene. Vector sequence was not analyzed. Deletion up to 6 bases could be performed in single step.

Table 10 oligonucleotides used for site directed mutagenesis

Primer name	sequence
AtKu70 R256E_f	CGTGTACTTGCCAAGgaAATAGCAAAAAGAAT
AtKu70 R256E_r	ATTCTTTTTGCTATTtcCTTGGCAAGTACACG
HsKu70 R35E_f	ACTATAAATATTCAGGAgaAGATAGTTTGATT
HsKu70 R35E_r	AATCAAACTATCTtcTCCTGAATATTTATAGT
HsKu70 R80E_f	ATCATAAGCAGTGATgaAGATCTCTTGGCTGT
HsKu70 R80E_r	ACAGCCAAGAGATCTtcATCACTGCTTATGAT
HsKu70 K160E_f	AGTGATGTCCAATTCgAGATGAGTCATAAGAG
HsKu70 K160E_r	CTCTTATGACTCATCTcGAATTGGACATCACT
HsKu70 R254E_f	CAAGGAGACCAGGAAGgaAGCACTCAGCAGGT
HsKu70 R254E_r	ACCTGCTGAGTGCTtcCTTCCTGGTCTCCTTG
HsKu70 R258E_f	AAGCGAGCACTCAGCgaGTTAAAGCTGAAGCT
HsKu70 R258E_r	AGCTTCAGCTTTAACtcGCTGAGTGCTCGCTT
HsKu70 K297E_f	ACAAATGAACCAGTGgAAACCAAGACCCGGAC
HsKu70 K297E_r	GTCCGGGTCTTGGTTTcCACTGGTTCATTTGT

HsKu70 R444E_f	TTGCTGATGATAAAgaGAAGATGCCCTTTACT
HsKu70 R444E_r	AGTAAAGGGCATCTTCtcTTTATCATCAGCAA
HsKu70 delta(301R, 302T)_f	CAGTGAAAACCAAGACCTTTAATACAAGTACAGG
HsKu70delta(301R, 302T)_r	CCTGTACTTGTATTAAAGGTCTTGGTTTTCACTG
HsKu80 D299R, D300R_f	GTTTATTGCTTAAATagaagaGATGAAACTGAAGT
HsKu80 D299R, D300R_r	ACTTCAGTTTCATCtcttctATTTAAGCAATAAAC
HsKu80 K543E, K544E, K545E_f	CTGATTGAAGCCgAGgAAgAGGATCAAGTGACT
HsKu80 K543E, K544E, K545E_r	AGTCACTTGATCCTcTTcCTcGGCTTCAATCAG
HsKu70 R254A_f	CAAGGAGACCAGGAAGgcAGCACTCAGCAGGT
HsKu70 R254A_r	ACCTGCTGAGTGCTgcCTTCCTGGTCTCCTTG
HsKu70 delta(299K, 300T, 301R, 302T)_f	ATGAACCAGTGAAAACCTTTAATACAAGTACAGG
HsKu70 delta(299K, 300T, 301R, 302T)_r	CCTGTACTTGTATTAAAGGTTTTCACTGGTTCAT
AtKu70 K28E_f	GAAAAAGAGGCTTCCgAAGAATTTGTAGTCTA
AtKu70 K28E_r	TAGACTACAAATTCTTcGGAAGCCTCTTTTTC
AtKu70 R76E_f	TCATATTATCAATgaGTCAAATGATGAAAT
AtKu70 R76E_r	ATTTCATCATTTGACtcATTGATAATATGA
AtKu70 K165E_f	AAAGGATCTTTAgAGACAGCAGATAAACGCA
AtKu70 K165E_r	TGCGTTTATCTGCTGTCTcTAAAGATCCTTT
AtKu70 R269E_f	AGgaAATAGCAAAAgaAATTACGTTTGTGAT
AtKu70 R269E_r	ATCACAAACGTAATTtcTTTTGCTATTtcCT
AtKu80 E276R_f	TACAAAGTTACTGCAagATCTACTGAGGTTATT
AtKu80 E276R_r	AATAACCTCAGTAGATctTGCAGTAACTTTGTA
AtKu80 K518E, L519E, K520E_f	AAGGAGAATCCAgAGgaGgAGAAGGCTTCTAAG
AtKu80 K518E, L519E, K520E_r	CTTAGAAGCCTTCTcCtcCTcTGGATTCTCCTT

5.5.3.3 Vectors for Insect cell expression of Ku

The coexpression vector pFastBac Dual (Invitrogen) contains two promoters: Polh and P10 and was used for insect cell expression. First, the HsKu80 or AtKu80 were cloned into pFastBac HTA (Invitrogen) vector to introduce the N'terminal 6xHis tag. AtKu80 cDNA was amplified from plasmid pCBJ02 from our laboratory using primers At80_HL/HR. Human HsKu70 and HsKu80 were amplified from HeLa cDNA kindly provided by Johannes Popov. Restriction enzyme combinations NcoI/NotI and

BamHI/NotI were used for AtKu80 and HsKu80 respectively to digest PCR products and vectors. Prior ligation by T4 ligase (Thermo scientific), vectors were treated by shrimp alkaline phosphatase (Thermo scientific).

AtKu80 was then digested from pFastBac HTA using CpoI/NotI. Overhang was filled in using Klenow fragment (Thermo scientific) and fragment was cloned into pFastBac Dual under PolH promoter in SmaI site. Ligation was done with T4 ligase (Thermo scientific). HsKu80 was amplified from pFastBac HTA using primers Hs80_DL/DR, digested and cloned into XhoI/NheI site.

AtKu70 was amplified from plasmid pCBJ01 from our laboratory using primers At70_DL/DR. HsKu70 was amplified from Hela cDNA using Hs70_DL/DR. Fragments and vectors were digested with BamHI/SpeI and Ku70 was ligated under the P10 promoter with no tag attached.

AtKu70 contained four mutations R117K, A155A, Q256Q, V462 that originated from template. R117K was corrected by site-directed mutagenesis *in vitro* using primers AtKu70 K117R_f/r. HsKu70 contained silent mutation T524T that was not corrected. All primers are listed in Table 11.

Table 11: List of primers used to clone Ku to pFastBac Dual

Primer name	sequence
At70_DL	ATATGGATCCATGGAATTGGACCCAGAT
At70_DR	ATATACTAGTTTATTTACCAATGTGAGT
At80_HL	ATATCCATGGCACGAAATCGGGAGGGTT
At80_HR	ATATGCGGCCGCTTAGCTCTCGAGCATTGAC
AtKu70 K117R_f	CCGTCCAACAGCGAGGCTGATTAAAGAATTCG
AtKu70 K117R_r	CGAATTCTTTAATCAGCCTCGCTGTTGGACGG
Hs80_HL	ATATGGATCCAGTGCGGTCGGGGAATAAGGCA
Hs80_HR	ATATGCGGCCGCTTATATCATGTCCAATAAATC
Hs70_DL	ATATGGATCCATGTCAGGGTGGGAGTCATAT
Hs70_DR	ATATACTAGTTTAGTCCTGGAAGTGCTTGGT
Hs80_DL	ATATCTCGAGGTCCGAAACCATGTCGTA
Hs80_DR	ATATGCTAGCTTATATCATGTCCAATAA

5.5.3.4 Vectors for complementation in human cells

HsKu70 and HsK80 were amplified from pFastBac Dual using primers Att_hKu70F/R, Att_hKu80F/R (Table 12). Forward primer includes Kozak sequence. Wild type and mutant subunits were used. According to the manufacturer's instructions

BP and LR clonase (Invitrogen) were used to first clone fragments to pDONR221 (Life technologies), afterwards to destination vector pPBSB_CG_DEST1_K (Eric Hendrickson).

Table 12: List of primers used to clone HsKu subunits

Primer name	sequence
Att_hKu80F	GGGGACAAGTTTGTACAAAAAAGCAGGCTGCCGCCACCATGGTG CGGTCGGGGAAT
Att-hKu80R	GGGGACCACTTTGTACAAGAAAGCTGGGTTTATATCATGTCCAAT AA
Att_hKu70F	GGGGACAAGTTTGTACAAAAAAGCAGGCTGCCGCCACCATGTCA GGGTGGGAGTCA
Att-hKu70R	GGGGACCACTTTGTACAAGAAAGCTGGGTTTAGTCCTGGAAGTG CTT

5.5.3.5 Vectors for complementation in A. thaliana

AtKu70 promoter, first exon and intron were amplified from genomic DNA of *A. thaliana* Col0 using primers AtKu705'F/R. Fragment was treated with Taq polymerase in presence of dNTPs at 72°C for 10 min to add A-overhangs. Afterwards, it was cloned into pGEM-T (Promega) according to the manufacturer's instructions. AtKu70 cDNA was amplified from pFastBac Dual using GEM_cF WT/GEM_cR or GEM_cF #2/GEM_cR primer combinations for wild type or Ku70#18 respectively. 3'UTR was amplified from gDNA of *A. thaliana* Col0 using GEM_uF/R primers. pGEM-T containing AtKu70 promoter region was digested with XbaI and respective cDNA fragments and 3'UTR was cloned using In-Fusion HD cloning kit (Clontech) according to manufacturer's protocols. XbaI restriction site that was introduced during cloning in between promoter region with first intron and the rest of cDNA was removed using site-directed mutagenesis with primers GEM_noXba_F/R. Mutation ID#2 had to be reintroduced by site-directed mutagenesis (AT back2KLK_F/R), because it was lost during cloning procedure. Plasmid pCBK05 for plant expression from our laboratory was modified using site-directed mutagenesis to introduce SmaI site using pCBKSma_F/R. The plasmid was cut open using SmaI. Sequence of AtKu70 promoter till 3'UTR were amplified using AtKu705'F/ GEM_uR from pGEM-T vector and phosphorylated by T4

polynucleotid kinase (Thermo scientific). Silent mutations were corrected by site-directed mutagenesis using primers AtKu70_A155A_f/r and AtKu70_Q256Q_f/r.

AtKu80 wild type and Ku80#13 were amplified from respective pFastBac Dual vectors using primers Ku80cSap_F/Ku80cBbvCI_r. Plasmid pCBA02 from our laboratory containing 12xC'Myc-tagged AtKu80 gene was digested with SapI/BbvCI (New England biolabs) enzymes and AtKu80 fragment was cloned using In-Fusion HD cloning kit (Clontech). Sequences of used primers are shown in Table 13.

Table 13: List of primers used to clone AtKu subunits

Primer name	sequence
AtKu705'F	CTATAACTCTTATGTACGAGA
AtKu705'R	GGAAGCCTCTTTTTCCTGCAACACCAACAGA
GEM_cF WT	GAAAAAGAGGCTTCCTCTAGAAAAGAATTTGTAGT
GEM_cF #2	GAAAAAGAGGCTTCCTCTAGAGAAGAATTTGTAGT
GEM_cR	TAACTCACGGTTAAAGTTATTTACCAATGTG
GEM_uF	CTTTAACCGTGAGTTATATAACTCCTGCTAGA
GEM_uR	CGCGGGAATTCGATTTCTAGATGTAAACAGAGATA
GEM_noXba_F	GAAAAAGAGGCTTCCAAAGAATTTGTAGTC
GEM_noXba_R	GACTACAAATTCTTTGGAAGCCTCTTTTTC
pCBKSma_F	TCTGGGGACCTGCAGCCCGGGTAATTCCCGATCTAG
pCBKSma_R	CTAGATCGGGAATTACCCGGGCTGCAGGTCCCCAGA
AtKu70_A155A_f	GCTCTCTGGGTTGCACAAGCACTACTGCGC
AtKu70_A155A_r	GCGCAGTAGTGCTTGTGCAACCCAGAGAGC
AtKu70_Q256Q_f	GACATGAAGGACCAACTGAAGAAGCGTGTA
AtKu70_Q256Q_r	TACACGCTTCTTCAGTTGGTCCTTCATGTC
Ku80cSap_F	AAGACGCAGCCTTTACGAAGAGCGAGTACACATTCCA
Ku80cBbvCI_r	AAGAAAGTGGCTGAGGAGAGACTTCCCACTCTAAA
AT back2KLK_F	TCAAGGAGAATCCAAAGTTGAAGAAGGCTTCTAAG
AT back2KLK_R	CTTAGAAGCCTTCTTCAACTTTGGATTCTCCTTGA

5.5.3.6 Cloning CrTBP1 and vectors for dimerization assay

CrTBP1 was amplified with primers CrTBP1_5UTR/3UTR from cDNA prepared from strain CC-4350 using oligo(dT) and two gene specific primers CrTBP1_E3Rnes, CrTBP1_E5Rnes (Table 14). Fragment was treated with Taq polymerase in presence of

dNTPs at 72°C for 10 min to add A-overhangs and cloned into pCR 2.1-TOPO vector using TOPO TA cloning kit (Invitrogen).

To introduce T7-6xHis tag, BamHI_CrTBP1/CrTBP1_HindIII primers were used to amplify fragment from previously constructed TOPO vector. For 6xHis tag without T7 tag primers NheI_CrTBP1/CrTBP1_HindIII were used. Fragments and vector pET28a (Novagen) were digested with BamHI/HindIII and NheI/HindIII respectively and ligated using T4 ligase (Thermo scientific). Fragments of CrTBP1 PreQ, QMyb and MYB were cloned in similar fashion with T7-6xHis tag using primer pairs BamHI_CrTBP1/HindIII_TAA_PreQ, BamHI_QMyb/CrTBP1_HindIII and BamHI_CrTBP1_MYB/CrTBP1_HindIII (Table 14).

CrTBP1 was cloned into pFastBac HTA for insect cell expression. Fragment was amplified from CrTBP1 cloned in TOPO vector using primers SF_TBP1F/R and cloned into CpoI/NotI site using restriction digest and T4 ligation as described above.

Table 14: List of primers used to clone CrTBP1

Primer name	sequence
CrTBP1_E3Rnes	TGGCACCTTCTTGT
CrTBP1_E5Rnes	TCGTAGTGGATGA
CrTBP1_5UTR	AGTTGTCCTGAGTCGCTGTA
CrTBP1_3UTR	ACTGCGGCTACCTGTCACAT
NheI_CrTBP1	ATATGCTAGCATGGCGAGAGTTCAAGTT
BamHI_CrTBP1	ATATGGATCCATGGCGAGAGTTCAAGTT
CrTBP1_HindIII	ATATAAGCTTTTATTACCCCAGCGGCCACTG
BamHI_CrTBP1_MYB	ATATGGATCCGCCGGTGGTGCCTACGGT
BamHI_QMyb	ATATGGATCCGAACTGCCGGACTTTGCGCCA
HindIII_TAA_PreQ	ATATAAGCTTTTACACCAGCCACTGCACCGCCGC
SF_TBP1F	ATATCCATGGTGGCGAGAGTTCAAGTTA
SF_TBP1R	ATATGCGGCCGCtTACCCCAGCGGCCACT

5.5.4 Native agarose gel electrophoresis

DNA samples were mixed 5:1 with 6x loading dye (60 % glycerol [VWR], 10 mM Tris-HCl pH 7,6, 0,03 % bromphenol blue (Sigma), 60 mM EDTA pH 8,0) and then size separated on 0,8 – 1,5 % agarose gels in 1x TAE buffer (40 mM TrisAc, 20 mM EDTA pH 8,0). Gels were either supplemented with 0,01 % ethidium bromide (AppliChem) or

post-stained by shaking the gel in 1x TAE with ethidium bromide for 20 min. The ethidium bromide stained DNA was visualized by UV with the GeldocTM (BioRad).

5.5.5 Southern blot

Agarose gels were washed for 7 min in 0.25M HCl, soaked for 30 min in denaturation buffer (1,5 M NaCl, 0,5 M NaOH) followed by 30 min washing with neutralization buffer (1,5 M NaCl, 0,5 M Tris.Cl, pH 7,0). The gels were then transferred onto a stack of blotting paper, one layer of Whatman paper, neutral nylon membrane (Hybond NX, GE Healthcare). Another layer of Whatman paper and a sponge saturated with 10x SSC (87,65 g/l NaCl, 44,1 g/l sodium citrate) was put on top of the stack and transfer of the DNA onto the membrane was allowed overnight. DNA was cross-linked with 1200 µJ to the membrane with UV Stratalinker 2400 (Stratagene).

5.5.6 Double stranded 5' Klenow labeled radioactive probes

25 to 50 ng of dsDNA PCR product was mixed with 0,3 µM of specific primers and boiled for 5' at 99°C. The sample was cooled on ice for 5 min and then mixed with 1x OLB (250 mM Tris-HCl (pH 8,0), 25 mM MgCl2, 5 mM β-mercaptoethanol, 2 mM each dCTP, dGTP and dTTP, 1 M HEPES (adjusted to pH 6,6 with NaOH), 1 mg/ml random oligonucleotides (hexamers)), 1,85 MBq of ^{32}P α-ATP (3000 Ci/mmol), and 5 units Klenow fragment (Fermentas). The mixture was incubated for 1 hr at 37°C and then the probe was purified with a Nucleotide Removal Kit (QIAGEN) according to the manufacturer's instructions and eluted twice in 100 µl elution buffer. The purified probe was boiled at 99 °C for 5 min to denature it and then added to the pre-hybridized nylon membrane.

For Micrococcal nuclease digest experiments with *C. reinhardtii* 18S-derived probe was used. Probe was amplified using primers Cr18S_PR1_F/R (Table 15) from genomic DNA of strain CC-4350.

5.5.7 Single stranded 5' PNK labeled radioactive probes

Primer (0,5 µM) of was incubated with 10 units of PNK (Fermentas), 1x PNK buffer A (500 mM Tris-HCl (pH 7,6), 100 mM MgCl2, 50 mM DTT, 1 mM spermidine), and 1,85 MBq of ^{32}P ɣ-ATP (6000 Ci/mmol) for 20 min at 37 °C. The probe was purified with a Nucleotide Removal Kit (QIAGEN) according to the manufacturer's instructions.

The purified probe was directly added to the pre-hybridized nylon membrane. Oligonucleotides used for EMSA were eluted in 50-100 µl elution buffer and stored on 20°C.

For TRF experiments, single stranded oligonucleotides (T3AG3)3 or (T4AG3)3 were end-labeled for *A. thaliana* or *C. reinhardtii* telomeres respectively.

For EMSA, annealing of single stranded oligonucleotides formed short double stranded DNA fragments ((T4AG3)3/(C3TA4)3, AthG-TEL24/ AthC-TEL24, HsG-TEL24/ HsC-TEL24, AtKu70 K117R_r/f) that were used as substrate for labeling. Alternatively, a 98 bp dsDNA was amplified from *A. thanliana* cDNA kindly provided by Jiradet Gloggnitzer using primers qF1/qF2 and gel-purified (Macherey-Nagel). Phusion polymerase formed blunt-ended products that served as substrate for end labeling. Primers and oligonucleotides are listed in Table 15.

Table 15: List of primers and oligonucleotides used for TRF and EMSA

Primer name	sequence
Cr18S_PR1_F	CTTCACTGTCTGGGACTCGGA
Cr18S_PR1_R	ACTAAGAACGGCCATGCACCA
(T3AG3)3	TTTAGGGTTTAGGGTTTAGGG
(TA3C3)3	TAAACCCTAAACCCTAAACCC
(T4AG3)3	TTTTAGGGTTTTAGGGTTTTAGGG
(C3TA4)3	CCCTAAAACCCTAAAACCCTAAAA
AthG-TEL24	TTTAGGGTTTAGGGTTTAGGGTTT
AthC-TEL24	AAACCCTAAACCCTAAACCCTAAA
HsG-TEL24	TTAGGGTTAGGGTTAGGGTTAGGG
HsC-TEL24	CCCTAACCCTAACCCTAACCCTAA
AtKu70 K117R_r	CGAATTCTTTAATCAGCcTCGCTGTTGGACGG
AtKu70 K117R_f	CCGTCCAACAGCGAgGCTGATTAAAGAATTCG
qF1	ATGAAAGCTGGGTTTGCTTTTG
qR1	CGTCCCTTACGCCCAAATT

5.5.8 Hybridization of membranes

Nylon membranes after southern blotting with cross-linked DNA were pre-hybridized in glass tubes for at least 20 min to 1 hr by adding 20 ml hybridization buffer (7% SDS, 0,25 M Na-phosphate buffer pH 7,2). Hybridization was performed at 55°C for

PNK labeled ssDNA probes, and at 65°C for Klenow labeled dsDNA probes. After pre-hybridization, the purified, and if applicable denatured, probe was added and hybridized overnight. Membranes were washed twice with 2x SSC, 0,1 % SDS for 10 min and once with 0,2x SSC, 0,1 % SDS for 40 min. Membranes were wrapped in Saran wrap and exposed to a phosopho-screen (GE Healthcare or Amersham). The phospho-screens were scanned with Molecular Imager FX or Pharo Plus FX (BioRad).

5.5.9 Stripping a membrane

To reprobe a membrane with a different probe, membrane was beforehand incubated with 0,4 M NaOH at 42°C for 30 min. the membrane was then rinsed twice with 200 mM Tris-HCl (pH 7,0), 0,1x SSC, 0,1 % SDS for 20 min at room temperature.

5.6 Telomere assays

5.6.1 Micrococcal nuclease digest

This method was based on literature (Lodha and Schroda 2005). To perform Micrococcal nuclease digest, 1 ml of nuclei isolated from *C. reinhardtii* in Buffer B (~ 8 reactions) were thawed on ice. To collect nuclei, sample was spun on maximal speed for 15 seconds and resuspended in 500 µl of 1x MN Buffer (50mM Tric-HCl pH 8,0, 5 mM CaCl2). Reactions of total volume of 110 µl were carried out in 1x MN Buffer using 60 µl of sample and different amounts of Micrococcal nuclease units (Fermentas). Genomic DNA from *C. reinhardtii* CC-4350 (~ 750 ng) was used as a control for enzyme activity and digested with 15 U of nuclease. Samples were incubated 3 minutes at room temperature and stopped by adding 110 µl STOP buffer (1% SDS, 50 mM EDTA). To purify DNA, proteins were denaturated 45min at 65°C and DNA was extracted using 500 µl phenol:chlorophorm:isoamyl alcohol (25:24:1) using phasetrap A (Peqlab). Aqueous phase was precipitated by adding 42 µl 3 M NaOAc and 840 µl of 96 % EtOH. DNA was pelleted 10 min on maximal speed. Pellet was washed with 70 % EtOH, dried and resuspended in 25 µl H2O. 6x loading dye (6 µl) was added prior loading onto 1,5 % agarose gel. DNA was stained with ethidium bromide (AppliChem 1 % solution) and blotted onto uncharged membrane (Amersham) and hybridized with (T3AG3)3 probe. After scanning, membrane was stripped and reprobed using 18S derived probe.

5.6.2 Terminal restriction fragment analysis (TRF)

To release the terminal restriction fragments from genomic DNA, 800 ng of genomic DNA was digested with 20 units of Tru1I or AluI (Fermentas) for *A. thaliana* or *C. reinhardtii* respectively. Reaction with Tru1I was supplied with 1x buffer R, in a total reaction volume of 100 µl at 65°C overnight. The reaction was done in thermocycler (Biorad) with heated lid to prevent evatoration. The AluI digest was done at 37°C in TANGO buffer overnight in final volume 100 µl. The DNA was then precipitated with 10 µl 3 M NaAc and 80 µl isopropanol, followed by centrifugation at 16100 xg for 10 min. The pellet was washed with 70 % ethanol and resuspended in 20 µl TE. The samples were separated on 0,8 or 1,2 % agarose gels respectively. After blotting were membranes hybridized with (T3AG3)3 or (T4AG3)3 probe respectively. Probe (T3AG3)3 hybridizes with 1 kb ladder (Thermo scientific) and was used additionally for *C. reinhardtii* to visualize the ladder.

Scanned membranes were analyzed for telomere length using TeloTool (Gohring et al. 2014).

5.6.3 In-gel hybridization

In-gel hybridization is used to detect single stranded overhangs on genomic DNA. Blunt-ended control was generates when 2 µg gDNA was incubated with 30 units T4 DNA polymerase (NEB) and 0,1 mM dNTPs in 1x NEB buffer #2 for 30 min at 37°C. The total volume of the reaction was 200 µl. Afterwards, the DNA was precipitated with 0,8 V isopropanol for 30 min at 13000 rpm. The pellet was washed with 70 % ethanol for 5 min at 13000 rpm and the dried pellet was resuspended in 175 µl dH2O.

The genomic DNA and blunt control was digested with 50 units HindIII (Thermo Scientific) in 1x Buffer R (Thermo Scientific) over night at 37°C. Afterwards, the DNA was precipitated with 0,8 V isopropanol and 1/10 V 3 M NaOAc for 30 min at 13000 rpm. Pellet was washed twice with 70 % ethanol, dried and finally resuspended in 25 µl dH2O. The samples were mixed with loading buffer and separated on a 0,8 % agarose gel. The gel run was performed at 2 V/cm for 15 h without ethidium bromide and post-stained in 200 ml 2x SSC supplied with 0,01 % ethidium bromide for 30 min while shaking. Afterwards, the gel was scanned with the Pharos FX Plus Molecular Imager (Bio Rad).

For the native In-gel hybridization the gel was sandwiched between two Whatman papers and dried under vacuum (240 mbar) for 10 min per side. Afterwards, the gel was prehybridized in 60 ml hybridization buffer (7 % SDS, 0,25 M Na-phosphate buffer pH= 7,2, 0,1 g/L BSA) at 50°C while shaking for 2 h at 35 rpm. Subsequently, the radioactive labeled G-strand probe (TA3C3)3 was added and the hybridization was performed over night at 50°C while shaking at 35 rpm. The solution was discarded and the gel was shortly rinsed with 100 ml washing solution (0,25x SSC, 0,01 % SDS). Afterwards, the gel was washed twice with 200 ml washing solution for 1 h at room temperature. Finally, the gel was rinsed twice with 200 ml 0,25x SSC for 1 h at 38°C. The gel was sandwiched between two Whatman papers and dried under vacuum (240 mbar) for 30 s. After that the gel was wrapped in Saran wrap and exposed for 3 - 4 days to a phosphor screen. The screen was scanned with the Pharos FX Plus Molecular Imager (Bio Rad).

For the denaturing in-gel hybridization the gel was soaked for 30 min in denaturation solution (150 mM NaCl, 0,5 M NaOH). Next, the gel was shortly rinsed with dH2O and then neutralized for 15 min in neutralization solution (150 mM NaCl, 0,5 M Tris-HCl pH 8,0). Finally, the gel was washed for 15 min in 5x SSC and prehybridized in 60 ml hybridization buffer at 50°C while shaking for 1 h at 35 rpm. The subsequent steps were performed as describe for the native in-gel hybridization.

5.7 Protein protocols

5.7.1 Protein structure prediction

Protein sequences of AtKu and ScKu subunits were aligned and predictions were made using HHPred and MODELLER available online (http://toolkit.tuebingen.mpg.de/hhpred). Assembly and alignment of the subunits with DNA was done using PyMol 1.3 and the align function.

5.7.2 Protein concentration determination by Bradford

Bradford protein assay was done according to the manufacturer's instructions. BSA was used as protein standard. Reactions were performed in volume of 250 µl and analyzed using Nanodrop spectrophotometer.

5.7.3 SDS polyacrylamide gel electrophoresis (SDS-PAGE)

The running gel (12 % polyacrylamide 29:1 (Sigma), 375 mM Tris-HCl pH 8,8, 0,025 % SDS, 0,1 % ammonium persulfate (APS, Fluka), 0,01 % Temed (Sigma)) was loaded into the SDS-PAGE gel apparatus, covered with a thin layer of isopropanol, allowed to polymerize, and then the stacking gel (6 % polyacrylamide 29:1 (Sigma), 125 mM Tris-HCl 6,8, 0,025 % SDS, 0,05 % APS, 0,01 % Temed) was loaded on top of the running gel. Protein sample was mixed with 4x SDS-PAGE sample buffer (200 mM Tris-HCl pH 6,8, 20 % glycerol, 0,02 % bromphenol blue, 20 % ß-mercaptoethanol, 10 % SDS), boiled for 5 min at 96°C prior loading. The gel was run in 1x electrophoresis buffer (6 mM Tris, 48 mM glycine, 0,025 % SDS) at 20 mA or 120 – 200V until the bromphenol blue migrated out of the gel. For protein size determination 4 µl of PageRuler (Thermo scientific) was used.

Gel was stained and destained with SimplyBlue SafeStain Coommassie G-250 (Life technologies) according to manufacturer's instructions and visualized on Odyssey® system (Li-Cor, Biosciences).

5.7.4 Western blot

Immobilon® FL (Millipore) membrane (Thermo Scientific) was activated by rinsing in pure methanol for 15 sec and rinsed in 1xTBE (89 mM Tris, 89 mM boric acid, 2 mM EDTA, pH of 10X TBE: 8,3). Transfer was done in Biorad wet transfer apparatus in 1x TBE at 380 mA for 1,5 hrs or 20 V overnight in cold room. Protein loading was visualized by staining the membrane with 1x Ponceau solution (0,2 % PonceauS (Fulka), 5 % acetic acid) for 5 min and subsequent destaining with dH20. Membrane was scanned using regular scanner. The membrane was blocked in 5 % milk with 1x TBS-T (150 mM NaCl, 10 mM Tris-Cl pH 8,0, 0,05 % Tween) for 30 min at room temperature. Primary antibody was added in 1x TBS-T and hybridized overnight at +4°C or 2 hr at room temperature. Membrane was washed three times for 5 minutes in 1x TBS-T and secondary antibody conjugated with IRDye fluorophore was added and incubated for 2 hrs at room temperature in dark. The fluorescent signal was detected with an Odyssey® Infrared imager (Li-Cor, Biosciences). Signal was quantified using Image Studio 1.3.4 software. Antibodies are listed in Table 16.

Table 16: List of antibodies for western blotting

Antibody	Organism	Dilution, pair	Company
Anti T7	Mouse monoclonal	1:10 000	Novagen
Anti AtKu70 #300	Rabbit polyclonal	1:15 000	Riha lab
Anti c-Myc A-14	Rabbit polyclonal	1:5000	Santa Cruz
Anti Ku86 sc-9034	rabbit	1:1000	Santa Cruz
Anti β-actin AB3280	mouse	1:2000	Abcam
IRDye®680 α - rabbit	goat	1:20 000 (anti T7)	LiCor
IRDye®800 CW α - rabbit	goat	1:20 000 (anti AtKu70, anti c-Myc)	LiCor
IRDye®800 CW α - rabbit	donkey	1:15 000 (anti Ku86)	LiCor
IRDye®680 LT α - mouse	donkey	1:20 000 (anti β-actin)	LiCor

5.7.5 *In vitro* translation

Backbone vector pET28a was used as for expression of proteins. Plasmid DNA was purified and collected from several plasmid extractions. Resuspended pDNA was than loaded on Nucleospin Extract II kit (Macherey Nagel) column in that it exceeds the binding capacity of column and eluted with 30 µl. 400-500 ng/µl were obtained and this was used as DNA template for TnT Quick coupled transcription/translation system (Promega). Protein LoBind tubes (Eppendorf) were used. Reaction was set up according to the manufacturer's instruction and 1 µg of pDNA for 50 µl reaction was added. To label newly translated protein, 2 µl of lysine Fluorotect (Promega) was added for 50 µl reaction. Translation was done at 30°C for 90 minutes and product was kept on ice when handling or frozen on -20°C.

5.7.6 Protein dimerization assay *in vitro*

Protocol was modified according to Nonradioactive Identification of protein::protein Interactions (Promega).

TnT translation reactions containing translated proteins were used as source of protein. For dimerization assay T7-tagged protein was incubated with protein without T7 tag, but labeled using Fluorotect. 10 µl of each protein were added to 50 µl of binding buffer (20 mM Tris pH 7,5, 150 mM NaCl, 0,2 % Triton X). As a control 10 µl of non-T7 Fluorotect labeled protein was mixed with 60 µl of binding buffer. Samples were incubated 1hr at RT while shaking. For immunoprecipitation antiT7 agarose (Novagen)

was used. 25 µl of slurry was blocked in 1 ml BSA (2 % BSA in PBS) 1hr at 4°C in rotation and washed once with 0,5 ml binding buffer prior adding the sample. Beads were incubated with sample 1-2 hours at RT, spun at 5000 rpm for 30 sec. Supernatant was removed and used as input (20 µl + 5 µl 4x protein loading dye). Beads were washed in several steps. During every step 1 ml of solution was added and tube was flipped 10-20 times. Buffers were used in this order: binding buffer, high salt buffer (20 mM Tris pH 7,5, 1 M NaCl, 0,2 %Triton), filtered dH2O, medium salt buffer (20 mM Tris pH 7,5, 500 mM NaCl, 0,5 %Triton), high triton buffer (20 mM Tris pH 7,5, 150 mM NaCl, 0,7 % Triton). Sample in high triton buffer was transferred into the new tube. Proteins were eluted by adding 5 µl of 4x protein loading dye to slurry and incubated at 69°C for 3 min and directly loaded to SDS PAGE gel at 20 mA for 1,5 hr. Fluorotect was visualized using Typhoon Trio with laser 488 nm and filter 520 nm. Afterwards, gel was used for western blotting to visualize T7 tagged proteins with monoclonal mouse antiT7 primary antibody (Novagen) in dilution 1:10000. The secondary antibody was used anti mouse IRDye680 (LiCor) in dilution 1:20000.

5.7.7 *E. coli* expression and purification

Chemically competent Rosetta (DE3)pLys were transformed using heat shock. Colonies were selected on LB medium containing chloramphenicol (34 µg/ml) and kanamycin (50 µg/ml). Overnight culture was diluted 1:10 in fresh LB medium and grown at 37°C to OD(590 nm) = 0,6. Protein expression was induced by supplementing culture with 1 mM IPTG for 3 hr at 28°C.

Pellet was obtained by centrifugation and resuspended in lysis buffer (50 mM sodium phosphate pH 8,0, 300 mM NaCl) supplemented with protease inhibitors Complete mini (Roche) and lysozyme (1 mg/ml). Lysis solution was incubated at RT for 30 min on rocking platform. Triton X-100 was added to final concentration 1 % and solution was further incubated at 4°C on rocking platform. After centrifugation was lysate filtered through 0,45 µm syringe filter (Millipore) and applied to HiTrap column (GE Healthcare) in ÄKTA protein purification system. Column was washed with lysis buffer supplemented with 20 mM imidazole. Protein was eluted with lysis buffer supplemented with 250 mM imidazole.

5.7.8 Insect cell expression and purification

Vectors pFastBac Dual with cloned Ku subunits and CrTBP1 in pFastbac HTA were delivered to Campus science support facilities (CSF) and technician carried out expression. Pellets were processed in our laboratory.

5.7.8.1 Bacmid generation

Constructs were transformed into *E. coli* containing the EMBacY bacmid. Transposition of the gene of interest into the bacmid was detected via blue/white screening. Bacmid DNA was purified and ethanol precipitated.

5.7.8.2 Generation of V0 virus stock

Each bacmid was transfected into 2 wells of a 6-well plate of Sf9 insect cells After 60-72 hrs media was collected (V0 stock). YFP fluorescence was used to monitor virus generation.

5.7.8.3 Small-scale expression analysis

After V0 harvest, fresh media was added and cells were incubated for a further 60 hours. Cells from 2 wells were harvested and resuspended in 800 µl cold 1X PBS. 50 µl cell suspension was used for SDS-PAGE analysis. Cells were lysed by addition of glass beads followed by vortexing at 4° C for 5 minutes. Lysate was centrifuged and supernatant was decanted. 100 µl supernatant was used for YFP analysis. 50 µl supernatant was used for SDS-PAGE analysis

5.7.8.4 Viral amplification

Cell line: Sf9, Ratio: 1:50, BIIC or virus: BIIC, BIIC's frozen after growth arrest. Virus harvested on DPA3 (DPA = Day Past Arrest).

5.7.8.5 Optimization

Cells were infected under the following conditions: Hi5 cells, 27°C, Harvest time: DPA2.5, final cell concentration: 1 x 10^6 cells/ml. Cell growth was monitored until growth arrest. YFP fluorescence was monitored starting at DPA 1 on DPA0-3 a sample of 1 x 10^6 cells were taken. Cells were resuspended in 1 ml 1X PBS. Cells were lysed by addition of glass beads followed by vortexing at 4°C for 6 min. The sample was centrifuged to remove beads and cell debris. YFP fluorescence of supernatant (S) was determined. Supernatant samples were analyzed via SDS-PAGE and Western blot.

Cells were grown in 50 ml of media and were used for protein purification for preliminary EMSA analysis.

5.7.8.6 Large scale expression

Cell line: Hi5, BIIC or Virus: Ratio: 1:150, Harvest time: DPA3, Final cell concentration: 1 x 10^6 cells/ml. Final cell viability: >90%. 1 x 10^6 cells were resuspended in 1 ml 1X PBS and YFP was monitored until plateau. Cells were grown in 1 liter of media and were used for protein purification for EMSA, fluorescence anisotropy and electron microscopy.

5.7.8.7 Protein purification

From optimization step we obtained 50 ml pellet of Hi5 cells with approx. 1,2 g. Pellet was frozen at -20°C or processed fresh. Alternatively, from large expression (1l) pellet was processed in similar fashion. Pellets were resuspended in 20 ml or 200 ml of Ku Lysis buffer (50 mM Tris-Cl, 250 mM KCl, 10% v/v glycerol, 1 mM DTT, pH 8,0 adjusted with HCl, supplemented with Roche complete MINI (1 tablet/10 ml) or complete ULTRA (1 tablet/50 ml) protease inhibitors). Cells in lysis buffer were frozen in aliquots (2 ml or 45 ml) in LN2 and stored at -80°C.

Thawed cells in lysis buffer were spun at 15 000 xg for 5min. Supernatant was mixed with 80 ul or 900 ul of His Mag Sepharose Ni (GE health care). Beads were washed once with Lysis buffer prior usage and incubated with sample overnight at 4°C on rotational shaker. Afterwards, beads were washed three times in Ku washing buffer (50 mM Tris-Cl, 250 mM KCl, 10% v/v glycerol, 50 mM imidazole) and eluted in 100 µl or 1000 µl of Ku elution buffer (50 mM Tris-Cl, 250 mM KCl, 10 % v/v glycerol, 250 mM imidazole). Proteins were filtered using Nanosep centrifugal colums (Pall) and stored at +4°C.

5.7.9 EMSA

Total protein concentration was determined by Bradford assay and it was corrected for amount of Ku protein via Ku70 western blot quantification. Total protein concentration of wild type complexes was set as reference concentration. Increasing amounts of protein were incubated with 0,38 ng of end labeled 98 bp dsDNA oligonucleotide (0,3 nM see PNK labeled radioactive probes) in final volume 20 µl binding buffer (35 mM Tris, 5 % glycerol, 150 mM KCl, 1 mM EDTA, 0,1 mM DTT).

Binding was carried out at room temperature for 30 min. Samples were loaded onto native polyacrylamide gel (5 % polyacrylamide 29:1 (Sigma), 0,5x TBE, 0,33 % APS, 0,06 % Temed) that had undergone pre-electrophoresis at 160 V for 10 minutes at 4°C in 0,5x TBE. Electrophoresis continued with samples in the same conditions for 3 hrs. Gels were dried and exposed to phospho-screen (GE Healthcare or Amersham). The phospho-screens were scanned with Molecular Imager FX or Pharo Plus FX (BioRad).

For non-radioactive EMSA, (T4AG3)3 oligonucleotide was labeled with 5' IRD800 (IDT) and hybridized to unlabeled complementary oligonucleotide. Conditions were as described above and images were acquired with Odyssey® Infrared imager (Li-Cor).

5.7.10 Fluorescence anisotropy

The fluorescence anisotropy was performed by Eliska Janouskova and Ctirad Hofr at CEITEC, Brno Czech republic. It is a spectroscopic method for studying fluorescently tagged molecules and their interaction with unlabeled molecules. FluoroMax-4 (Horiba) with software Origin Fluoresence 2.1.6. was used to measure increase in anisotropy of fluorescein (FITC) tagged DNA upon protein binding. Oligonucleotides s25 and s75 (Table 17) were hybridized in water. 1 μM protein solution was added to 5 nM DNA solution (25 mM Tris, 150 mM KCl, pH 8,0) 10 min prior each measurement. The anisotropy data were collected using an excitation wavelength of 494 nm and the emission from 521 nm. The band pass was 9 nm for excitation and 9 nm for emission. The integration time was 3 s. Typically three measurements were collected and averaged for each point. Kd was calculated using SigmaPlot.

Table 17: oligonucleotides used for fluorescence anisotropy

Primer name	sequence
5'F_s25	5' FITC_GAACGAAAACATCGGGTACGAGGAC
s25R	GTCCTCGTACCCGATGTTTTCGTTC
5'F_s75	5'FITC_GAACGAAAACATCGGGTACGAGGACGAAGACTGACCACGA CATACTAACAGGGACATGACTCACAGAACAGAGCG
s75R	CGCTCTGTTCTGTGAGTCATGTCCCTGTTAGTATGTCGTGGTCAGT CTTCGTCCTCGTACCCGATGTTTTCGTTC

5.7.11 Electron microscopy

Purified mutant and wild type Ku complexes of 3,62 µM HsKu and AtKu were mixed with 1,53 nM of 1100 bp blunt dsDNA (amplified by AtKu70 LP/RP primers (Table 9) from genomic DNA of *A. thaliana*). Sample preparation and imaging was done in CSF, Vienna. Sample was diluted to 1:5 in spraying buffer containing 100 mM ammonium bicarbonate (pH 7,5) and 30% (v/v) glycerol and sprayed onto freshly cleaved mica chips and immediately transferred into a Bal-Tec MED020 high vacuum coated equipped with electron guns. The dry rotating samples were coated with 0,7 nm platinum at an elevation angle of 5° and backed with 10 nm C at 45°. The produced replicas were floated off, picked up on 400 mesh Cu/Pd grids and inspected in an FEI T20 G2 transmission electron microscope operated at 80 kV. Prior inspection Bal-Tec SCD 005 glow discharge was used to remove glycerol. Electron micrographs were acquired using an FEI Eagle 4k CCD camera.

Images were analyzed in ImageJ software by tracing segmented line manually along the DNA. Measurements were set to shape descriptors and scale was set in pixels (1 pixel/px). Only DNA/Ku complexes were analyzed, because amount of free DNA could not be accurately determined. Criteria were set for high quality DNA/Ku complexes: total DNA length was in range of 800-1000 px, DNA was not overlapping and only Ku proteins that were centered along the DNA axis were considered. Ku protein was at least 30 px in diameter and the distance from DNA end was less than 10 px to be considered attached. Four zones were defined as distance of Ku from DNA end. For Terminal, no protruding DNA had to be detectable. Subterminal Ku was ⟨1-155) px away from DNA terminus, Medial ⟨155-310) px and Central ⟨310-465⟩ px. In DNA longer than 930 px all complexes in central region outside defined boundaries were considered part of left central region.

References

Arosio, D., et al. (2004), 'Fluorescence anisotropy studies on the Ku-DNA interaction: anion and cation effects', *J Biol Chem,* 279 (41), 42826-35.

Arosio, D., et al. (2002), 'Studies on the mode of Ku interaction with DNA', *J Biol Chem,* 277 (12), 9741-8.

Aubert, G. (2014), 'Telomere dynamics and aging', *Prog Mol Biol Transl Sci,* 125, 89-111.

Bae, N. S. and Baumann, P. (2007), 'A RAP1/TRF2 complex inhibits nonhomologous end-joining at human telomeric DNA ends', *Mol Cell,* 26 (3), 323-34.

Balestrini, A., et al. (2013), 'The Ku heterodimer and the metabolism of single-ended DNA double-strand breaks', *Cell Rep,* 3 (6), 2033-45.

Baumann, P. and Cech, T. R. (2001), 'Pot1, the putative telomere end-binding protein in fission yeast and humans', *Science,* 292 (5519), 1171-5.

Bennett, C. B., et al. (1993), 'Lethality induced by a single site-specific double-strand break in a dispensable yeast plasmid', *Proc Natl Acad Sci U S A,* 90 (12), 5613-7.

Betermier, M., Bertrand, P., and Lopez, B. S. (2014), 'Is non-homologous end-joining really an inherently error-prone process?', *PLoS Genet,* 10 (1), e1004086.

Blackburn, E. H. (2001), 'Switching and signaling at the telomere', *Cell,* 106 (6), 661-73.

--- (2005), 'Telomeres and telomerase: their mechanisms of action and the effects of altering their functions', *FEBS Lett,* 579 (4), 859-62.

Blackburn, E. H. and Gall, J. G. (1978), 'A tandemly repeated sequence at the termini of the extrachromosomal ribosomal RNA genes in Tetrahymena', *J Mol Biol,* 120 (1), 33-53.

Blackburn, E. H., Greider, C. W., and Szostak, J. W. (2006), 'Telomeres and telomerase: the path from maize, Tetrahymena and yeast to human cancer and aging', *Nat Med,* 12 (10), 1133-8.

Blackburn, G. L. and Mun, E. C. (2004), 'Effects of weight loss surgeries on liver disease', *Semin Liver Dis,* 24 (4), 371-9.

Blier, P. R., et al. (1993), 'Binding of Ku protein to DNA. Measurement of affinity for ends and demonstration of binding to nicks', *J Biol Chem,* 268 (10), 7594-601.

Bliss, T. M. and Lane, D. P. (1997), 'Ku selectively transfers between DNA molecules with homologous ends', *J Biol Chem,* 272 (9), 5765-73.

Bombarde, O., et al. (2010), 'TRF2/RAP1 and DNA-PK mediate a double protection against joining at telomeric ends', *EMBO J,* 29 (9), 1573-84.

Bonetti, D., et al. (2009), 'Multiple pathways regulate 3' overhang generation at S. cerevisiae telomeres', *Mol Cell,* 35 (1), 70-81.

Boukamp, P. and Mirancea, N. (2007), 'Telomeres rather than telomerase a key target for anti-cancer therapy?', *Exp Dermatol,* 16 (1), 71-9.

Boulton, S. J. and Jackson, S. P. (1996), 'Saccharomyces cerevisiae Ku70 potentiates illegitimate DNA double-strand break repair and serves as a barrier to error-prone DNA repair pathways', *EMBO J,* 15 (18), 5093-103.

Bowater, R. and Doherty, A. J. (2006), 'Making ends meet: repairing breaks in bacterial DNA by non-homologous end-joining', *PLoS Genet,* 2 (2), e8.

Burge, S., et al. (2006), 'Quadruplex DNA: sequence, topology and structure', *Nucleic Acids Res,* 34 (19), 5402-15.

Cary, R. B., et al. (1997), 'DNA looping by Ku and the DNA-dependent protein kinase', *Proc Natl Acad Sci U S A,* 94 (9), 4267-72.

Cesare, A. J., et al. (2003), 'Telomere looping in P. sativum (common garden pea)', *Plant J,* 36 (2), 271-9.

Chai, W., et al. (2006), 'The involvement of the Mre11/Rad50/Nbs1 complex in the generation of G-overhangs at human telomeres', *EMBO Rep,* 7 (2), 225-30.

Chan, S. R. and Blackburn, E. H. (2004), 'Telomeres and telomerase', *Philos Trans R Soc Lond B Biol Sci,* 359 (1441), 109-21.
Chen, L. Y. and Lingner, J. (2013), 'CST for the grand finale of telomere replication', *Nucleus,* 4 (4), 277-82.
Cockell, M., et al. (1995), 'The carboxy termini of Sir4 and Rap1 affect Sir3 localization: evidence for a multicomponent complex required for yeast telomeric silencing', *J Cell Biol,* 129 (4), 909-24.
Cohen, S. B., et al. (2007), 'Protein composition of catalytically active human telomerase from immortal cells', *Science,* 315 (5820), 1850-3.
Collins, K. (2006), 'The biogenesis and regulation of telomerase holoenzymes', *Nat Rev Mol Cell Biol,* 7 (7), 484-94.
Court, R., et al. (2005), 'How the human telomeric proteins TRF1 and TRF2 recognize telomeric DNA: a view from high-resolution crystal structures', *EMBO Rep,* 6 (1), 39-45.
d'Adda di Fagagna, F., et al. (2003), 'The Gam protein of bacteriophage Mu is an orthologue of eukaryotic Ku', *EMBO Rep,* 4 (1), 47-52.
de Lange, T. (2004), 'T-loops and the origin of telomeres', *Nat Rev Mol Cell Biol,* 5 (4), 323-9.
--- (2005), 'Shelterin: the protein complex that shapes and safeguards human telomeres', *Genes Dev,* 19 (18), 2100-10.
de Vries, E., et al. (1989), 'HeLa nuclear protein recognizing DNA termini and translocating on DNA forming a regular DNA-multimeric protein complex', *J Mol Biol,* 208 (1), 65-78.
Debuchy, R., Purton, S., and Rochaix, J. D. (1989), 'The argininosuccinate lyase gene of Chlamydomonas reinhardtii: an important tool for nuclear transformation and for correlating the genetic and molecular maps of the ARG7 locus', *EMBO J,* 8 (10), 2803-9.
Dmitriev, P. V., Petrov, A. V., and Dontsova, O. A. (2003), 'Yeast telosome complex: components and their functions', *Biochemistry (Mosc),* 68 (7), 718-34.
Doherty, A. J., Jackson, S. P., and Weller, G. R. (2001), 'Identification of bacterial homologues of the Ku DNA repair proteins', *FEBS Lett,* 500 (3), 186-8.
Downs, J. A. and Jackson, S. P. (2004), 'A means to a DNA end: the many roles of Ku', *Nat Rev Mol Cell Biol,* 5 (5), 367-78.
Dynan, W. S. and Yoo, S. (1998), 'Interaction of Ku protein and DNA-dependent protein kinase catalytic subunit with nucleic acids', *Nucleic Acids Res,* 26 (7), 1551-9.
Falzon, M., Fewell, J. W., and Kuff, E. L. (1993), 'EBP-80, a transcription factor closely resembling the human autoantigen Ku, recognizes single- to double-strand transitions in DNA', *J Biol Chem,* 268 (14), 10546-52.
Fattah, F., et al. (2010), 'Ku regulates the non-homologous end joining pathway choice of DNA double-strand break repair in human somatic cells', *PLoS Genet,* 6 (2), e1000855.
Fattah, F. J., et al. (2008), 'Ku70, an essential gene, modulates the frequency of rAAV-mediated gene targeting in human somatic cells', *Proc Natl Acad Sci U S A,* 105 (25), 8703-8.
Feldmann, E., et al. (2000), 'DNA double-strand break repair in cell-free extracts from Ku80-deficient cells: implications for Ku serving as an alignment factor in non-homologous DNA end joining', *Nucleic Acids Res,* 28 (13), 2585-96.
Fisher, T. S. and Zakian, V. A. (2005), 'Ku: a multifunctional protein involved in telomere maintenance', *DNA Repair (Amst),* 4 (11), 1215-26.
Fox, B. A., et al. (2009), 'Efficient gene replacements in Toxoplasma gondii strains deficient for nonhomologous end joining', *Eukaryot Cell,* 8 (4), 520-9.
Fulcher, N., et al. (2014), 'If the cap fits, wear it: an overview of telomeric structures over evolution', *Cell Mol Life Sci,* 71 (5), 847-65.
Fulneckova, J., et al. (2012), 'Dynamic evolution of telomeric sequences in the green algal order Chlamydomonadales', *Genome Biol Evol,* 4 (3), 248-64.
Gallego, M. E., Jalut, N., and White, C. I. (2003), 'Telomerase dependence of telomere lengthening in Ku80 mutant Arabidopsis', *Plant Cell,* 15 (3), 782-9.

Gohring, J., et al. (2014), 'TeloTool: a new tool for telomere length measurement from terminal restriction fragment analysis with improved probe intensity correction', *Nucleic Acids Res,* 42 (3), e21.
Gorman, D. S. and Levine, R. P. (1965), 'Cytochrome f and plastocyanin: their sequence in the photosynthetic electron transport chain of Chlamydomonas reinhardi', *Proc Natl Acad Sci U S A,* 54 (6), 1665-9.
Greider, C. W. and Blackburn, E. H. (1985), 'Identification of a specific telomere terminal transferase activity in Tetrahymena extracts', *Cell,* 43 (2 Pt 1), 405-13.
--- (1987), 'The telomere terminal transferase of Tetrahymena is a ribonucleoprotein enzyme with two kinds of primer specificity', *Cell,* 51 (6), 887-98.
Griffith, J. D., et al. (1999), 'Mammalian telomeres end in a large duplex loop', *Cell,* 97 (4), 503-14.
Grundy, G. J., et al. (2014), 'One ring to bring them all--the role of Ku in mammalian non-homologous end joining', *DNA Repair (Amst),* 17, 30-8.
Hails, T., Huttner, O., and Day, A. (1995), 'Isolation of a Chlamydomonas reinhardtii telomere by functional complementation in yeast', *Curr Genet,* 28 (5), 437-40.
Hanakahi, L. A. (2007), '2-Step purification of the Ku DNA repair protein expressed in Escherichia coli', *Protein Expr Purif,* 52 (1), 139-45.
Holohan, B., Wright, W. E., and Shay, J. W. (2014), 'Cell biology of disease: Telomeropathies: an emerging spectrum disorder', *J Cell Biol,* 205 (3), 289-99.
Horn, S., et al. (2013), 'TERT promoter mutations in familial and sporadic melanoma', *Science,* 339 (6122), 959-61.
Horvath, M. P., et al. (1998), 'Crystal structure of the Oxytricha nova telomere end binding protein complexed with single strand DNA', *Cell,* 95 (7), 963-74.
Hutner, S. H. (1950), 'Anaerobic and aerobic growth of purple bacteria (Athiorhodaceae) in chemically defined media', *J Gen Microbiol,* 4 (3), 286-93.
Jiang, W., et al. (2013), 'Demonstration of CRISPR/Cas9/sgRNA-mediated targeted gene modification in Arabidopsis, tobacco, sorghum and rice', *Nucleic Acids Res,* 41 (20), e188.
Karamysheva, Z. N., et al. (2004), 'A C-terminal Myb extension domain defines a novel family of double-strand telomeric DNA-binding proteins in Arabidopsis', *J Biol Chem,* 279 (46), 47799-807.
Kazda, A., et al. (2012), 'Chromosome end protection by blunt-ended telomeres', *Genes Dev,* 26 (15), 1703-13.
Konig, P., et al. (1996), 'The crystal structure of the DNA-binding domain of yeast RAP1 in complex with telomeric DNA', *Cell,* 85 (1), 125-36.
Kysela, B., et al. (2003), 'Ku stimulation of DNA ligase IV-dependent ligation requires inward movement along the DNA molecule', *J Biol Chem,* 278 (25), 22466-74.
Larrivee, M., LeBel, C., and Wellinger, R. J. (2004), 'The generation of proper constitutive G-tails on yeast telomeres is dependent on the MRX complex', *Genes Dev,* 18 (12), 1391-6.
Lehman, J. A., Hoelz, D. J., and Turchi, J. J. (2008), 'DNA-dependent conformational changes in the Ku heterodimer', *Biochemistry,* 47 (15), 4359-68.
Lei, M., Podell, E. R., and Cech, T. R. (2004), 'Structure of human POT1 bound to telomeric single-stranded DNA provides a model for chromosome end-protection', *Nat Struct Mol Biol,* 11 (12), 1223-9.
Li, G., Nelsen, C., and Hendrickson, E. A. (2002), 'Ku86 is essential in human somatic cells', *Proc Natl Acad Sci U S A,* 99 (2), 832-7.
Liang, F. and Jasin, M. (1996), 'Ku80-deficient cells exhibit excess degradation of extrachromosomal DNA', *J Biol Chem,* 271 (24), 14405-11.

Lingner, J. and Cech, T. R. (1996), 'Purification of telomerase from Euplotes aediculatus: requirement of a primer 3' overhang', *Proc Natl Acad Sci U S A,* 93 (20), 10712-7.
Lingner, J., Cooper, J. P., and Cech, T. R. (1995), 'Telomerase and DNA end replication: no longer a lagging strand problem?', *Science,* 269 (5230), 1533-4.
Liu, D., et al. (2004), 'Telosome, a mammalian telomere-associated complex formed by multiple telomeric proteins', *J Biol Chem,* 279 (49), 51338-42.
Lodha, M. and Schroda, M. (2005), 'Analysis of chromatin structure in the control regions of the chlamydomonas HSP70A and RBCS2 genes', *Plant Mol Biol,* 59 (3), 501-13.
Longhese, M. P. (2008), 'DNA damage response at functional and dysfunctional telomeres', *Genes Dev,* 22 (2), 125-40.
Lopez, C. R., et al. (2011), 'Ku must load directly onto the chromosome end in order to mediate its telomeric functions', *PLoS Genet,* 7 (8), e1002233.
Louis, E. J. (2002), 'Are Drosophila telomeres an exception or the rule?', *Genome Biol,* 3 (10), REVIEWS0007.
Ma, Y. and Lieber, M. R. (2001), 'DNA length-dependent cooperative interactions in the binding of Ku to DNA', *Biochemistry,* 40 (32), 9638-46.
Mahaney, B. L., Meek, K., and Lees-Miller, S. P. (2009), 'Repair of ionizing radiation-induced DNA double-strand breaks by non-homologous end-joining', *Biochem J,* 417 (3), 639-50.
Maringele, L. and Lydall, D. (2002), 'EXO1-dependent single-stranded DNA at telomeres activates subsets of DNA damage and spindle checkpoint pathways in budding yeast yku70Delta mutants', *Genes Dev,* 16 (15), 1919-33.
Mimori, T. and Hardin, J. A. (1986), 'Mechanism of interaction between Ku protein and DNA', *J Biol Chem,* 261 (22), 10375-9.
Mimori, T., et al. (1981), 'Characterization of a high molecular weight acidic nuclear protein recognized by autoantibodies in sera from patients with polymyositis-scleroderma overlap', *J Clin Invest,* 68 (3), 611-20.
Mimori, T., et al. (1990), 'Isolation and characterization of cDNA encoding the 80-kDa subunit protein of the human autoantigen Ku (p70/p80) recognized by autoantibodies from patients with scleroderma-polymyositis overlap syndrome', *Proc Natl Acad Sci U S A,* 87 (5), 1777-81.
Mitton-Fry, R. M. and Wuttke, D. S. (2002), '1H, 13C and 15N resonance assignments of the DNA-binding domain of the essential protein Cdc13 complexed with single-stranded telomeric DNA', *J Biomol NMR,* 22 (4), 379-80.
Mladenov, E. and Iliakis, G. (2011), 'Induction and repair of DNA double strand breaks: the increasing spectrum of non-homologous end joining pathways', *Mutat Res,* 711 (1-2), 61-72.
Myung, K., et al. (2004), 'Regulation of telomere length and suppression of genomic instability in human somatic cells by Ku86', *Mol Cell Biol,* 24 (11), 5050-9.
Nelson, A. D. and Shippen, D. E. (2012), 'Surprises from the chromosome front: lessons from Arabidopsis on telomeres and telomerase', *Cold Spring Harb Symp Quant Biol,* 77, 7-15.
O'Sullivan, R. J. and Karlseder, J. (2010), 'Telomeres: protecting chromosomes against genome instability', *Nat Rev Mol Cell Biol,* 11 (3), 171-81.
Olovnikov, A. M. (1971), '[Principle of marginotomy in template synthesis of polynucleotides]', *Dokl Akad Nauk SSSR,* 201 (6), 1496-9.
--- (1973), 'A theory of marginotomy. The incomplete copying of template margin in enzymic synthesis of polynucleotides and biological significance of the phenomenon', *J Theor Biol,* 41 (1), 181-90.
Osterhage, J. L. and Friedman, K. L. (2009), 'Chromosome end maintenance by telomerase', *J Biol Chem,* 284 (24), 16061-5.
Palm, W. and de Lange, T. (2008), 'How shelterin protects mammalian telomeres', *Annu Rev Genet,* 42, 301-34.

Peska, V., Schrumpfova, P. P., and Fajkus, J. (2011), 'Using the telobox to search for plant telomere binding proteins', *Curr Protein Pept Sci,* 12 (2), 75-83.
Petracek, M. E. and Berman, J. (1992), 'Chlamydomonas reinhardtii telomere repeats form unstable structures involving guanine-guanine base pairs', *Nucleic Acids Res,* 20 (1), 89-95.
Petracek, M. E., et al. (1990), 'Chlamydomonas telomere sequences are A+T-rich but contain three consecutive G-C base pairs', *Proc Natl Acad Sci U S A,* 87 (21), 8222-6.
Pfingsten, J. S., et al. (2012), 'Mutually exclusive binding of telomerase RNA and DNA by Ku alters telomerase recruitment model', *Cell,* 148 (5), 922-32.
Qi, Y., et al. (2013), 'Increasing frequencies of site-specific mutagenesis and gene targeting in Arabidopsis by manipulating DNA repair pathways', *Genome Res,* 23 (3), 547-54.
Raices, M., et al. (2008), 'C. elegans telomeres contain G-strand and C-strand overhangs that are bound by distinct proteins', *Cell,* 132 (5), 745-57.
Rathmell, W. K. and Chu, G. (1994), 'Involvement of the Ku autoantigen in the cellular response to DNA double-strand breaks', *Proc Natl Acad Sci U S A,* 91 (16), 7623-7.
Ribes-Zamora, A., et al. (2007), 'Distinct faces of the Ku heterodimer mediate DNA repair and telomeric functions', *Nat Struct Mol Biol,* 14 (4), 301-7.
Ribes-Zamora, A., et al. (2013), 'TRF2 interaction with Ku heterotetramerization interface gives insight into c-NHEJ prevention at human telomeres', *Cell Rep,* 5 (1), 194-206.
Riha, K. and Shippen, D. E. (2003), 'Ku is required for telomeric C-rich strand maintenance but not for end-to-end chromosome fusions in Arabidopsis', *Proc Natl Acad Sci U S A,* 100 (2), 611-5.
Riha, K., Heacock, M. L., and Shippen, D. E. (2006), 'The role of the nonhomologous end-joining DNA double-strand break repair pathway in telomere biology', *Annu Rev Genet,* 40, 237-77.
Riha, K., et al. (2002), 'Telomere length deregulation and enhanced sensitivity to genotoxic stress in Arabidopsis mutants deficient in Ku70', *EMBO J,* 21 (11), 2819-26.
Riha, K., et al. (2000), 'Analysis of the G-overhang structures on plant telomeres: evidence for two distinct telomere architectures', *Plant J,* 23 (5), 633-41.
Roberts, S. A. and Ramsden, D. A. (2007), 'Loading of the nonhomologous end joining factor, Ku, on protein-occluded DNA ends', *J Biol Chem,* 282 (14), 10605-13.
Schrumpfova, P. P., et al. (2014), 'Telomere repeat binding proteins are functional components of Arabidopsis telomeres and interact with telomerase', *Plant J,* 77 (5), 770-81.
Sfeir, A. and de Lange, T. (2012), 'Removal of shelterin reveals the telomere end-protection problem', *Science,* 336 (6081), 593-7.
Shee, C., et al. (2013), 'Engineered proteins detect spontaneous DNA breakage in human and bacterial cells', *Elife (Cambridge),* 2, e01222.
Shiotani, B. and Zou, L. (2009), 'Single-stranded DNA orchestrates an ATM-to-ATR switch at DNA breaks', *Mol Cell,* 33 (5), 547-58.
Siede, W., et al. (1996), 'The Saccharomyces cerevisiae Ku autoantigen homologue affects radiosensitivity only in the absence of homologous recombination', *Genetics,* 142 (1), 91-102.
Smogorzewska, A., et al. (2002), 'DNA ligase IV-dependent NHEJ of deprotected mammalian telomeres in G1 and G2', *Curr Biol,* 12 (19), 1635-44.
Symington, L. S. and Gautier, J. (2011), 'Double-strand break end resection and repair pathway choice', *Annu Rev Genet,* 45, 247-71.
Tamura, K., et al. (2002), 'Identification of Ku70 and Ku80 homologues in Arabidopsis thaliana: evidence for a role in the repair of DNA double-strand breaks', *Plant J,* 29 (6), 771-81.
Tarsounas, M. and Tijsterman, M. (2013), 'Genomes and G-quadruplexes: for better or for worse', *J Mol Biol,* 425 (23), 4782-9.

Turchi, J. J., Henkels, K. M., and Zhou, Y. (2000), 'Cisplatin-DNA adducts inhibit translocation of the Ku subunits of DNA-PK', *Nucleic Acids Res,* 28 (23), 4634-41.
Tuteja, N., et al. (1994), 'Human DNA helicase II: a novel DNA unwinding enzyme identified as the Ku autoantigen', *EMBO J,* 13 (20), 4991-5001.
van Steensel, B., Smogorzewska, A., and de Lange, T. (1998), 'TRF2 protects human telomeres from end-to-end fusions', *Cell,* 92 (3), 401-13.
Venteicher, A. S. and Artandi, S. E. (2009), 'TCAB1: driving telomerase to Cajal bodies', *Cell Cycle,* 8 (9), 1329-31.
Venteicher, A. S., et al. (2008), 'Identification of ATPases pontin and reptin as telomerase components essential for holoenzyme assembly', *Cell,* 132 (6), 945-57.
Venteicher, A. S., et al. (2009), 'A human telomerase holoenzyme protein required for Cajal body localization and telomere synthesis', *Science,* 323 (5914), 644-8.
Verdun, R. E. and Karlseder, J. (2007), 'Replication and protection of telomeres', *Nature,* 447 (7147), 924-31.
Wahlin, J. and Cohn, M. (2000), 'Saccharomyces cerevisiae RAP1 binds to telomeric sequences with spatial flexibility', *Nucleic Acids Res,* 28 (12), 2292-301.
Walker, J. R., Corpina, R. A., and Goldberg, J. (2001), 'Structure of the Ku heterodimer bound to DNA and its implications for double-strand break repair', *Nature,* 412 (6847), 607-14.
Wang, Y., Ghosh, G., and Hendrickson, E. A. (2009), 'Ku86 represses lethal telomere deletion events in human somatic cells', *Proc Natl Acad Sci U S A,* 106 (30), 12430-5.
Watson, J. D. (1972), 'Origin of concatemeric T7 DNA', *Nat New Biol,* 239 (94), 197-201.
Wu, L., et al. (2006), 'Pot1 deficiency initiates DNA damage checkpoint activation and aberrant homologous recombination at telomeres', *Cell,* 126 (1), 49-62.
Wu, P., et al. (2010), 'Apollo contributes to G overhang maintenance and protects leading-end telomeres', *Mol Cell,* 39 (4), 606-17.
Xin, H., Liu, D., and Songyang, Z. (2008), 'The telosome/shelterin complex and its functions', *Genome Biol,* 9 (9), 232.
Ye, J. Z., et al. (2004), 'TIN2 binds TRF1 and TRF2 simultaneously and stabilizes the TRF2 complex on telomeres', *J Biol Chem,* 279 (45), 47264-71.
Yoo, S., Kimzey, A., and Dynan, W. S. (1999), 'Photocross-linking of an oriented DNA repair complex. Ku bound at a single DNA end', *J Biol Chem,* 274 (28), 20034-9.
Zellinger, B. and Riha, K. (2007), 'Composition of plant telomeres', *Biochim Biophys Acta,* 1769 (5-6), 399-409.
Zellinger, B., et al. (2007), 'Ku suppresses formation of telomeric circles and alternative telomere lengthening in Arabidopsis', *Mol Cell,* 27 (1), 163-9.
Zhang, R., et al. (2014), 'High-Throughput Genotyping of Green Algal Mutants Reveals Random Distribution of Mutagenic Insertion Sites and Endonucleolytic Cleavage of Transforming DNA', *Plant Cell,* 26 (4), 1398-409.
Zhou, B. B. and Elledge, S. J. (2000), 'The DNA damage response: putting checkpoints in perspective', *Nature,* 408 (6811), 433-9.

Abbreviations

4-OHT	4-hydroxytamoxifen
alt-NHEJ	alternative NHEJ
AtKu	Ku heterodimer from *A. thaliana*
C-NHEJ	canonical NHEJ
DNA	deoxyribonucleic acid
dsDNA	double stranded DNA
DSB	DNA double strand break
EMSA	electrophoretic mobility shift assay
HR	homologous recombination
HsKu	Ku heterodimer from human cells
Kd	the equilibrium dissociation constant
MNase	micrococcal nuclease
NHEJ	non-homologous end joining
PCR	polymerase chain reaction
RNA	ribonucleic acid
ScKu	Ku heterodimer from *S. cerevisiae*
ssDNA	single stranded DNA
TBP	telomere binding protein
TRF	terminal restriction fragment analysis

Curriculum Vitae

Personal data

Name: Sona Valuchova
Birth: 04.08.1986, Bratislava Slovakia
E-mail: sona.valuchova@gmail.com

Education

2010 – present Ph.D. Molecular Biology, University of Vienna, Vienna Biocenter, Austria
2010 to Present (graduating in Septeber 2014)
Thesis: “Insights into telomere protection by the Ku heterodimer”
Supervisor: Karel Riha, Ph.D.

2008 – 2010 M.Sc. Genetics of microorganisms, Comenius University, Bratislava, Slovakia
Thesis: “Telomeres of *Chlamydomonas reinhardtii* and their response to under-expression of Ku80”
Supervisor: Doc. Mgr. Miroslava Slaninova, Ph.D.

2005 – 2008 B.Sc. Genetics, Comenius University, Bratislava, Slovakia
Thesis: “Green fluorescent protein”
Supervisor: Doc. Mgr. Miroslava Slaninova, Ph.D.

Conferences

June 2014 16th International meeting: Cell and Molecular Biology of Chlamydomonas, Asilomar Conference Grounds, Pacific Grove, CA, June 8 - June 13, 2014.
Poster: “Putative telomere-binding protein in *Chlamydomonas reinhardtii*.”

April 2014 EMBO Telomeres, telomerase and disease, Brussels, Belgium, Aril 30 - May 4, 2014.
Poster: “Insights into telomere protection by the Ku heterodimer”

June 2012 15th International Conference on the Cell and Molecular Biology of Chlamydomonas, Potsdam, Germany, June 5-10, 2012.
Poster: “Comparative analysis of the structure of telomeres in *A. thaliana* and *C. reinhardtii*”

2010 Student scientific conference, Comenius University, Bratislava 2010
Poster: “Telomeres of *Chlamydomonas reinhardtii* and their response to miRNA mediated under-expression of Ku80”

2009 Student scientific conference, Comenius University, Bratislava 2009
Poster: “Complementation of nitrate reductase in *C. reinhardtii* using constructs from *Volvox carterii*“

Fellowships

2014 EMBO short-term fellowship, January 01 - February 26, 2014
Project title: “Functional analysis of human Ku complexes with altered DNA interaction properties and their effect on DNA double strand break repair and telomere biology”

Other activities

2011 – 2012 Member of the organizing committee of the 10th VBC PhD Symposium “Biomimetics – inspired by nature”

2011 – 2012 PhD student representative at the Gregor Mendel Institute of Molecular Plant Biology

Publications

Fulcher N, Derboven E, Valuchova S, Riha K. If the cap fits, wear it: an overview of telomeric structures over evolution. Cell Mol Life Sci. 2014 Mar;71(5):847-65.

Plecenikova A, Mages W, Andrésson OS, Hrossova D, Valuchova S, Vlcek D, Slaninova M. Studies on Recombination Processes in two *Chlamydomonas reinhardtii* Endogenous Genes, NIT1 and ARG7. Protist. 2013 Jul;164(4):570-82.

Acknowledgments

This work could not be done without many people that helped me throughout my whole studies in scientific and non-scientific way.

I would like to thank Karel for the opportunity to work in world-class conditions, his ever-lasting optimism and enthusiasm, great ideas and his extremely kind nature. Furthermore, for the enormous patience with my scientific writing. None of this would have happened without him.

The Riha lab team, that slowly changed over the years was always a supportive and great place to work. The sentence “I am coming on Sunday, do you need something?” or “Lunch?” became matter of course, but never taken for granted. If I were to list everything I am thankful for, this thesis would double in size. I can hardly thank for everything that Svetlana Akimcheva have done. Besides being the best technician and teacher, she was always there in my weak moments to cheer me up. For this thesis, it was the help with in-gel hybridization that made it to the result section. I would like to thank Matt Watson for being the most patient and generous lab-mate. All your advice was highly appreciated. Anita Kazda for being the fun heart of the lab. Nick Fulcher that contributed not only by protein alignment of TBPs and TRF hybridization of T3 Ku80, but for his fun nature and helpful advice. Branislav Kusenda for introducing me to Karel, pushing me to learn Perl and always trying to help. Petra Bulankova for never ending patience and support. Andrea Plecenikova for being an amazing friend and support in the Chlamy-world. Elisa Derboven for being a great friend, bench neighbor, inspiration and being my partner in crime in PhD Symposium and PhD represention. Claudio Capitao for introducing me to HHPred and MODELLER, countless discussions about the project, talks about the ocean and for being an amazing colleague and friend. Jiradet Gloggnitzer for being an extraordinary and amazing person that fascinates and inspires me. For all scientific and non-scientific discussions we had. Thank you for the ultimate unicorn dust sprinkler and cello vibrations. Sorin Tanasa, Albert Cairo and Kate Vashutina for being brave at the beginning of the RihaReborn and taking the spirit from the former lab to Brno. I am especially thankful to Kate for enormous support in the hard times. Last but not least, Jaroslav Fulnecek and Pavlina Mikulkova for support in the new lab.

All great people from Vienna Biocenter that I had the honour meeting and interacting with: Monika Maronova for being a good friend, but mostly all this would not happen without you. Thank you for answering my email. I do not want to leave anybody behind, but some people stand out from the crowd: Tomas Eichler, Iulia Danciu, Radka Slovak, Jasmin Bassler, Ivan Lebovka and Benoit Pignard.

A lot of people contributed to this work scientifically. Peggy Stoldt-Bergner for her incredible patience and answering all my questions. For her help with designing the baculovirus expression, providing necessary vectors, introducing me to PyMol and helping me to get into the structural biology, and for running the awesome protein department in CSF facility that allowed my research to progress much faster. Johannes Popow for HeLa cDNA and for extensive discussion about transient expression and siRNA knockdown in human cells. Luis Valledor for mass spectrometry of *C. reinhardtii*. Anton Polyansky and Bojan Zagrovic for helpful tips in protein structure modeling and alignment. Eric Hendrickson and his team for making my months in cold Minnesota warm. Eu Han Lee for expression vector and helpful advice. Brian Ruis for help with the transfection, generating stable cell lines and teaching me how to work with cell culture. Elisabeth Thompson for help with proteins. Adam Harvey and Yinan Kan contributed with helpful advice and funny stories. I am sorry Yinan that rAAV did not work out and it could not be included into the work. Marco Repic from Knoblich group for pDONR plasmid. Guenter Resch and Harald Kottisch for help with electron microscopy. Ctirad Hofr and Eliska Janouskova for fluorescence anisotropy.

I would like to thank members of my PhD committee Peter Schloegelhofer and Stefan Westermann for their helpful suggestions.

My friends were a great support. Katarina Harmatova-Finch for staying my best friend even when I was not around. The best gift you can ever give. Alexander Aigner for being there for me when I needed it. Being from IT specialist to psychotherapist, but most of all, my best friend. My thanks goes also to Lisi and Robert Aigner.

My family was a great support throughout my life and nothing would have been the same without Janka Valuchova, Igor Valuch, Michal Valuch and Eduard Valuch, Ludmila Valuchova, Helena Kulikova and Jan Kulik.

Thank you!